TOWARDS A MORE RATIONAL USE OF METABOLISM-TARGETING DRUGS AS ANTICANCER TREATMENTS

CATHERINE VANDER LINDEN

2022

SUPERVISOR: Pr. OLIVIER FERON

CO-SUPERVISOR: Pr. CYRIL CORBET

Acknowledgements

As I step forward on a new path after more than 4 years in the FATH laboratory, I do so with humble thanks to many people who have contributed to the achievement of this thesis.

First of all, I would like to thank the Télévie and all its volunteers who raise money all year long tirelessly, without whom this project would simply not have been possible.

I am grateful to the two external members of my jury, Pr. Chiara Riganti and Pr. Akeila Bellahcène, for having accepted to take the time to revise my manuscript with all their expertise in the field and for all the questions and comments addressed during my private defense that gave me food for thought. I also thank the UCLouvain internal members of my thesis committee, Pr. Bénédicte Jordan and Pr. Raphaël Frédérick for all their suggestions which have contributed to the excellent follow-up of my project during the past 4 years, and Pr. Jean-Pascal Machiels for presiding over my private defense and for your kind words of encouragement.

Then, I would like to deeply thank my promoter, Pr. Olivier Feron, for having allowed me to complete a thesis in your laboratory. I am grateful for the trust you have placed in me during the initiation of the immuno project which has really made me evolve both scientifically and personally. Thank you for always pushing me forward and challenging me with your outstanding scientific expertise, for all your precious corrections and the fruitful coachings before presentations. I also warmly thank my co-promoter, Pr. Cyril Corbet, for having supervised my work with all the pedagogy I could have asked for, for your unfailing patience with all my questions, for all the pleasant discussions about science or at the corner of a corridor and for your comprehension and humanity when I needed to be encouraged. It was a true pleasure to work under your supervision and I wish you much success in your future promising career.

To my esteemed past and present colleagues from Olivier's team, you have been part of my daily life and I'll miss each of you. Many thanks to the

post-docs, Natalia for your extreme kindness, your patience, and the transfer of your knowledge in immunology which was so important to me. Octavia, I will not forget your enthusiasm and your smile that have made my days more beautiful, your inspirational words and all our precious discussions. Léo and Marianela, thank you for your scientific help and personal words. Estelle, thank you for having become a friend over the past years, with whom I know I can openly talk and confide with trust. Your encouraging words and our numerous discussions around a coffee were so important to me, thank you for your unconditional support and your contagious passion for always crazier experiment protocols. I also thank all the "OF-CC" PhD student team, Charline, Elena and Françoise for your smile and enthusiasm that light up the team, and I thank more particularly my office neighbours Bastien, Joao, Kasia and Valentin who have taken the work to another dimension with all the good moments shared, the laughs, the mutual support we addressed to each other and all the precious afterwork drinks and dinners. Last but not least, I would like to mention a special thanks to probably the most important people in the team, the technicians. Alizée, I will not forget your positivity, your frankness but also your great sensitivity which make you a great and unique person. Laurenne, thank you for all our complicity moments inside but also outside of the lab (Couleur Café was a great one); we used to understand each other with a simple look in the eyes and to think in the same way for a lot of things. Céline, I can't thank you enough for all your help with the experiments that you always performed in a masterly way but also for your unwavering support, for the long discussions about our respective private lives, and for your kindness and your generosity. You are a beautiful person that everyone deserves to meet.

I would also like to thank all the PIs from the FATH laboratory, Pr. Jean-Luc Balligand and Pierre Sonveaux for the precious remarks during the FATH data clubs, and Pr. Chantal Dessy for your "maternal" side and your support during difficult times two years ago that I will not forget. For the great atmosphere, the laughs and the infinite number of discussions, I deeply thank all the FATH members: Hrag, Delphine, Charlotte, Lauriane, Thibault, Lucas, Justin, Tania, Deborah, Justine, Laurent, Virginie, and more specifically Roxane, Loïc, Marie and Dorothée

who have become friends. I also particularly would like to mention Emilie, Flavia, Lucie and Ramona for the memorable girls' office. Besides FATH, I warmly thank the members of the IREC platforms, Aurélie, Michèle for the great talks about Nodebais during my cryostat sessions, Caroline for our small but fruitful collaboration on spheroid clearing protocols topped by a fabulous road trip to Liège and Davide for your availability and your more-than-precious help with the flow cytometry and immuno protocols. I also thank Pedro from DDUV animal facility for your kindness, your flexibility and all the mice provided at the end of my thesis. Thank you Guillaume and Olivier, my old GYNE's colleagues and nofilter team for our endless conversations during the lockdown and the support you always provided to me. Guillaume, thank you for having aroused my scientific curiosity, for our numerous (not) always deep conversations, for your encouragements and for having pushed me to send the e-mail that definitively changed my future.

Emeline, my genuine friend, this thesis would definitely not have the same taste without you. Thank you for the inseparable duo that we form since the beginning, for your friendship and your open arms in all circumstances. I have lost the count of our laugh sessions, profound discussions and complicity moments by your side during these 4 years. Working with you has been such a wonderful experience and it is with heart that I wish you the absolute best for your future, although I am sure that we will continue to keep in touch and that nothing will change despite our respective new lives.

Finally, I am grateful to my parents who are giving me all their love since my birth and who have always believed in me regardless of the decisions I was making. You keep saying that you are proud of your daughter, but today I can tell you that if I am who I am today it is to a great extent thanks to you. John, the true love of my life since more than 10 years, thank you simply to stand by my side every day and to allow me to be the best part of myself thanks to your infinite support. Today I can confirm that we perfectly fit together as everybody says and that day after day you bring me all the elements I need to evolve and flourish. I look forward to many more years with you and to discover what the future holds for us.

Summary

Metabolic plasticity in cancer cells makes very challenging the use of metabolism-targeting agents as monotherapy. Indeed, although tumor metabolism is becoming a major source of inspiration to develop new anticancer drugs, numerous examples where tumors were shown to adapt their metabolic preferences to counteract a specific pathway inhibition have been reported. Direct consequences of metabolic adaptation are the development of resistance and the progressive loss of activity of the drug. Besides metabolism-targeting treatments, there is nowadays an increasing interest for immunotherapy. Despite some remarkable effects of immunotherapy in the last decade, many metabolic alterations occurring in cancer cells lead to the elaboration of an immunosuppressive microenvironment. Moreover, the use of metabolism-targeting drugs as anticancer treatments will not only affect cancer cells, but also healthy cells from the tumor microenvironment including immune cells and thereby might abrogate the beneficial effects of immunotherapy. For these reasons, the major objective of this thesis is to bring new insights on the use of metabolism-targeting treatments as anticancer therapy, to efficiently kill plastic cancer cells and to stimulate (or maintain) anticancer immune response. In the first part of our work, we report that exposure to 3-bromopyruvate (3-BrPA), a glycolysis inhibitor, leads to the epigenetic inactivation of the monocarboxylate transporter MCT1 in cancer cells, thereby driving resistance but also preventing the use of extracellular lactate

as a fuel. We further observe that unexpectedly 3-BrPA-resistant cancer cells mostly rely on glycolysis to grow, with MCT4 becoming essential to support lactate flux. Finally, we demonstrate that genetic and pharmacological blockade of MCT4 activity in 3-BrPA-exposed cancer cells prevents cancer cells to grow. In the second part of this thesis, the effects of three compounds blocking the activity of electron transporter chain (ETC) complex I, MCT4 transporter and CPT1A enzyme are used to assess the effects of mitochondrial metabolism, glycolysis or fatty acid oxidation (FAO) inhibition, respectively on T cell phenotype. We show that acute treatment of activated T cells with FAO inhibitor leads to an increase of their proliferation *in vitro*, and to higher cytotoxic capacities towards melanoma cancer cells. Conversely, we also show that pre-treatment of cancer cells with ETC complex I inhibitor before co-incubation with activated T cells potentiates T cell cytotoxic activity. Altogether our data offer metabolism-targeting therapeutic strategies to overcome resistance from plastic cancer cells and to potentiate benefits of immunotherapies.

Table of content

List of abbreviations

α-KG	Alpha-ketoglutarate
1,3-BPG	1,3-bisphosphoglycerate
2-DG	2-deoxyglucose
3-BrPA	3-bromopyruvate
3-BrPA-R	3-bromopyrvate-resistant
5-aza-dC	5-aza-deoxycytidine
5-FU	5-fluorouracil
ACC	Acetyl-CoA carboxylase
ACLY	ATP-citrate lyase
ACT	Adoptive cell therapy
ADP	Adenosine diphosphate
AML	Acute myeloid leukemia
AMPK	AMP-dependent protein kinase
APC	Antigen presenting cell
ASCT2	Alanine-serine-cystein transporter 2
ATP	Adenosine triphosphate
BCAA	Branched-chain amino acid
CAF	Cancer-associated fibroblast
CAR	Chimeric antigen receptor
CFSE	Carboxyfluorescein succinimidyl ester
CIC	Cancer immunity cycle
CoA	Coenzyme A
COX	Cyclo-oxygenase
CPT	Carnitine-palmitoyl transferase
CTL	Cytotoxic T lymphocyte
CTLA-4	Cytotoxic T lymphocyte-associated protein 4

DALYs	Disability-adjusted life years
EGFR	Epidermal growth factor receptor
ER	Endoplasmic reticulum
ETC	Electron transporter chain
FA	Fatty acid
$FADH_2$	Reduced flavin adenine dinucleotide
FAO	Fatty acid oxidation
FAOi	Inhibitor of fatty acid oxidation
FAS	Fatty acid synthase
G6P	Glucose-6-phosphate
GA3P	Glyceraldehyde-3-phosphate
GAPDH	Glyceraldehyde-3-phosphate dehydrogenase
GFP	Green fluorescent protein
GLS	Glutaminase
GLUT	Glucose transporter
HER2	Human epidermal growth factor receptor 2
HIF	Hypoxia-inducible factor
HK	Hexokinase
IC_{50}	Half-maximal inhibitory concentration
ICI	Immune checkpoint inhibitor
IDH	Isocitrate dehydrogenase
IDO1	Indoleamine 2,3 dioxygenase
IFN	Interferon
IL	Interleukin
IL4I1	Interleukin-4-induced protein 1
IMM	Inner mitochondrial membrane
ITAM	Immunoreceptor tyrosine-based activation motif
K_i	Inhibitory constant

K_m	Michaelis-Menten constant
KRAS	Kirsten rat sarcoma virus
LAG-3	Lymphocyte-activation gene 3
LAT1	L-type amino acid transporter 1
LDH	Lactate dehydrogenase
MAPK	Mitogen-activated protein kinase
MeDIP	Methylated DNA immunoprecipitation
MCT	Monocarboxylate transporter
MCTi	Inhibitor of monocarboxylate transporters
MDSC	Myeloid-derived suppressor cell
MHC	Major histocompatibility complex
MPC	Mitochondrial pyruvate carrier
mtDNA	Mitochondrial DNA
mTOR	Mammalian target of rapamycin
NAD	Nicotinamide adenine dinucleotide
NADP	Nicotinamide adenine dinucleotide phosphate
NK	Natural killer
NFAT	Nuclear factor of activated T cells
NO	Nitric oxide
NRF2	Nuclear factor erythroid 2-related factor 2
NSAID	Non steroidal anti-inflammatory drug
NSCLC	Non-small-cell lung cancer
OCR	Oxygen consumption rate
OVA	Ovalbumin
OXPHOS	Oxidative phosphorylation
OXPHOSi	Inhibitor of oxidative phosphorylation
PD-1	Programmed cell death protein 1
PD-L	Programmed death ligand

PDAC	Pancreatic ductal adenocarcinoma
PDH	Pyruvate dehydrogenase
PGC1α	Peroxisome proliferator-activated receptor gamma coactivator 1-alpha
PHD	Prolyl hydroxylase
pHe	Extracellular pH
PFK	Phosphofructokinase
PI3K	Phosphatidylinositol 3 kinase
PK	Pyruvate kinase
PPP	Pentose phosphate pathway
RCC	Renal cell carcinoma
ROS	Reactive oxygen species
shRNA	Short hairpin RNA
siRNA	Small interfering RNA
SREBP	Sterol regulatory element-binding protein
STAT	Signal transducer and activator of transcription
TAG	Triacylglycerol
TCA	Tricarboxylic acid
TCR	T cell receptor
TDO2	Tryptophan 2,3-dioxygenase
T_{EFF}	Effector T cell
T_{EXH}	Exhausted T cell
TGF-β2	Transforming growth factor β2
TIL	Tumor-infiltrating lymphocyte
Tim-3	T cell immunoglobulin-3
TKI	Tyrosine kinase inhibitor
TLS	Tertiary lymphoid structure
TME	Tumor microenvironment
T_{MEM}	Memory T cell

TNBC	Triple negative breast cancer
TNF	Tumor necrosis factor
Tregs	Regulatory T cells
TSG	Tumor suppressor gene
VEGF	Vascular endothelial growth factor

List of figures

List of tables

Introduction

1. Cancer at a glance

Obesity, tobacco, alcohol, exposure to some chemicals… Despite an increasing investment in prevention and screening campaigns, the modern world that we have created is a source of risk factors to promote cancer. In 2017, according to the Belgian Cancer Registry, prostate and breast cancers were the most frequently diagnosed cancers in Belgium among men and women, respectively. In 2018, 70,468 new cases were registered in the country. Today, cancer has become a worldwide phenomenon, representing the highest clinical, social and economic burden in terms of Disability-Adjusted Life Years (DALYs) among all human diseases and the leading cause of mortality around the world [1]. Interestingly, the discovery of a 1.7-million-year-old osteosarcoma from South Africa has demonstrated that cancer is not a recent disease and has raised the question of the origin of cancer and its determinants [2]. If only 5-10% of cancers are known to be hereditary (*i.e.* caused by germline mutations inherited from our ancestors), somatic mutations randomly acquired during lifetime due to mutagenic exposures or defects in DNA surveillance are far more common to cause cancer [3]. These somatic mutations include base substitutions, insertions or deletions of DNA segments, DNA rearrangements after a DNA double-strand break, and increase/reduction of gene copy number [4]. Tumor-suppressor

genes and oncogenes (*i.e.* genes that protect or favor cancer development, respectively) are counted among the most frequently mutated genes. Indeed, these mutant genes will lead to survival and/or growth advantages and thereby to the clonal development of the tumor [5]. Since natural selection will foster cells carrying the most advantageous mutations in harsh conditions, cancer is frequently considered as a Darwinian evolutionary process.

Neoplastic diseases are complex to characterize due to their extremely high heterogeneity and diversity. Indeed, it is now well documented that two tumors can exhibit different behaviors and response to therapy, even if they originate from the same organ [6]. In 2000, Douglas Hanahan and Robert A. Weinberg proposed six essential alterations in cell physiology that dictate malignant growth: self-sufficiency in growth signals, insensitivity to anti-growth signals, tissue invasion and metastasis capacities, limitless replicative potential, sustained angiogenesis and ability to evade programmed cell death (*i.e.* apoptosis) [7]. These six peculiarities have been called the hallmarks of cancer. Eleven years later, after a decade of cutting-edge research, emerging hallmarks involved in cancer pathogenesis have been added to the list. Among them are the reprogramming of energy metabolism and the escape from immune destruction [8] (**Figure 1**). These two characteristics are of particular interest in the context of my thesis project. In the next pages of my introduction, I will therefore detail some aspects of cancer cell bioenergetics as well as the influence of tumor metabolism on the immune response.

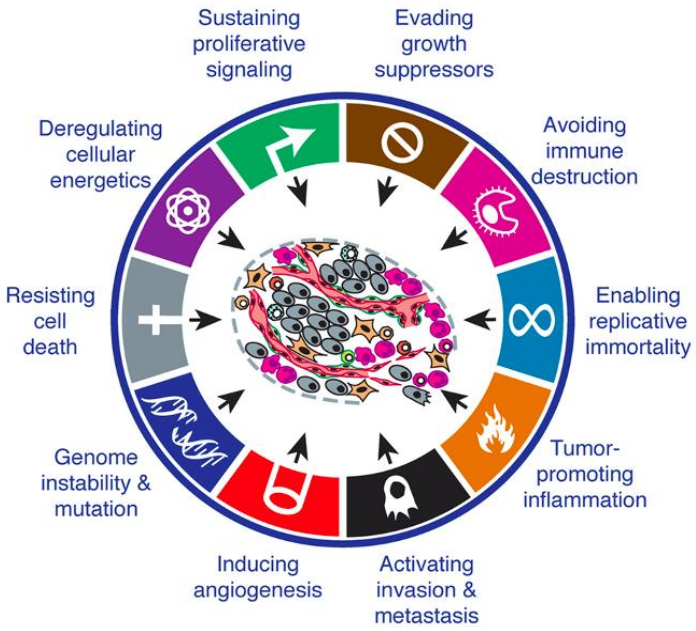

Figure 1: The hallmarks of cancer: new generation.
This figure illustrates a cancer cell in close connection (represented by arrows) with the tumor microenvironment. Ten alterations involved in pathogenesis of most of the cancers and rationalizing the complexity of neoplastic diseases are surrounding the tumor mass. Adapted from [8].

2. Metabolic reprogramming and cancer progression

Along tumor progression, cancer cells constantly face microenvironment-driven metabolic pressures (*e.g.* limited access to nutrients and/or oxygen, local accumulation of protons and the presence of tumor-associated stroma cells) forcing them to adapt to maintain the production of biosynthetic precursors, energy (adenosine triphosphate (ATP)) and reduced cofactors (nicotinamide adenine dinucleotide (NADH)

and nicotinamide adenosine dinucleotide phosphate (NADPH)) [9]. Indeed, from the tumor initiation to metastasis formation, a number of mechanisms largely driven by changes in the local microenvironment such as alterations in sensing and signaling pathways and induction of transcription factors directly contribute to reprogram cancer cell metabolism [9]. Moreover, oncogenic mutations are known to be associated with metabolic rewiring and unique oncogene-driven metabolic signatures have been identified in several cancer types, including non-small cell lung cancer (NSCLC) and triple-negative breast cancer (TNBC) [10, 11]. This continuous metabolic reprogramming required *flexibility* (*i.e.* the ability of a cell to use different nutrients), as well as *plasticity* (*i.e.* the ability of a cell to metabolize the same nutrient differently) [12]. Additionally, tumor cells can either cooperate (metabolic symbiosis) or compete with other (non-) cancer cell populations (**Figure 2**). These scenarios are not mutually exclusive and offer cancer cells multiple adaptations and escape options to maintain selective growth/survival advantages even when evolving under harsh microenvironmental conditions.

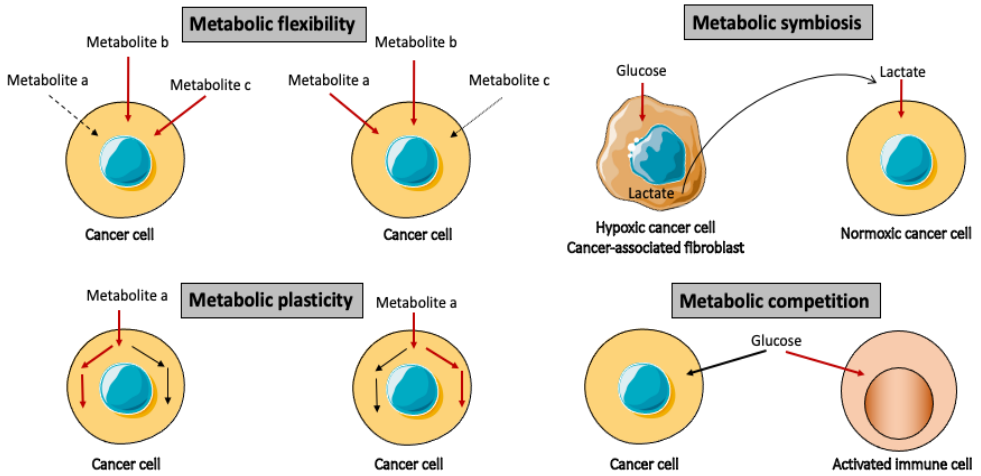

Figure 2: Microenvironment-driven tumor metabolic heterogeneity.
Microenvironmental peculiarities and oncogenic mutations can determine tumor metabolic adaptability via the (co-)existence of different metabolic "scenarios". Intratumor metabolic heterogeneity actually relies on high capacities of flexibility and plasticity but also on the capacities of distinct tumor cell populations (e.g., normoxic vs hypoxic cancer cells) to cooperate together or with stromal cells, such as cancer-associated fibroblasts and adipocytes. Tumor cells can also compete with immune cells for specific bioenergetic substrates, thereby impairing efficient immune response.

Differences in terms of tissue of origin, genetic background and microenvironment composition make cancer extremely heterogenous. Moreover, even in the same primary tumor or between distinct metastatic sites originating from the same primary tumor, cancer cells can exhibit different metabolic preferences, thereby creating metabolic heterogeneity at inter-tumor, intra-tumor and inter-metastatic levels [13] (**Figure 3**).

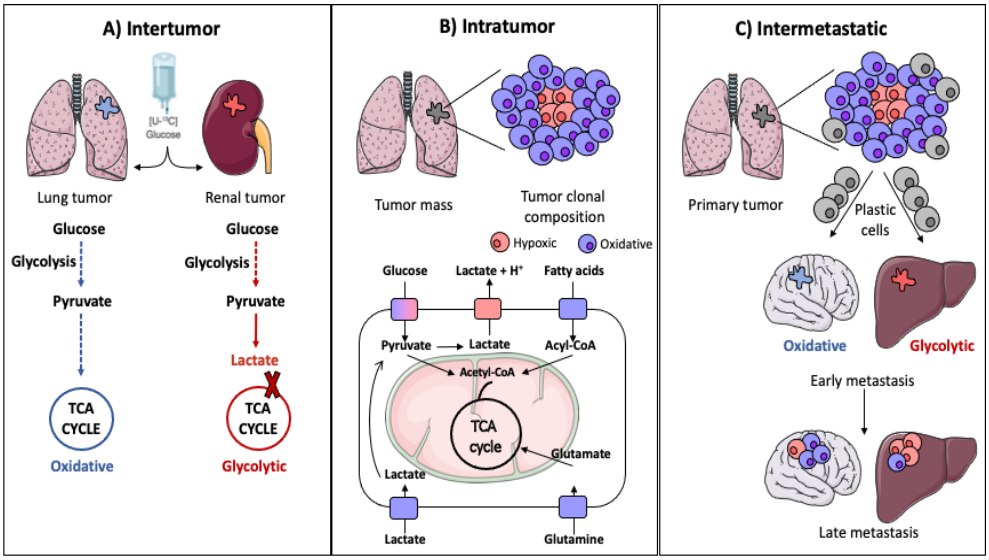

Figure 3: Different levels of metabolic heterogeneity.

Tumor tissue origin can dictate different metabolic preferences leading to inter-tumor heterogeneity (A). For instance, while human lung tumors are reported to be oxidative and rely on mitochondrial respiration, human renal carcinoma are glycolytic and produce high amounts of lactate. Intra-tumor metabolic heterogeneity is found within the tumor mass upon the influence of local TME conditions, as illustrated here with the co-existence of hypoxic and oxidative tumor cells (B). While hypoxic cells are mostly glycolytic, oxidative cancer cells can fuel the mitochondrial TCA cycle with a large diversity of nutrients. Cancer cells that implant to a metastatic site will rely on new metabolic addictions dictated by the local environment within the metastatic niche to sustain ATP production (C) [14]. Abbreviations: CoA, Coenzyme A; TCA, tricarboxylic acid.

2.1 Glycolysis and pyruvate oxidation

Glucose is the most abundant monosaccharide in nature and it is today very well known that all physiologically active and dividing cells are avid for this substrate. Glucose possesses 6 carbons and enters into eukaryotic cells *via* two different types of membrane-associated carrier proteins, the Na^+-coupled glucose transporter and glucose transporter facilitators (GLUT) [15]. In the cytoplasm, glucose will undergo glycolysis initiated upon its phosphorylation by hexokinase (HK) II to form glucose-6-phosphate (G6P) (**Figure 4**). This reaction is determinant for the glycolysis pathway because negatively-charged G6P is not permeable to cell membrane, and the phosphorylation of glucose facilitates its further oxidation. Of note, G6P is the starting element of the pentose phosphate pathway (PPP), a metabolic pathway parallel to glycolysis which is essential for NADPH production (further supporting fatty acid synthesis) and for nucleotide and amino acid precursor generation. When trapped in the cytoplasm, G6P will isomerize to fructose-6-phosphate and undergo a second phosphorylation reaction to form fructose-1,6-bisphosphate upon phosphofructokinase (PFK) enzyme activity. The latter will next split into two molecules of 3 carbons (dihydroxyacetone phosphate and glyceraldehyde-3-phosphate (GA3P)). Of note, the spontaneous degradation of these two triose phosphate intermediates leads to the formation of methylglyoxal, a highly reactive α-oxoaldehyde detoxified via cytosolic glyoxalase I and II with the production of S-D-lactoylglutathione and D-lactate as intermediate and end-product, respectively [16, 17]. The transformation of GA3P in 1,3-

bisphosphoglycerate (1,3-BPG) by the glyceraldehyde 3-phosphate dehydrogenase (GAPDH) initiates the second phase of glycolysis. Importantly, this second phase allows the generation of two molecules of ATP by the conversion of 1,3-BPG to 3-phosphoglycerate. After a series of transformations, the final step of glycolysis leads to the production of two molecules of pyruvate upon phosphorylation of phosphoenolpyruvate by pyruvate kinase (PK).

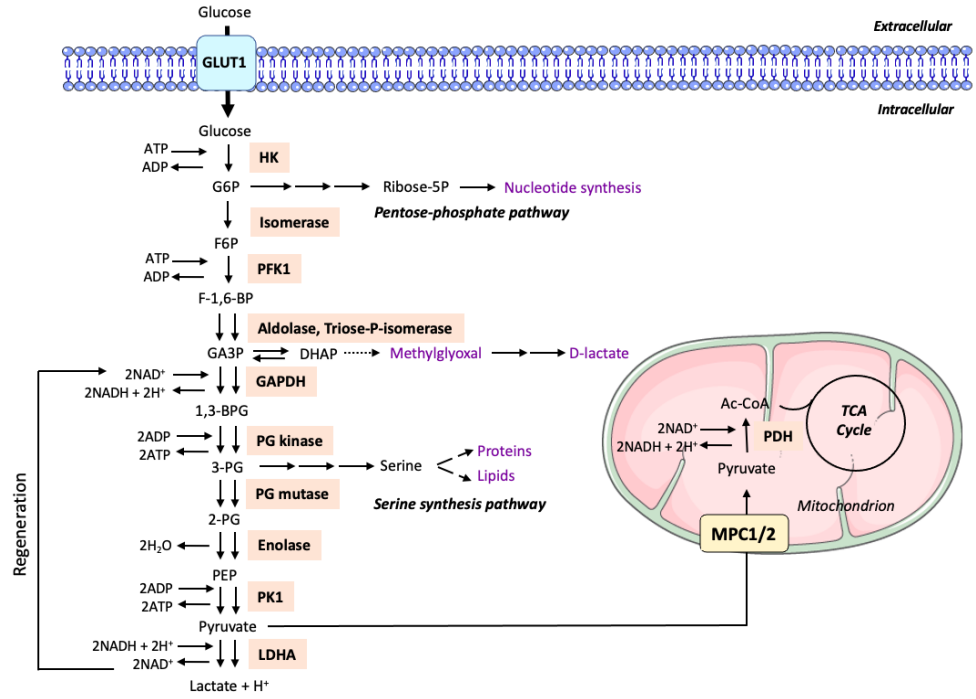

Figure 4: Glycolysis and pyruvate oxidation.
Glycolysis is a series of metabolic reactions, driven by nine specific enzymes, through which one mole of glucose is catabolized to two moles of pyruvate, two moles of NADH with a net gain of two ATP. As indicated, several intermediates can fuel glycolysis branching metabolic pathways such as pentose phosphate pathway, methyglyoxal pathway and serine synthesis pathways. When oxygen is available in

adequate concentrations, pyruvate is imported into the mitochondrial matrix to fuel the TCA cycle after conversion in acetyl-CoA. Abbreviations: Ac-CoA, acetyl Coenzyme A; ADP, adenosine diphosphate; ATP, adenosine triphosphate; BPG, bisphosphoglycerate; DHAP, dihydroxyacetone phosphate; F-1,6-BP, fructose-1,6-bisphosphate; F6P, fructose-6-phosphate; G6P, glucose-6-phosphate; GA3P, glyceraldehyde-3-phosphate; GAPDH, glyceraldehyde 3-phosphate dehydrogenase; GLUT1, glucose transporter 1; HK, hexokinase; LDHA, lactate dehydrogenase A; NAD, nicotinamide adenine dinucleotide; PEP, phosphoenolpyruvate; PDH, pyruvate dehydrogenase; PFK1, phosphofructokinase 1; PG, phosphoglycerate; PK1, pyruvate kinase 1; TCA, tricarboxylic acid.

When oxygen is available in adequate concentrations, pyruvate is transported across the inner mitochondrial membrane (IMM) through a hetero-oligomeric complex formed by two proteins named mitochondrial pyruvate carrier (MPC) 1 and 2, into the mitochondria where it is oxidized in acetyl-Coenzyme A (acetyl-CoA) by pyruvate dehydrogenase (PDH) complex, producing NADH and one carbon dioxide molecule (CO_2) (**Figure 4**). Acetyl-CoA can then enter into the tricarboxylic acid (TCA) cycle, a key metabolic pathway carried out by eight enzymes and releasing the reduced cofactors NADH and flavin adenine dinucleotide ($FADH_2$). NADH and $FADH_2$ produced by TCA cycle will be used as electron donors by the oxidative phosphorylation (OXPHOS) machinery to generate ATP, an energy-carrying organic compound found in the cells of all living organisms (**Figure 5)**. During OXPHOS, electrons are transferred from NADH and $FADH_2$ to a series of electron acceptors through redox reactions catalyzed by protein complexes (*i.e.* complexes I, II, III and IV of the electron transporter chain (ETC)) localized in the IMM. This electron transport process will create an electrical potential and a pH gradient across the membrane, that is used by the ATP

synthase (ETC complex V) to transform adenosine diphosphate (ADP) to ATP *via* a phosphorylation reaction. In total, under aerobic conditions, glycolysis coupled to OXPHOS can produce around 36 ATP molecules per glucose molecule.

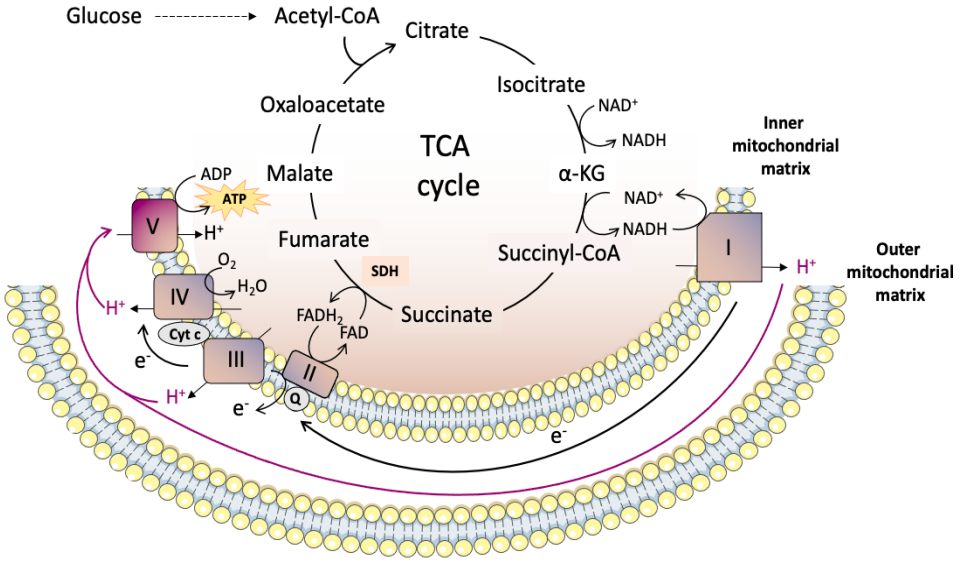

Figure 5: Connection between TCA cycle and OXPHOS.
In a series of enzymatic reactions, the TCA cycle generates the reducing equivalents NADH and $FADH_2$, which are required to transfer electrons to the electron transporter chain (ETC). As the electrons pass through the complexes in the inner mitochondrial membrane, a functional ETC generates a mitochondrial membrane potential that is used to produce ATP. This process requires oxygen and is known as oxidative phosphorylation (OXPHOS). Mitochondrial ETC complexes I and II replenish NAD^+ and FAD, respectively, allowing the TCA cycle to function. Abbreviations: ADP, adenosine diphosphate; ATP, adenosine triphosphate; CoA, Coenzyme A; Cyt C, cytochrome C; FAD, flavin adenine dinucleotide; KG, ketoglutarate; NAD, nicotinamide adenine dinucleotide; SDH, succinate dehydrogenase. Adapted from [18].

2.2 Glycolysis, hypoxia and Warburg effect

The scientist Otto Warburg observed in the 1920s that cancer cells exhibit dramatic increase of glucose uptake and enhanced rates of lactate production despite the presence of adequate oxygen levels (**Figure 6**). This phenomenon is generally called aerobic glycolysis or the « Warburg effect ». Warburg originally hypothesized that such behavior of cancer cells resulted from impaired mitochondrial metabolism [19]. Today we know that only few tumors exhibit a deficit in mitochondrial functions (*e.g.* through mutations in genes coding for TCA cycle enzymes) [20-22]. In most tumors, high lactate production rates are actually observed in the presence of fully functional mitochondria. Aerobic glycolysis has been proposed to offer a growth advantage to cancer cells (over the full glucose oxidation) because of the acidification of the extracellular medium (associated with lactate release) which is toxic for normal cells [23]. For one molecule of glucose, aerobic glycolysis is less efficient than mitochondrial respiration to generate ATP (2 ATP molecules *versus* 36 ATP molecules, respectively). However, the extremely fast turnover rate of aerobic glycolysis is such that the production of lactate from glucose occurs 10-100 times faster than complete oxidation in the mitochondria [24]. This major difference of kinetics can reasonably explain why cancer cells employ aerobic glycolysis to gain energy. Still, the rationale for the Warburg effect is multiple and several biological explanations have been proposed in the last few years. For instance, aerobic glycolysis may be described as an adaptation mechanism to support specific biosynthetic requirements of uncontrolled proliferation. The regeneration

of NAD^+ from NADH in the pyruvate to lactate step actually maintains a high glycolytic turnover and thus generates a large pools of glycolytic intermediates. Those may in turn be engaged in the pentose-phosphate and serine pathways [24-26].

In cancer, hypoxia is a well-known peculiarity of the tumor micro-environment. Indeed, the rapid and uncontrolled proliferation of cancer cells leads to a quick development of the tumor and thereby the positioning of some cancer cells at distance from blood vessels and thus from nutrient and oxygen supplies. This induces the production of angiogenic factors in hypoxic regions of the tumor, like the vascular endothelial growth factor (VEGF). Still, the resulting newly formed blood vessels will often present a chaotic architecture and a non-laminar blood flow [27]. Inadequacy in tumor perfusion will thus also lead to metabolic adaptation of cancer cells to survive under hypoxia. Hypoxia-inducible factor (HIF) is the main regulator of adaptive processes induced by hypoxia (**Figure 6**).

In oxygenated conditions, the proline residues of HIF-α subunits are hydroxylated by oxygen-dependent prolyl-4-hydroxylase (PHDs) (**Figure 6**). The hydroxylated HIF-α creates a binding site for the E3 ubiquitin ligase Von Hippel-Lindau tumor suppressor protein which will further direct the polyubiquitylation of HIF and thereby ensure its degradation by the proteasome [28]. Hypoxic conditions lead to the loss of activity of PHDs, and HIF-α subunits may then translocate into the nucleus to bind HIF-β. This heterodimer of HIF act as a master transcription factor responsible for the induction of hundreds of genes impacting the reprogramming of energy

metabolism, and notably anaerobic glycolysis by positively regulating the expression of GLUT1, HKII, GAPDH, lactate dehydrogenase (LDH) A and monocarboxylate transporter (MCT) 4 responsible for lactate export after pyruvate reduction [29]. Of note, HIF family is composed of 3 different isoforms (*i.e.* HIF-1, HIF-2, and HIF-3). HIF-1α and HIF-2α are more closely related (*vs.* HIF-3α) but still play nonredundant roles and have distinct transcriptional targets [30]. Interestingly, while the transcription of genes encoding glycolytic enzymes cited herein above in response to hypoxia appears to be mostly regulated by HIF-1α, tumor acidosis leads to an increase in HIF-2α abundance either by directly inducing *EPAS1*/HIF-2α gene transcription or by promoting HIF-2α protein stabilization [31]. HIF-2α supports glutamine metabolism in acidic cancer cells (and thereby participates to a decrease in glucose dependence) through the upregulation of glutamine transporter Na^+-dependent alanine-serine-cystein transporter 2 (SLC1A5/ASCT2) and glutaminase (GLS) 1 enzyme [32] (see also paragraph 3.1 Tumor acidosis). HIF-2α can also regulate stem cell functions and/or differentiation through induction of Oct-4 expression [33] and stimulate the production of angiogenic factors such as VEGF and interleukin-8 (IL-8) [34].

In certain circumstances and especially in the context of cancer, HIF-1α regulation may be independent of external oxygen levels. These non-canonical mechanisms include the regulation of PHDs activity by oncometabolites (*e.g.* succinate and fumarate), the emergence of additional mediators of HIF-1α regulation acting regardless of its hydroxylation status and the direct increase of HIF-1α transcription and translation by aberrant

stimulation of pro-survival pathways (*e.g.* ERK/MAPK, JAK/STAT and PI3K/Akt/mTOR) [35].

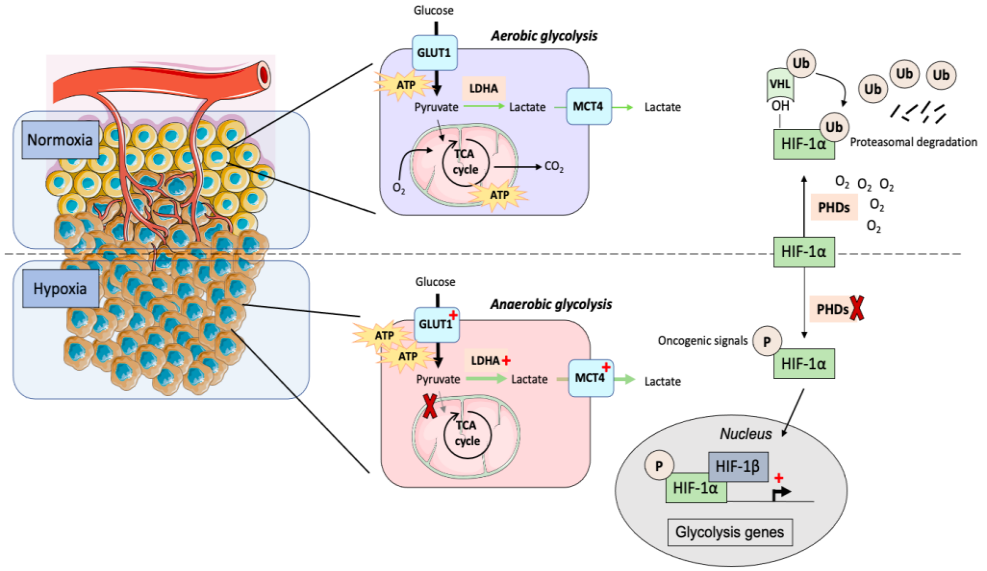

Figure 6: Warburg effect and HIF-1α regulation.

In normoxia, HIF-1α is hydroxylated by prolyl hydroxylase domain (PHD) proteins. The resulting hydroxylated HIF-1α is then recognized by von Hippel-Lindau E3 ubiquitin ligase (VHL) and subjected to be degraded via proteasome. In hypoxia, HIF-1α becomes stable due to inactivation of PHDs and dimerizes with HIF-1β in the nucleus to regulate the transcription of target genes involved in glycolysis. Aerobic glycolysis (the so-called Warburg effect) is a hallmark of proliferative metabolism frequently associated with cancer cells, stating that the majority of glucose consumed by tumors is fermented to lactate rather than oxidized in the mitochondria, even in the presence of adequate oxygen concentrations. Abbreviations: ATP, adenosine triphosphate; GLUT1, glucose transporter 1; HIF, hypoxia inducible factor; LDHA, lactate dehydrogenase A; MCT4, monocarboxylate transporter 4; TCA, tricarboxylic acid; Ub, ubiquitin.

2.3 Glutaminolysis

Glutamine, the most abundant circulating amino acid in the human body, has an important role to produce ATP and reducing equivalents as well as replenishing TCA cycle intermediates [36] (**Figure 7**). After transport inside the cell through diverse transporters including ASCT2 responsible for neutral amino acid transport, glutamine is hydrolyzed in glutamate by GLS1 enzyme and consecutively deaminated into α-ketoglutarate (α-KG) by one of the three following enzymes: glutamate dehydrogenase, glutamic oxaloacetate transaminase or glutamic pyruvate transaminase. Previous work has suggested that glutamine influx *via* ASCT2 triggers the entry of essential amino acid (*e.g.* leucine, phenylalanine, etc.) independently of Na^+ *via* the L-type amino acid transporter 1 (SLC7A5/LAT1) [37]. Both ASCT2 and LAT1 are coordinately upregulated in human cancers where among other roles, they are thought to drive mechanistic target-of-rapamycin (mTOR) growth signaling [38] (**Figure 7**).

Glutamine is frequently used by cancer cells as a major energetic fuel. Recently, Oizel et al. demonstrated through an orthotopic mouse model that aggressive mesenchymal glioblastoma display increased glutamine uptake and utilization compared to other glioblastoma subtypes [39]. Some proto-oncoproteins known for their capacity to regulate cell energetics have been reported to impact glutamine metabolism. For instance, myelocytomatosis oncogene (MYC) was shown to promote glutamine uptake by directly transactivating the expression of ASCT2 and LAT1, and to stimulate glutaminolysis by increasing the expression of GLS via

transcriptional suppression of the GLS repressor micro RNAs (miR)-23a/b [40]. A NRAS-driven dependence of glutamine of melanoma cells resistant to mitogen-activated protein kinase (MAPK) inhibitors was also reported [41].

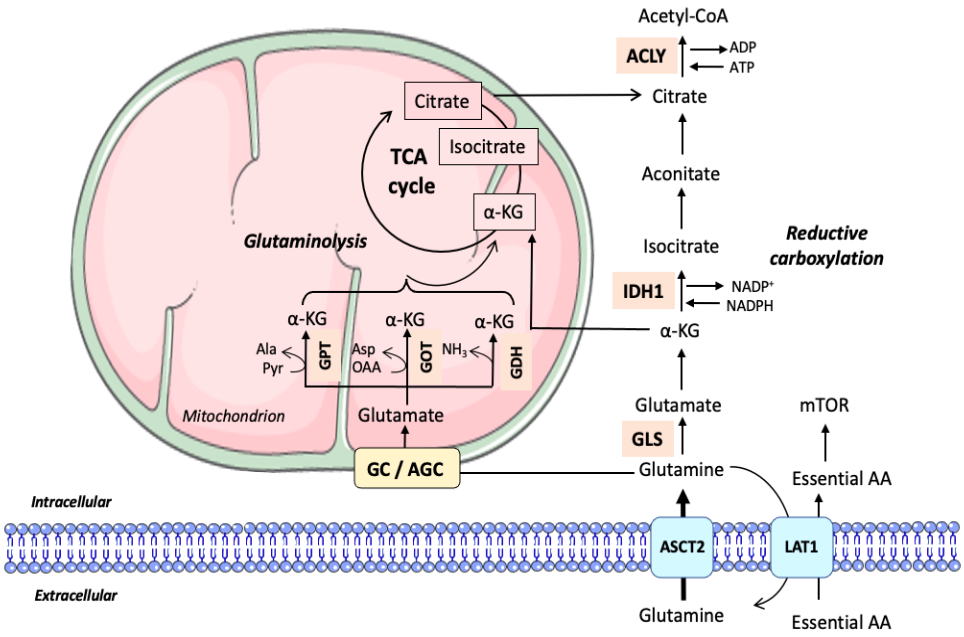

Figure 7: Glutaminolysis and glutamine reductive carboxylation.
Glutaminolysis, which catabolizes glutamine to generate ATP, is a metabolic pathway that involves the initial deamination of glutamine by glutaminase (GLS) forming glutamate. Glutamate is then converted to α-ketoglutarate (α-KG), a TCA cycle intermediate, a reaction catalyzed either by glutamate dehydrogenase (GDH) or transaminases such as glutamate pyruvate transaminase (GPT) and glutamate oxaloacetate transaminase (GOT) which convert α-ketoacids into their corresponding amino acids. Reductive carboxylation of glutamine occurs in the cytoplasm and leads to the production of citrate to supply the cytoplasmic pool of acetyl-Coenzyme A (acetyl-CoA) after conversion in oxaloacetate by ATP-citrate lyase enzyme (ACLY). Glutamine influx via Na^+-dependent alanine-serine-

cystein transporter 2 (SLC1A5/ASCT2) triggers entry of essential amino acid via the L-type amino acid transporter 1 (LAT1) that further activate mechanistic target of rapamycin (mTOR) and stimulate cell growth. Abbreviations: ADP, adenosine diphosphate; AGC, aspartate/glutamate carrier; ATP, adenosine triphosphate; GC, glutamate carrier; IDH1, isocitrate dehydrogenase 1; NADP, nicotinamide adenine dinucleotide phosphate; TCA, tricarboxylic acid.

Besides anaerobic glycolysis, HIF-1α drives also glutamine reductive carboxylation and activation of *de novo* fatty acid synthesis [42, 43]. In hypoxic conditions or when mitochondria are not fully functional, glutamine reductive carboxylation in the cytoplasm is a major cellular carbon source for fatty acid (FA) *de novo* synthesis (lipogenesis) and thereby contributes to the formation of new phospholipid membranes [44] (**Figure 8**). In this case, glutamine is transformed in isocitrate by isocitrate dehydrogenase (IDH) 1 and finally in citrate. Citrate supplies the cytoplasmic pool of acetyl-CoA (together with acetate) by being converted in oxaloacetate through ATP-citrate lyase enzyme (ACLY) [45]. Acetyl-CoA is in turn transformed by acetyl-CoA carboxylase (ACC) in malonyl-CoA which will undergo a series of reactions with new acetyl-CoA molecules. This process is catalyzed by the multi-enzymatic complex fatty acid synthase (FAS) and *in fine* leads to the production of one acyl-CoA molecule. Lipid metabolism is frequently dysregulated in cancer cells and its importance to sustain tumor progression is today well demonstrated. For instance, enzymes from *de novo* lipogenesis are found upregulated in most cancers while normal cells rely on fatty acids coming from the diet or from the liver to sustain their energy needs [46].

2.4 Fatty acid β-oxidation

Besides their principal role of structural components of the membrane matrix, FAs are also important secondary messengers and can serve as substrates for energy production [47]. After uptake by cancer cells *via* CD36/FAT transporters, exogenous free fatty acid will be transformed in acyl-CoA by long-chain-fatty-acid-CoA ligase 1 enzyme in the cytoplasm. Acyl-CoA can be transported *via* the carnitine-palmitoyl transferase (CPT) system into the mitochondria. The CPT system is composed of two separated proteins located in the outer (CPT1) and inner (CPT2) mitochondrial membranes. While CPT2 is an ubiquitous protein, three tissue-specific CPT1 isoforms are described: the so-called « liver » CPT1A, « muscle » CPT1B and « brain » CPT1C [48]. When in the mitochondria, acyl-CoA molecules will be degraded through β-oxidation (FAO) (**Figure 8**). Each cycle of β-oxidation leads to the production of one molecule of acetyl-CoA to supply TCA cycle but also one molecule of $FADH_2$ and one molecule of NADH + H^+ [49]. The energy balance of β-oxidation is hence important: for one molecule of palmitic acid (C16:0), not less than 129 ATP molecules can be generated. However, while lactate is produced by glycolytic (tumor) cells in the *second* range upon exposure to glucose [50], the generation of acetyl-CoA is usually observed *in vitro* in the *minute* range after palmitate addition (O. Feron, unpublished data) and actually reaches a steady-state in men a few hours after administration of palmitate [51]. Therefore, although offering a higher ATP production yield per substrate unit (*i.e.*, palmitate *vs* glucose), the kinetics of FA β-oxidation is slower than glycolysis.

FAO has been reported to be upregulated in several aggressive cancers. For instance, high expression of CPT1A has been associated with bad prognosis and tumor progression for breast, prostate, lymphoma, leukemia, ovarian and lung cancers [52]. FAO was also found to be dramatically increased in MYC-expressing TNBC [53]. Of note, increased lipid uptake and/or synthesis can lead to the emergence of lipid droplet formation, constituting a storage place for excess FAs. Lipid droplets are composed of neutral lipids (*e.g.* triacylglycerol and sterol esters) surrounded by a phospholipid monolayer and help cancer cells to produce energy, in particular when exogenous nutrients are lacking, by releasing FAs upon lipolysis or lipophagy [54]. Moreover, storage of FAs in lipid droplets prevents the toxic effects of a lipid overload in the cytosol, such as endoplasmic reticulum (ER) stress and lipid peroxidation [55].

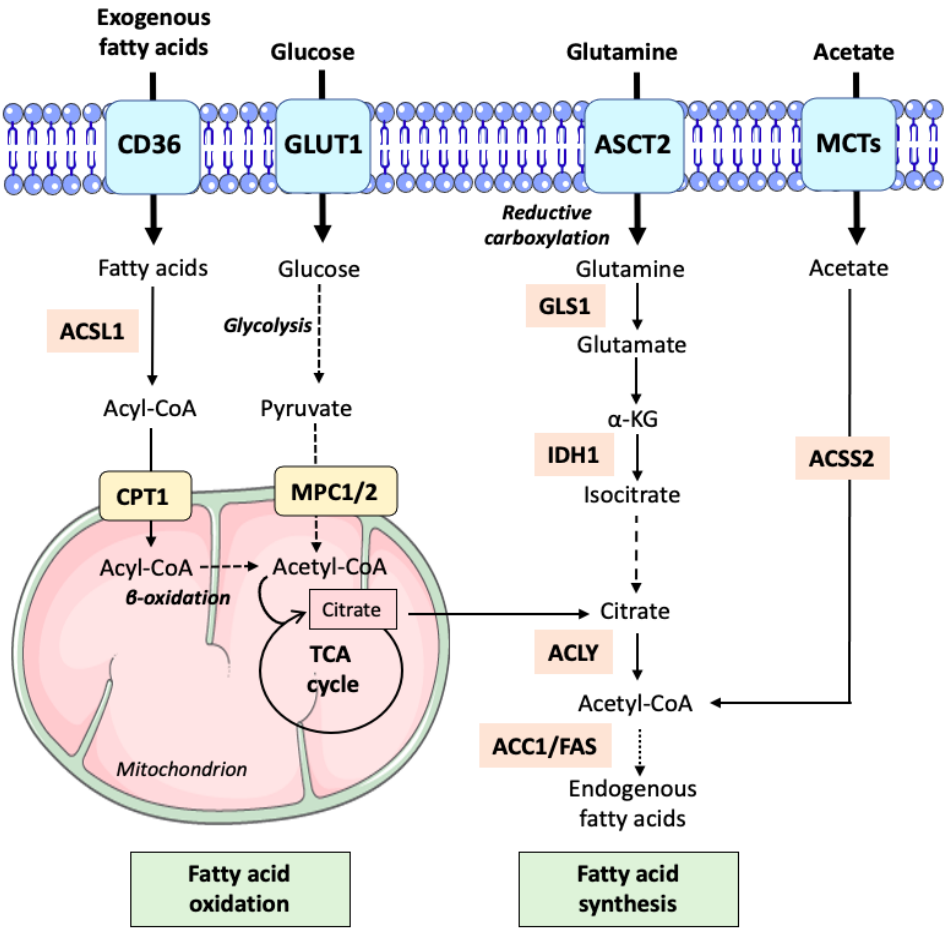

Figure 8: Fatty acid β-oxidation and de novo fatty acid synthesis.

Fatty acid (FA) oxidation is a multistep process by which fatty acids are broken down to produce energy. Exogenous FA firstly enter in the cytoplasm via CD36/FAT transporter. Once in the cell, a Coenzyme A (CoA) group is added to the FA by long-chain-fatty-acid-CoA ligase 1 (ASCL1) enzyme, forming acyl-CoA. Acyl-CoA is transported into the mitochondria by carnitine-palmitoyl transferase system (CPT) and enters the FA β-oxidation pathway, which results in the production of one acetyl-CoA molecule from each cycle of β-oxidation to feed the TCA cycle. On the other hand, cancer cells can also synthesize fatty acids de novo from a cytoplasmic pool of acetyl-CoA, furnished either from exogenous acetate or from glucose- and glutamine-derived citrate. Abbreviations: ACC, acetyl-CoA carboxylase; ACLY, ATP

citrate lyase; ACSS2, acetyl-CoA synthetase 2; ASCT2, alanine-serine-cystein transporter 2; FAS, fatty acid synthase; GLS1, glutaminase 1; GLUT1, glucose transporter 1; IDH1, isocitrate dehydrogenase 1; MPC, mitochondrial pyruvate carrier; TCA tricarboxylic acid. Adapted from [31].

2.5 Other tumor fuels

Besides glutamine, cancer cells may rely on other non-essential amino acids such as aspartate, glycine and serine to sustain bioenergetics and proliferation. Aspartate was shown to represent a limiting metabolite under hypoxia for various types of tumors [56, 57], whereas glycine consumption was strongly correlated with high rates of cancer cell proliferation [58]. Serine starvation and suppression of phosphoglycerate dehydrogenase (*i.e.* the enzyme catalyzing the first step of the serine biosynthesis pathway) efficiently affect the growth of p53-deficient tumors and certain breast cancers, respectively [59, 60]. A variety of cancers are also capable of capturing and metabolizing exogenous acetate to maintain cancer cell growth under low oxygen and lipid-depleted conditions [61-63]. Recently, branched-chain amino acids (BCAAs; *i.e.* valine, leucine and isoleucine) metabolism was demonstrated to influence multiple cancer phenotypes and even act as a cancer biomarker [64, 65]. Indeed, BCAAs are important metabolic substrates because their degradation contributes to the pool of acetyl-CoA and/or provides anaplerotic substrates for the TCA cycle [66].

Access of cancer cells to nutrients can also be supported by macropinocytosis, an ubiquitous pathway for the bulk uptake of

extracellular fluids and substrates into cells through large vesicles known as macropinosomes [67]. Ras-transformed cells were shown to internalize protein *via* macropinocytosis to sustain amino acids pools after proteolytic degradation [68]. More recently, macropinocytosis has been exploited to specifically target oncogenic KRAS in pancreatic cancer through administration of engineered exosomes [69]. Cancer cells can also activate autophagic degradation of macromolecules when lacking nutrients [66]. Autophagy was documented to be crucial for the growth of many cancer types, including the agressive $BRAF^{V600E}$ lung cancer [70] and KRAS-driven pancreatic and lung tumors [71, 72].

2.6 *In vivo* evidence of metabolic heterogeneity in cancer patients

Stable isotope-based metabolic analyses can be performed to assess how the cellular metabolism of a variety of potential biosynthetic fuels is altered during cancer progression. Within the past ten years, this approach has dramatically modified our knowledge of the *in vivo* tumor metabolism in mice [73-75] but also in human cancer patients [76-81]. For this purpose, stable isotopically ^{13}C-labeled substrates are administered as a bolus followed by an intra-operative infusion, through a peripheral intravenous line, before surgical tumor resection and analysis of isotope enrichment downstream of labeled nutrients via ^{13}C NMR spectroscopy [82]. Several recent studies using [U-^{13}C]glucose infusion in cancer patients have revealed a metabolic heterogeneity between different tumor types (**Figure 2**). Indeed, some tumors, like clear cell renal cell carcinoma, were found to be highly

glycolytic and produce high amounts of lactate through aerobic glycolysis [81] while a preferred glucose oxidation through mitochondrial oxidative metabolism was documented in glioma, brain metastases and NSCLC [76-79, 83]. Moreover, infusion of [U-^{13}C]glucose in patients with FDG-PET-positive tumors within the brain and lungs reveals the preferred use of pyruvate by the mitochondria (vs. reduction into lactate), even to a larger extent than in adjacent tissues [78, 79]. Moreover, only 50% of the acetyl-CoA pool has been found to derive from blood-borne glucose in human brain tumors [77], suggesting that additional substrates contribute to tumor bioenergetics (**Figure 2**). Other studies have indeed highlighted the role of alternative respiratory fuels, including acetate and lactate, in complementing glucose oxidation to support biomass and energy production in living tumors [62, 75, 79, 80]; the specific role of lactate as a metabolic fuel will be discussed in the section 3.2.1. Interestingly, the metabolic profile of tumors has been found to be dependent on both the genotype and the tissue of origin. For instance, *MYC*-driven liver cancers and TNBCs are more glutamine-dependent than *MET*-driven liver and *MYC*-driven lung tumors [74, 84, 85]. *In vivo* ^{13}C-based metabolic profiling also led to demonstrate the important role of PDH and pyruvate carboxylase to support tumor growth in human lung cancer patients [76, 78, 83], making them attractive therapeutic targets in this specific tumor type.

This paragraph is derived from "Catherine Vander Linden and Cyril Corbet, Seminars in Cells and Developmental Biology, https://doi.org/10.1016/j.semcdb.2019.05.016"

Besides studies measuring which nutrients contribute carbon to the tumor TCA metabolites, a recently-developed *in vivo* dynamic isotope tracing-mass spectrometry strategy has been validated to evaluate TCA flux quantification (*i.e.* how fast the cycle turns) [86]. By applying this technique to all major mouse organs and to five tumor models, authors have reported that, compared to the tissue of origin, tumor TCA flux is markedly suppressed. Complementary glycolytic flux measurements confirmed tumor glycolysis acceleration, but the majority of tumor ATP is made aerobically, and total tumor ATP is suppressed compared to healthy tissues. Thus, instead of being hypermetabolic as commonly accepted, tumors apparently produce ATP at a lower than normal rate. Authors proposed the hypothesis that when cells de-differentiate into cancer, they escape ATP-intensive processes characteristic of the host tissue, and that the resulting low ATP requirement contribute to the Warburg effect and helps cancer growth in the nutrient-poor tumor microenvironment [86].

3. Microenvironment-driven intratumoral metabolic heterogeneity

As briefly detailed above, cancer cells can use a variety of substrates to fulfill their need in energy and/or biosynthetic precursors according to the local tumor microenvironment (TME) [49, 87, 88]. The latter is itself influenced by the gradients of nutrients, oxygen and protons as well as by the presence of tumor-associated stromal cells (*e.g.* cancer-associated fibroblasts (CAFs), immune cells, endothelial cells, etc.) [88-90].

3.1 Tumor acidosis

Besides hypoxia, acidosis is now considered as a hallmark of the microenvironment in solid tumors with mean values of extracellular pH (pHe) ranging from 6.2 to 6.8 [91, 92]. Although initially described as a consequence of the exacerbated glycolysis in tumor cells and the disorganized tumor vasculature, accumulation of H^+ ions in the TME also results from the mitochondrial respiration-derived CO_2 hydration [45, 93]. Direct measurements of both intratumoral pO_2 and pH have indeed revealed a spatial heterogeneity as well as an imperfect overlapping of hypoxia and acidosis gradients, with the existence of acidic areas that are also well-oxygenated [94, 95].

Tumor acidosis is thus initially a metabolic collateral effect of uncontrolled dividing cancer cells. Importantly, cancer cells will have to adapt to the environmental acidosis that they have themselves generated, by progressively shifting from glucose metabolism to lipid metabolism. They will for instance develop a strong dependence to glutamine in a SIRT1/HIF2α-dependent manner while reducing the release of glycolysis-derived protons (Figure 9) [32]. Even though malonyl-CoA is reported to be an allosteric inhibitor of CPT1 activity to avoid futile cycles between fatty acid formation and degradation, Corbet et al. documented that cancer cells in tumor acidic compartments have the ability to concomitantly use fatty acid oxidation and synthesis because of ACC2 downregulation (itself resulting from sirtuin-mediated histone deacetylation) [96]. In parallel, acidosis-driven activation of sterol regulatory element-binding protein

(SREBP) 2 increases FAS from acetate by promoting the expression of acetyl-CoA synthetase 2 [45]. More recently, acidic pH was found to promote autocrine transforming growth factor β2 (TGF-β2) signaling, which in turn leads to the membrane translocation of CD36 and a significant increase in FA uptake (**Figure 9**) [97]. FAs are then either readily oxidized to generate ATP or stored as triglycerides in lipid droplets that represent potential energy reservoir for invading cancer cells [97]. In addition to glutaminolysis and FA metabolism, acidosis was also reported to activate p53, which contributes to redirect glucose away from lactate production and towards the oxidative branch of the PPP; consecutive increase in NADPH production can thereby counter the enhanced basal reactive oxygen species (ROS) production in cancer cells exposed to extracellular acidosis [98].

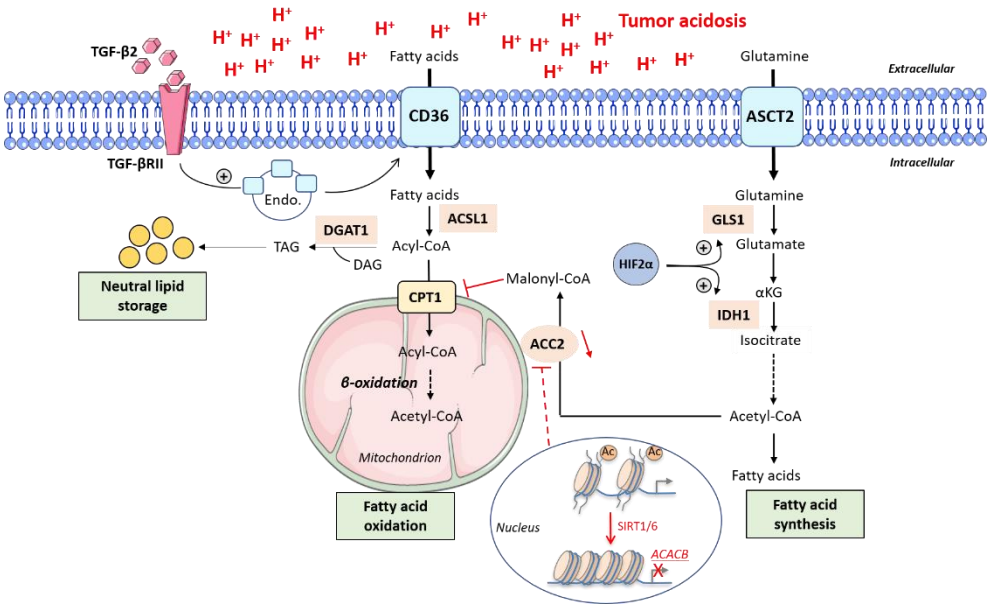

Figure 9: Fatty acid metabolism dysregulation in acidic cancer cells.

Tumor cells, exposed to low pH conditions, exhibit profound alterations in lipid metabolism, with a concomitance of fatty acid oxidation in mitochondria and synthesis from glutamine in the cytoplasm, rendered possible through a sirtuin 1 and 6 (SIRT1/6)-mediated downregulation of the acetyl-CoA carboxylase 2 (ACC2). Acidosis also triggers transforming growth factor β2 (TGF-β2) signaling upregulation which favors the translocation of CD36 fatty acid translocase to the plasma membrane, thereby enhancing the uptake of long-chain fatty acids. Fatty acids can then be either oxidized in mitochondria for energy production, or stored as neutral lipids (triacylglycerols, TAGs) in lipid droplets, in a diacylglycerol acyltransferase 1 (DGAT1)-dependent manner. Abbreviations: ACSL1, acyl-Coenzyme A synthetase 1; ASCT2, alanine-serine-cystein transporter 2; CoA, Coenzyme A; CPT1, carnitine-palmitoyl transferase 1; DAG, diacylglycerol; Endo, endosomes; GLS1, glutaminase 1; HIF2α, hypoxia-inducible factor 2α; IDH1, isocitrate dehydrogenase 1; TGF-βRII, transforming growth factor β receptor 2. Adapted from [97] and [31].

3.2 Metabolic crosstalk between (tumor) cell types

The different components of the TME accounts for intratumor metabolic heterogeneities that give rise to metabolite exchanges between different populations of cancer cells and/or between tumor cells and stromal cells, including CAFs, adipocytes and immune cells [9] (**Figure 10**).

3.2.1 Lactate-mediated metabolic symbiosis between tumor cell populations

In 2008, our lab documented the existence of a process of lactate exchange between lactate-generating and lactate-consuming cancer cells [99], a phenomenon recapitulating the lactate shuttle between fast-twitch and slow-twitch skeletal muscle fibers. This capacity of lactate to be used as a fuel was further proven by other investigators in our lab documenting that the upregulation of MCT1 offered p53-deficient cancer cells the possibility to facilitate lactate import or export depending on glucose availability [100]. This role of lactate as a *bona fide* tumor fuel was recently confirmed by infusing NSCLC cancer patients with ^{13}C-lactate and showing that lactate is actually more extensively used than glucose by lung cancer cells to sustain tumor metabolism [80]. More than a unidirectional exchange of substrate, our lab demonstrated that the use of lactate as an energy fuel by oxidative cancer cells contributes to spare glucose and makes it more available for hypoxic cancer cells (**Figure 10**) [99, 101]. Indeed, poorly oxygenated cancer

cells are forced to meet their energy needs through glycolysis, leading to the production of lactate. Rather than being a waste metabolite, lactate is secreted out of the cytoplasm of hypoxic cells mainly through MCT4 (together with H^+) and taken up by oxidative tumor cells through MCT1 where it may act as a fuel for TCA cycle after being converted in pyruvate by LDHB enzyme. This use of lactate thus reduced the extent of consumed glucose which can instead be used for anaerobic glycolysis by hypoxic cancer cells [99, 101].

Recently, MCT1 expression and lactate utilization by tumor cells have been linked to a more aggressive and oncological behavior in different types of cancers [102, 103]. In melanoma patient-derived xenografts, $MCT1^{high}$ cells were found responsible for a higher metastatic disease burden than $MCT1^{low}$ cells derived from the same tumor, further illustrating intratumor metabolic heterogeneity [104].

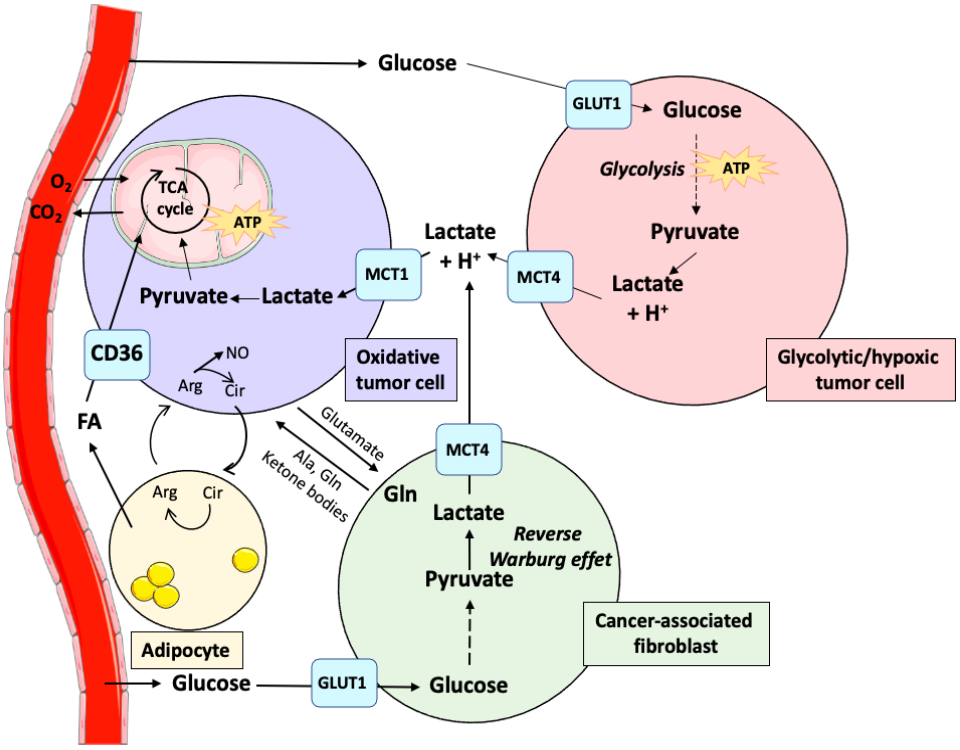

Figure 10: Metabolic communication between (tumor) cells.

Blood vessels feed glucose and oxygen to cancer cells. Hypoxic cancer cells far from blood vessels perform anaerobic glycolysis to survive and in consequence consume high amounts of glucose. Lactate provided by glycolytic cells (MCT4-dependent process) is preferentially used than glucose as an oxidative fuel by oxidative cancer cells close to blood vessels (MCT1-dependent process), in order to increase glucose availability for glycolytic cancer cells. Cancer cells also communicate with stroma cells such as cancer-associated fibroblasts and adipocytes to exchanges various nutrients (e.g. glutamine, glutamate, amino acids, ketone bodies, fatty acids and lactate through the so-called « reverse Warburg effect »). Abbreviations: ATP, adenosine triphosphate; GLUT1, glucose transporter 1; MCT, monocarboxylate transporter; NO, nitric oxide; TCA, tricarboxylic acid. Adapted from [105].

3.2.2 Monocarboxylate transporters (MCTs)

MCTs belong to family of 14 transmembrane proteins, encoded by solute carrier 16 (*SLC16*) genes. MCT1-4 are the most characterized in the literature and their role is to catalyze the proton-linked transport of monocarboxylates, including pyruvate, L-lactate, ketone bodies aceto-acetate and β-D-hydroxybutyrate and short chain FA propionate and butyrate, across the plasma membrane [105]. These passive transporters can work bidirectionally depending on the concentration gradient of their substrates, even though they all possess distinct relative affinity values that can dictate the import or export of molecules. For instance, the high affinity of MCT1 for lactate (K_m ~3.5 mM) renders MCT1 more prone to import lactate inside oxidative cells, while MCT4 is mostly known for lactate export due to lesser lactate affinity (K_m ~30 mM) (**Figure 9**). Moreover, the very low affinity of MCT4 for pyruvate (K_m ~150 mM) prevents the loss of pyruvate from the cell and thus permits high rates of glycolysis [106] (**Table 1**).

MCT proteins possess 12 transmembrane domains, and a large cytosolic loop between domains 6 and 7 [107]. In the presence of L-lactate, the amino and carboxyl terminal domains enclose a cavity that opens to the extracellular side, a state defined as « outward-open » [108]. The central pocket is positively charged due to two basic residues Lys38 and Arg313 (in the transmembrane domains 1 and 8, respectively) that are also suggested to be responsible for the recognition of acidic substrates [109]. Importantly, the outward-open structure of MCT1 is observed when key residues for substrate-binding and proton coupling are in a deprotonated state. Hence,

when the residues are in a constitutive protonated state (*i.e.* due to mutations or to lower pHe values), the structure of MCT1 is locked in « inward-open » state which prevents lactate from entering the central cavity [108].

MCTs are widely active in normal tissue with different patterns of expression to ensure important metabolic processes, such as lactate-fueled gluconeogenesis in the liver after exercise through MCT1 [110] or lactate shuttle between MCT4-expressing glycolytic white muscle fibers and MCT1-expressing oxidative red muscle fibers [111]. *SLC16A1*/MCT1 transcription is reported to be controlled by MYC oncogenic transcription factors [112]. MCT2 is less ubiquitous and is mostly expressed in neurons at the postsynaptic density. MCT3 expression is limited to the retinal pigment epithelium and choroid plexus epithelia [113]. To be properly expressed at the plasma membranes, MCTs need ancillary proteins: translocation of MCT1, MCT3 and MCT4 needs the chaperone protein basigin (also known as CD147) while MCT2 relies on embigin (gp70) [114] (Table 1).

Besides their physiological roles in transporting the above listed monocarboxylates, MCTs have also been reported to mediate the transport of exogenous drugs (*e.g.* salicylic, valproic, simvastatin, 3-bromopyruvic acids and γ-hydroxybutyrate) and can therefore influence drug pharmacokinetics [115, 116].

Table 1: Main characteristics of monocarboxylate transporters 1-4.
This table summarizes main substrates of monocarboxylate transporters (MCT)1-4 along with their respective Michaelis constant (K_m) values, as well as tissue distribution and chaperone proteins.

	MCT1	MCT2	MCT3	MCT4
Human gene name	*SLC16A1*	*SLC16A7*	*SLC16A8*	*SLC16A3*
Main substrates	Lactate, pyruvate, ketone bodies	Pyruvate, lactate, ketone bodies	Lactate	Lactate, ketone bodies
Tissue distribution	Ubiquitous except β cells of the endocrine pancreas	High expression in testis, moderate to low in spleen, heart, kidney, pancreas, skeletal muscle, brain and leucocytes	Retinal pigment epithelium, choroid plexus	Skeletal muscle, chondrocytes, leucocytes, testis, lung, brain, ovary, placenta, heart
K_M lactate	3.5-10 mM	0.5-0.75 mM	5-6 mM	22-28 mM
K_M pyruvate	1 mM	0.1 mM	-	153 mM
K_M β-hydroxybutyrate	12.5 mM	1.2 mM	-	-
K_M acetoacetate	5.5 mM	0.8 mM	-	-
Chaperone protein	Basigin (CD147)	Embigin (gp70)	Basigin (CD147)	Basigin (CD147)

*References related to K_m values of **MCT1**: [113], [117], [118] and [119]; of **MCT2**: [117], [120], [121], [122] and [123]; of **MCT3**: [120], [121] and [122]; of **MCT4**: [117] and [124].*

3.2.3 Metabolic crosstalk with cancer-associated fibroblasts and adipocytes

The harsh tumor microenvironment determines a large part of metabolic adaptations in cancer cells, including through competition for substrates with neighboring stromal cells [125] (**Figure 10**).

CAFs are a key component of TME with multiple functions, including matrix deposition and remodeling, cyto$_{ki}$ne secretion and reciprocal signaling interactions with cancer cells [126]. Regarding metabolism, cancer cells and CAFs communicate through several mechanisms. The « reverse Warburg effect » states that CAFs use aerobic glycolysis to produce lactate, which is utilized by adjacent cancer cells to fuel mitochondrial TCA cycle and subsequent ATP production *via* OXPHOS [127]. Whitaker-Menezes et al. further documented that breast cancer cells MCF7 specifically induce the expression of MCT4 in CAFs and that MCT1 is reciprocally upregulated in MCF7 cells when co-cultured with fibroblasts, both supporting the reverse Warburg effect [128]. Besides glucose and lactate metabolism, activated pancreatic stellate cells (*i.e.* the major type of pancreatic CAFs) are critical for pancreatic ductal carcinoma (PDAC) through the secretion of non-essential amino acids, and more specifically alanine which outcompetes glucose and glutamine to fuel the TCA cycle in PDAC and thereby decreases the tumor's dependence on glucose and serum-derived nutrients, often limited in the pancreatic TME [129]. Under nutrient deprivation, CAFs can instead provide ovarian cancer cells with glutamine and use cancer-cell-derived glutamate to regenerate glutamine [130].

Obesity-associated changes in the TME have been implicated in several hallmarks of cancer (*e.g.* chronic inflammatory state, epithelial-to-mesenchymal transition, tumor-related fibrosis, angiogenesis and genomic instability) [131]. It is now well documented that adipocytes provide a source of extracellular FAs to cancer cells upon lipolysis, and thereby participate to

tumor growth by supplying lipids for cancer cell membrane and cellular organelle constitution and/or by providing an efficient source of energy production through the FAO pathway [132, 133] (**Figure 10**). Moreover, omental adipocytes reprogram ovarian tumor metabolism through the activation of key transcription factors (*e.g.* STAT1, HIF-1α, FOXO1 and PPARγ coactivator-related 1) known to be involved in the regulation of CD36 activation and plasma membrane recruitment, resulting in FA uptake, cholesterol and lipid droplets accumulation [134]. Ovarian adipose stromal cells have also been shown to metabolically communicate with cancer cells by engaging in an arginine cycling pathway to increase nitric oxide (NO) synthesis in cancer cells and reduce oxidative stress [135].

The numerous metabolic cross-talks existing between cancer cells and immune cells will be described in the « immuno-metabolism » chapter of this introduction.

4. Therapeutic strategies to interfere with metabolic pathways

The existence of various metabolic addictions in cancer cells renders anti-metabolic drugs very attractive as innovative therapeutic approach to treat cancer (**Figure 11**).

Regarding ***glucose metabolism***, several inhibitors of GLUT1 have been reported to decrease glucose uptake in cancer cells. A group of tyrosine

kinase inhibitors (TKIs) that include natural products of the family of flavones and isoflavones and synthetic compounds such as tyrphostins have been shown to inhibit the activity of GLUT1 [136]. Kinetic analysis of transport data indicated that only TKIs with specificity for ATP binding sites inhibited the transport activity of GLUT1 in a competitive manner, while TKIs that are competitive with tyrosine but not with ATP failed to inhibit hexose uptake or did it in a noncompetitive manner. Recently, other natural small molecules such as the anti-inflammatory resveratrol have also demonstrated to block GLUT activity [137]. Besides GLUT1 targeting, 2-deoxyglucose (2-DG) and 3-bromopyruvate (3-BrPA) that are analog molecules of glucose and pyruvate, respectively, have been abundantly exploited to block glycolysis. While 2-DG competitively inhibits the production of G6P thereby blocking downstream glycolytic reactions, 3-BrPA is an alkylating agent with antiglycolytic properties via preferential alkylation of HKII and GAPDH enzymes [115]. Potential therapeutic drugs targeting other key glycolytic enzymes like PFK, PK and LDHs are also currently investigated [138].

The roles of MCTs in supporting lactate shuttle (*i.e.* metabolic symbiosis) between oxidative and hypoxic cancer cells also offers new perspectives to therapeutically target the hypoxic tumor compartment by a bystander effect [99, 101] but also to tackle tumor angiogenesis [139]. Pharmacological inhibition of lactate transport can be obtained by AZD3965, a MCT1/2 inhibitor with a higher affinity for MCT1 (K_i MCT1 2.3 nM versus MCT2 <10 nM) [140] and the orally available BAY-8002 small molecule (IC_{50} ~85 nM in MCT1-expressing DLD-1 cells) [141]. Recently, the mode of action

of these two inhibitors was unraveled by Wang et al. who documented that they both occupy the MCT1 substrate binding site (via polar interactions between the carboxylate group of BAY-8002 with Lys38, Ser154, Asp309, Arg313 and Ser371 of MCT1 and hydrophobic contacts between Leu281 of MCT1 with pyrazol and isoxazolidinyl groups of AZD3965), and trap MCT1 in the outward-open state [108]. Interestingly, the non-steroidal anti-inflammatory drug (NSAID) diclofenac has been recently repurposed to target MCT1 and MCT4 activity, with a 10-fold higher affinity for MCT4 than MCT1. Diclofenac was shown to reduce lactate export and consequently glucose uptake, thereby delaying tumor growth *in vivo* and inducing a better response to immune checkpoints inhibitors (ICIs) [142].

The relevance of targeting ***lipid metabolism*** in cancer therapies has been highlighted in many recent reviews [143, 144]. Fatty acid uptake can be blocked at the CD36 level with the small molecule inhibitor sulfosuccinimidyl oleate [145] or with monoclonal antibodies. Etomoxir was shown to block FAO by inhibiting CPT1A activity. In glioblastoma, etomoxir was further shown to exert anti-tumor effects by impairing NADPH production and increasing ROS [146] while in leukemia, mitochondrial damages and apoptosis induction were reported [147]. Several strategies to block lipogenesis have also recently been documented, including the inhibition of ACLY [148], ACC [149, 150] and FAS [151]. Finally, our laboratory also demonstrated that instead of blocking lipid metabolic pathways, one could take advantage of the addiction of acidic cancer cells for FA. Indeed, the administration in excess of specific toxic FA like omega-3 and omega-6

polyunsaturated can lead to ferroptosis-mediated cytotoxic effects in the tumor acidic compartment [152].

Glutamine metabolism can be prevented either through GLS inhibition by the preclinical compound bis-2-(5-phenylacetamido-1,2,4-thiadiazol-2-yl)ethyl sulfide (BPTES) or its clinical derivative CB-839 (Telaglenastat) [153] or through glutamine depletion using L-asparaginase [154].

Other therapeutic approaches deal with targets shared by several metabolic pathways. The recent development of ***OXPHOS inhibitors*** is one example of a strategy that may considerably impact tumor bioenergetics. Originally, however, OXPHOS-interfering compounds were thought to be incompatible with the survival of healthy tissues. Furthermore, intrinsic issues with the first OXPHOSi prevented their use in the clinic, including "off-target" effects (*e.g*. rotenone) or a limited pharmacokinetic profile (*e.g*. oligomycin) [155]. Today, there are increasing evidence that OXPHOS inhibition may represent a viable option. For instance, biguanides (*e.g*. metformin, phenformin) which are safely used to treat diabetes were documented to act as (albeit weakly potent) complex I inhibitors. IM156 and IM188 (ImmunoMet) are novel biguanides currently in late stage lead optimization. IM156, currently in phase I clinical study is very promising and has demonstrated efficacy to treat cancers with molecular signatures of sensitivity to OXPHOS inhibition, while IM188 is targeting OXPHOS-dependent immune suppressor cells to enhance the response of current immunotherapies.

Recent studies have identified *bona fide* OXPHOS inhibitors, namely IACS-010759 [156] and gboxin [157], as potent anticancer drugs in various tumor subtypes. IACS-010759 has been reported as a selective inhibitor of the ND1 subunit of complex I of the ETC and shown to preferentially inhibit the growth of certain "OXPHOS-dependent" tumors such as chemo-resistant acute myeloid leukemia (AML), glycolysis-deficient glioma, SWI/SNF mutant lung cancer and brain metastases from melanoma [156, 158, 159]. IACS-010759 is currently being evaluated in phase I clinical trials in relapsed/refractory AML and solid tumors (NCT02882321 and NCT03291938, respectively). In another study, gboxin has been found to specifically inhibit the growth of primary mouse and human glioblastoma stem-like cells while not affecting the viability of mouse embryonic fibroblasts or neonatal astrocytes. Gboxin reduces OXPHOS by interacting with respiratory chain proteins and inhibiting the ATP synthase activity [157]. The risk of side effects is certain with OXPHOSi, the main question is whether the benefit-risk balance will be favorable (in particular for therapy-refractory cancer patients). While the high therapeutic index of IACS-010759 and gboxin is encouraging, phase I clinical trial with BAY87-2243, another complex I inhibitor, had to be stopped several years ago for toxicity issues [160]. BAY87-2243 had however been reported to alleviate hypoxia and improved radiation response without toxicity in mice. It is noteworthy that, such radiosensitizing effects (*via* tumor reoxygenation) can be obtained with drugs acting on more specific metabolic paths. Our lab for instance reported that 7ACC2, an inhibitor of MPC1 could promote tumor reoxygenation by blocking both lactate and glucose-fueled TCA cycle [161].

This paragraph is derived from "Catherine Vander Linden and Cyril Corbet, Seminars in Cells and Developmental Biology, https://doi.org/10.1016/j.semcdb.2019.05.016 ».

Chemical structures and affinity values of key compounds used in the Results part of this thesis (*i.e.* 3-bromopyruvate, diclofenac, CIM203070 (ETC complex I inhibitor) and etomoxir) are summarized in the Scope and Aims section (see paragraph 2. Specific aims).

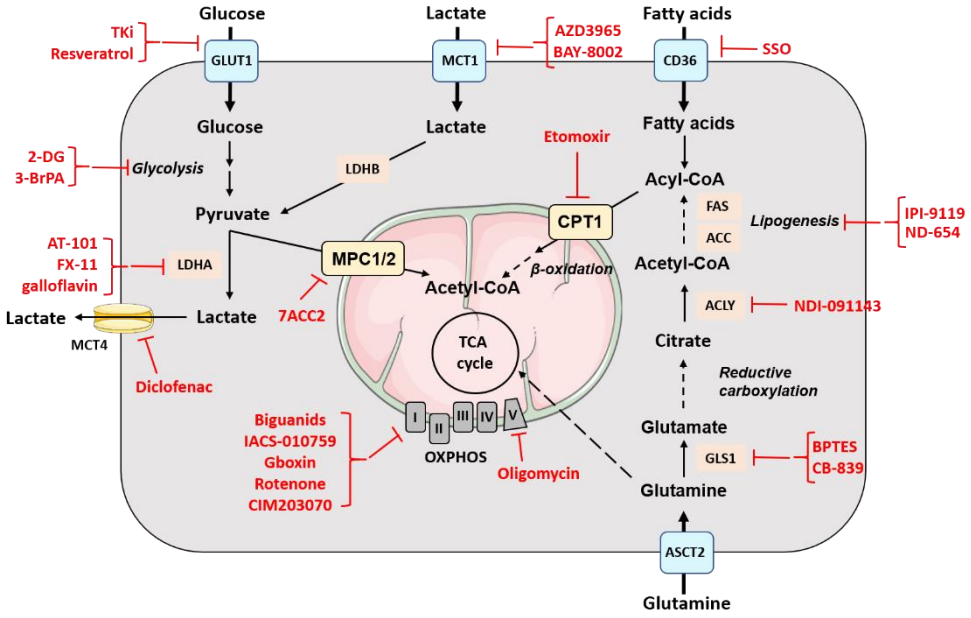

Figure 11: Therapeutic options to interfere with metabolic pathways.
This figure represents the principal metabolic pathways and their inter-connections supporting cancer phenotype. Metabolic inhibitors aiming to disrupt these networks and to affect tumor growth are depicted in red. Abbreviations: 2-DG, 2-deoxyglucose; 3-BrPA, 3-bromopyruvate; ACC, acetyl-CoA carboxylase; ACLY, ATP-citrate lyase; ASCT2, alanine-serine-cystein transporter 2; BPTES, bis-2-(5-phenylacetamido-1,2,4-thiadiazol-2-yl)ethyl sulfide; CoA, Coenzyme A; FAS, fatty

acid synthase; GLUT1, glucose transporter 1; GLS1, glutaminase 1; LDH, lactate dehydrogenase; MCT, monocarboxylate transporter; MPC, mitochondrial pyruvate carrier; OXPHOS, oxidative phosphorylation; SSO, sulfosuccinimidyl oleate; TCA, tricarboxylic acid; TKIs, tyrosine kinase inhibitors.

4.1 Metabolic plasticity as a driver of therapy resistance

Development of innovative tumor metabolism-targeting drugs is challenging due to the ability of cancer cells to shift their metabolic preferences to survive and/or keep growing. Interestingly, metabolic plasticity is also a driver of resistance to anticancer treatments, from conventional chemotherapy to recently developed targeted therapies (**Figure 12**).

4.1.1 Chemotherapy resistance

Cancer cells relying on aerobic glycolysis due to defective mitochondrial activity and hypoxia are described to be less sensitive to conventional chemotherapeutic agents [162]. In addition, lactate is today not only recognized as a waste but rather as an active metabolite causing anticancer therapy resistance by enhancing cellular DNA damage repair process [163]. In ovarian cancer cells, increased glycolysis and lactate production are associated with poor prognosis and cisplatin resistance [164]. Two anthracyclines, doxorubicin and epirubicin elicit distinct primary metabolic vulnerabilities in human breast cancer cells through differences in

Gene Set Enrichment Analysis. While doxorubicin-resistant cells rely on glutamine to drive OXPHOS and glutathione synthesis, epirubicin-resistant cells show increased bioenergetic capacity and mitochondrial ATP production [165]. These observations further revealed that for the same tumor subtype, metabolic adaptations may vary according to the therapeutic agent. Lipid metabolism was also associated with chemoresistance by investigators who documented that inhibiting SREBP1 and reducing lipogenic pathways could sensitize colorectal cancer cells to gemcitabine [166]. Lipid droplet accumulation is also thought to play an active role in inducing chemoresistance in breast cancer due to their capacity to sequester lipophilic drugs such as docetaxel [167].

Since chemotherapy is known to specifically target cells under high division rates, recent studies support the concept that cancer cells can become chemotherapy-resistant by promoting OXPHOS that leads to a reduced proliferation (vs. highly glycolytic tumors). This metabolic switch is observed in different types of cancer (*e.g.* ovarian cancer, KRAS-driven pancreatic cancer and colon cancer) where it is respectively driven by inflammatory mediators, by expansion of quiescent tumor cells surviving oncogene ablation and changes in mitochondrial biomass [168]. In TNBC, doxorubicin resistant clones exhibit a metabolic shift to a greater dependence on fatty acid storage in lipid droplets and mitochondrial OXPHOS [169]. Besides OXPHOS, mutations in mitochondrial DNA (mtDNA) have been associated with chemo-resistance in colorectal cancer patients [170] and a somatic mutation in ND4 complex I subunit correlates with resistance to chemotherapy in serous ovarian cancer [171]. Accordingly, low

mtDNA content has been correlated with a better outcome in breast cancer patients receiving anthracycline-based chemotherapy [172].

4.1.2 Endocrine-therapy resistance

Besides chemotherapy, metabolic reprogramming can also be inherent to endocrine-therapy resistance, the standard of care for hormone-positive breast cancers [168]. Indeed, HIF-1α hyper-activation via Akt/mTOR signaling pathway and hence increased aerobic glycolysis is closely associated with tamoxifen resistance in estrogen receptor-positive breast cancers [173]. Feng et al. recently observed that metabolic rewiring of breast cancer cells towards exogenous FA uptake *via* CD36 over *de novo* FA synthesis confers resistance to human epidermal growth factor receptor 2 (HER2) tyrosine-kinase inhibition [145]. Epithelial growth factor receptor (EGFR)/HER2 inhibition with lapatinib resistance is described to be supported by overexpression of LDHA and by phosphorylation changes in glycolysis-mediating enzymes (*e.g.* LDHA, enolase 1, phosphoglycerate mutase) [174]. The transcription of *MPC* gene is regulated by the androgen receptor and the mitochondrial pyruvate import has been shown indispensable to support the growth of hormone-responsive and castration-resistant prostate adenocarcinoma [175].

4.1.3 Targeted therapy resistance

The efficacy of targeted therapies can also be dampened by metabolic features of cancer cells. Targeting KRAS mutations, known to be drivers of pancreatic ductal adenocarcinomas has been proved challenging. Indeed, Viale et al. showed that a subpopulation of dormant cancer cells exhibiting cancer stem cell features and surviving oncogene ablation are responsible for tumor relapse and strongly relies on OXPHOS for survival [176]. Accordingly, surviving cells show high sensitivity to OXPHOS inhibitors.

An adaptive resistance mechanism to tyrosine-kinases inhibitors (TKIs) was recently observed in lung cancer patients based on a metabolic shift toward increased glycolysis and lactate production [177]. Similarly, increased glycolytic activity has been associated with resistance to the multi-TKI axitinib in PDAC cell lines [178] and HIF-1α-mediated HKII overexpression was shown to contribute to resistance to sorafenib, a multi-kinase inhibitor in hepatocellular carcinoma cells [179].

The occurrence of a lactate-shuttle between hypoxic and oxidative cancer cells leads to major resistance phenomenon to anti-angiogenic therapies in pancreatic neuroendocrine tumors [180], murine breast cancer models [181], patient-derived renal cell carcinoma (RCC) models and in clinical human RCC samples [182]. Indeed, after an initial regression, murine and human tumors, treated with antiangiogenics, resume growth in the absence of active neo-vascularization by exhibiting a compartmentalized expression of MCT1 and MCT4 whereby hypoxic cancer cells import glucose and export lactate, while normoxic cells import and catabolize lactate

(**Figure 12**). In TNBC, a similar metabolic symbiosis with lactate being used as a primary source of energy allows cancer cells to survive long-term glucose deprivation and confers resistance to PI3K/mTOR inhibitors [183]. Metabolic crosstalks between cancer cells, CAFs, adipocytes and immune cells have also beenshown to support therapy resistance. For instance, secreted lactate has the capacity to instruct CAFs to produce hepatocyte growth factor activating MET-dependent signaling in cancer cells [177].

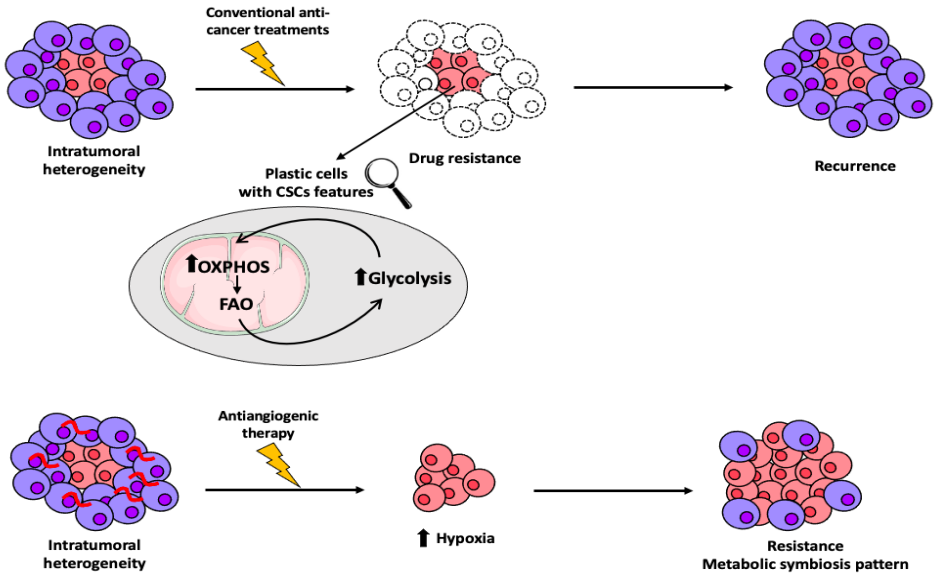

Figure 12: Metabolic plasticity as a driver of therapy resistance.

Conventional anti-cancer treatments mostly focusing on the inhibition of tumor growth result in the death of bulk tumor cells. A few population of plastic cells with cancer stem cell (CSC) features, including the ability of modifying their metabolic preferences according to specific needs, are able to survive and subsequently give rise to cancer recurrence. In contrast, antiangiogenic therapy primarily triggers hypoxia-dependent metabolic plasticity, involving topographic distribution of cancer cells presenting different metabolic phenotypes depending on oxygen and

nutrient concentrations within the tumor. Abbreviations: FAO, fatty acid oxidation; OXPHOS, oxidative phosphorylation. Adapted from [184] and [168].

4.2 The concept of collateral lethality to circumvent treatment resistance

The various interconnections between metabolic pathways together with cancer cell metabolic plasticity make very challenging the use of anti-metabolic treatments as anticancer therapy, although widely investigated in the last few years. The therapeutic blockade of a specific enzyme or the inhibition of nutrients uptake will frequently lead to metabolic rewiring of the cancer cell in order to sustain ATP production and proliferation. However, instead of representing a therapeutic failure, these new metabolic peculiarities may also become an Achille's heel for the cancer cell that can be specifically targeted in a second time to promote cell death. This emerging concept can be seen alongside with the collateral deletion of metabolic genes neighboring a major tumor suppressor locus, representing in our model a first hit with an anti-metabolic drug (**Figure 13**). The genomic deletion of tumor suppressor genes (TSG) is actually observed in almost every human cancer and a large number of genes playing diverse functions in cell homeostasis are co-deleted due to chromosomal proximity with the target TSG, although they have no apparent role in cancer progression (*i.e.* passenger deletion) [185]. These secondary deletions may correspond to genes encoding for metabolic enzymes. For instance, the homozygous deletion of the 1p36 locus targets various TSG but also *ENO1* (glycolysis), *NMNAT1* (NAD^+ synthesis) and *PGD* (pentose phosphate shunt). These

collateral deletions of passenger genes may thus lead to metabolic vulnerabilities that can be specifically tackled with an appropriate drug. This collateral lethality concept can be extended if considering that the first hit (instead of TSG deletion) can derive from stable alterations in metabolic preferences of cancer cells exposed to a given (first) drug. The vulnerability can then be targeted by a second drug that may induce lethality in cells unable to escape.

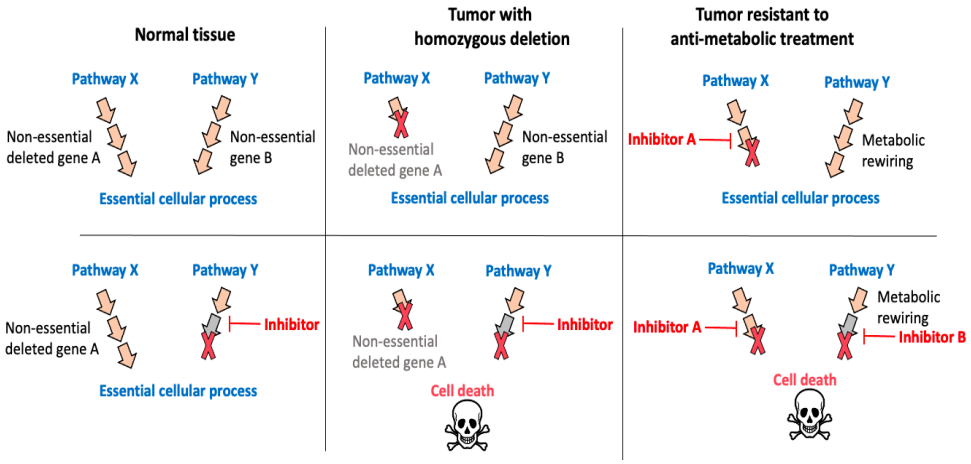

Figure 13: The concept of collateral lethality to circumvent anti-metabolic treatment resistance.

The fact that two (or greater) biochemical pathways can lead to the same essential cellular process drives therapy resistance establishment to inhibitors targeting a specific pathway. Passenger homozygous deletions can affect one of those pathways while leaving the other intact, thus having no detrimental effect on cancer cell viability but causing the remaining pathway to become essential. In line with this idea, targeting a specific metabolic pathway with an inhibitor can lead to new addictions in cancer cells after metabolic rewiring. Using selective inhibitors against the non-deleted essential pathway can lead to tumor specific cell death while leaving normal tissues unharmed. Adapted from [185].

5. Immuno-metabolism in cancer

If cancer cells can modulate their metabolic preferences and therefore adapt to specific nutrients availability and/or TME peculiarities, immune cells are not as plastic in their capacity to adapt to new mechanisms of immune escape continuously developed by progressing tumors [186]. Consequently, immune cells are often irreversibly affected and may fail to efficiently curb cancer progression. Moreover, immune cells rely on different metabolic pathways depending on their activation state, and those may be perturbed by the TME. Here below I will describe cancer-related immune system with a specific focus on CD8+ cytotoxic T cells including their reliance on distinct metabolic routes along the differentiation process, and discuss how metabolic regulation can affect the cancer-immunity cycle and thereby the efficacy of immunotherapy.

5.1 Immune contexture in human cancers

Histopathological analyses of human tumors have provided evidence that multiple infiltrating immune cells are found in different locations, within and around a tumor [187] (**Figure 14**).

While the conventional model describes the cross-presentation of tumor antigens to T cells by dendritic cells in the tumor-draining lymph nodes (or by tumor cells that have migrated there), the tumor mass is an attractive site of T cell priming. Tumor-infiltrating lymphocytes (TILs) are comprised primarily of cytotoxic (CD8+) and helper (CD4+) T cells, and a

smaller proportion of natural killer (NK) and B cells [188]. Named for their capability of killing cancer cells autonomously, NK cells represent the main effector cells toward cancer in innate immunity. B cells are mostly located in the invasive part of growing tumors but can also be found in tertiary lymphoid structures (TLS) adjacent to the tumor bulk [189]. TLS contain also memory T cells and mature dendritic cells (*i.e.* antigen-presenting cells) in close contact with naive T cells, supporting the possibility to develop an immune response independently of secondary lymphoid organs (such as lymph nodes and spleen).

Other immune cells localized in the tumor bed include macrophages, mast cells, granulocytes and myeloid-derived suppressor cells (MDSCs, *i.e.* heterogeneous population of cells inhibiting T cell activation). Initially macrophages were artificially divided into two subtypes (based on the cell polarization concept of helper T cell type 1 and 2). While M1 macrophages have an anti-tumor role, secrete pro-inflammatory cytokines (*i.e.* IL-1, IL-6 and tumor necrosis factor (TNF)) and express effector molecules such as iNOS, M2 macrophages exhibit anti-inflammatory functions, promote angiogenesis and favor tumor progression [190]. Today, the concept of continuum in the tumor macrophage phenotypes is established and the terms M1-like and M2-like macrophages are preferred.

More generally, the distribution of immune cells in the tumor bulk and in the associated stroma varies between tumor types and may considerably influence prognosis and treatment outcomes. For instance, in

colorectal cancer, high density of TILs at the invasive margin of liver metastases is associated with better chemotherapy efficacy [191].

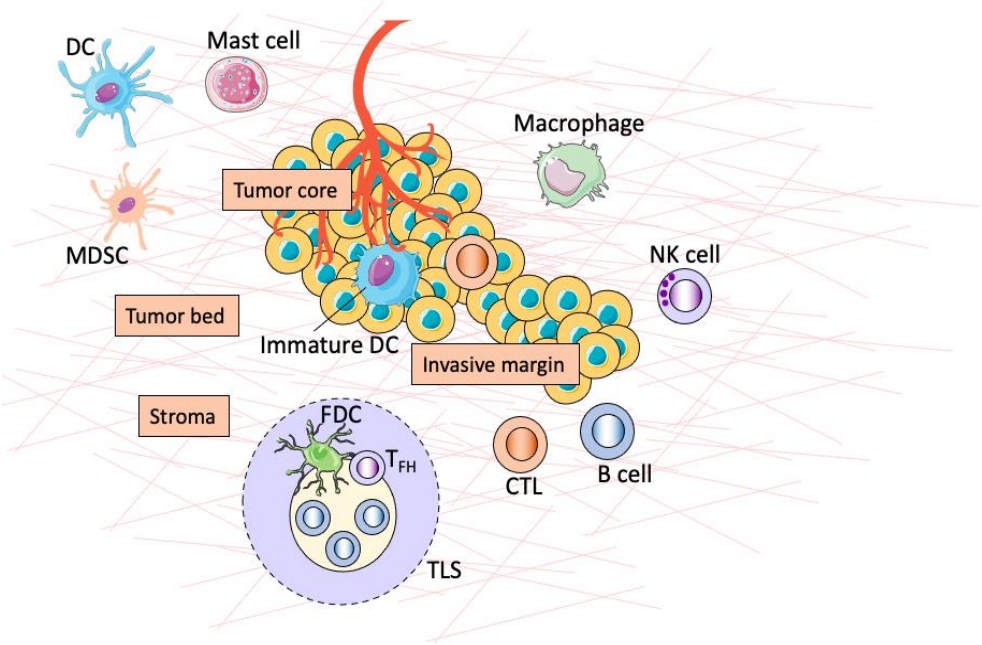

Figure 14: Immune contexture in cancer.
This figure depicts tumor anatomy, including the tumor core, the invasive margin, tertiary lymphoid structures (TLS) and the tumor microenvironment. Different immune cells are also represented according to their tumor distribution. Abbreviations: CTL, cytotoxic T lymphocyte; DC, dendritic cell; FDC, follicular dendritic cell; MDSC, myeloid-derived suppressor cell; NK, natural killer; T_{FH}, T follicular helper cell. Adapted from [187].

5.1.2 Focus on cytotoxic CD8+ T cells

CD8-expressing T cells, also known as cytotoxic T lymphocytes (CTLs), are the key players of anticancer immunity due to their essential role in killing cancer cells [192] and therefore form the backbone of successful

immunotherapies. To efficiently carry on their cytotoxic functions, CD8+ T cells first need to be properly primed and activated by antigen-presenting cells to become effector CTLs. When they are activated, effector CTLs proliferate and migrate to the tumor site where they will induce cancer cell death after antigen recognition and adherence mechanisms.

5.1.2.1 Activation process of naive T cells

Naive lymphocytes permanently circulate in the blood and in secondary lymphoid organs as long as they do not encounter their specific antigen. Hence, several billions of lymphocytes pass through lymph nodes every single day [193]. CD8+ T cells interact with major histocompatibility complex (MHC) I molecules on the surface of antigen-presenting cells (APCs) and target cells, which present foreign antigenic peptide fragments produced by proteasomal protein degradation [194] (**Figure 15**). When a CD8+ T cell engages an APC, it will attach to it and scan the surface by crawling over it. These direct contact and movements of the cells generate mechanical energy at the immunological synapse to drive biochemical signaling playing important role in the activation of the CD8+ T cell receptor (TCR) complex [195]. The TCR complex is composed of the antigen-binding subunit, non-covalently bound to three CD3 co-receptor signaling subunits that possess immunoreceptor tyrosine-based activation motifs (ITAMs), which are required for TCR surface expression, intracellular assembly and signal transduction [196] (**Figure 16**). CD8 domain stabilizes the tight contact between TCR and MHC-I by bringing the lymphocyte specific protein tyrosine

kinase (LCK) at the proximity of the complex, which can afterwards phosphorylate the CD3-associated ITAMs [197].

Following transduction of the TCR-activating signal, a co-stimulatory signal from the CD28 co-receptor must be received before the killing machinery is activated. This second signal is mediated by the interaction of CD28 receptors on CD8+ T cells with CD80/B7.1 or CD86/B7.2, both highly expressed on APCs, and enhances T cell proliferation and cytokine production (especially IL-2). Stimulation of CD28 receptor leads to the recruitment of phosphatidylinositol 3-kinase (PI3K) that will further promote T cell survival through activation of protein kinase B (PKB/Akt) and NF-κB [194]. If a naive lymphocyte recognizes its antigen without adequate co-stimulation, it will not only stay naive but any further re-activation becomes impossible, even in the presence of an adequate co-stimulus [198]. These lymphocytes are also characterized by reduced IL-2 production [199]. This particular state is referred as T cell anergy.

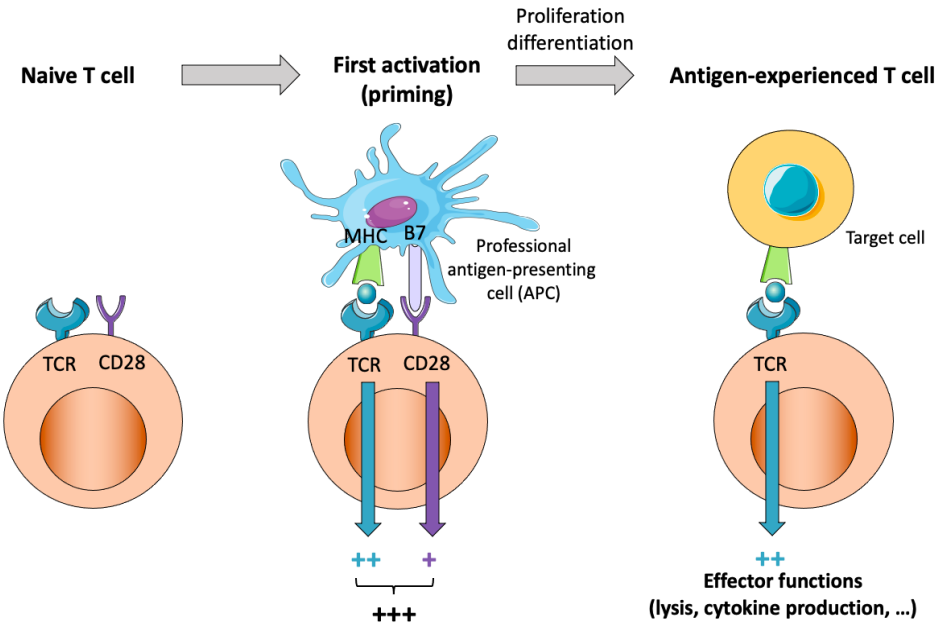

Figure 15: T cell activation.

Naive T cells become activated when they encounter a professional antigen-presenting cell (APC) such as a dendritic cell, displaying antigen fragments bound to its major histocompatibility complex (MHC) molecules. Activation results from the simultaneous engagement between the T cell receptor (TCR) and the complex MHC-peptide and between co-stimulatory molecules (CD28/B7). After priming, activated T cells proliferate, differentiate and acquire effector functions allowing them to recognize and kill a target cell presenting the same antibody on its surface.

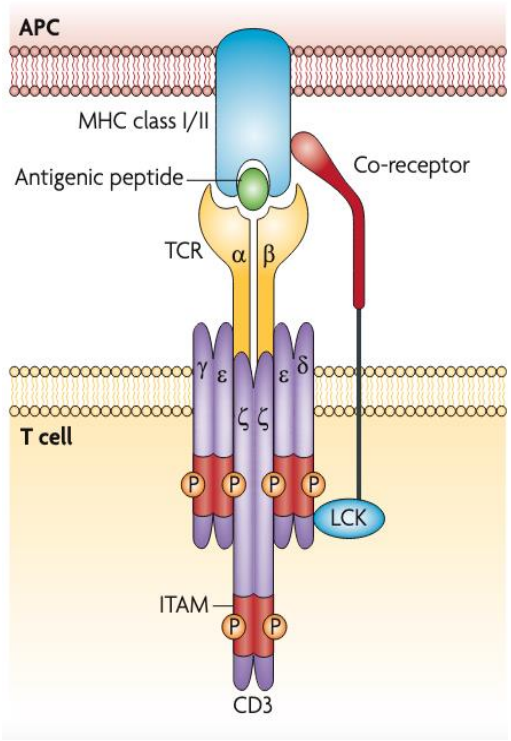

Figure 16: T cell receptor.

T cell receptor (TCR) is a heterodimer composed of one alpha chain and one beta chain. The interaction between the TCR and the major histocompatibility complex (MHC)-antigenic peptide complex of an antigen presenting cell (APC) is stabilized by CD8 domain which brings the lymphocyte-specific protein tyrosine kinase (LCK) to the proximity of the complex and further phosphorylates immunoreceptor tyrosine-based activations motifs (ITAMs) bound to CD3 co-receptors for signal transduction. Reproduced from [197].

5.1.2.2 Cancer cell lysis mechanism

The lysis of a target cell by a CTL requires a contact between the TCR and the MHC-I, strengthened by additional linking of adhesion molecules (*e.g.* T cell integrin LFA-1 with ICAM-1 on target cell) [200]. This phase is accompanied by a rapid and coordinate reorientation of the perinuclear Golgi apparatus and the microtubule-organizing center so that the two organelles face the bound target [201], as well as an accumulation of granules at the T cell pole in contact with the target cell. These granules contain several proteins, including perforin and granzyme (**Figure 17**). When secreted in the extracellular medium, perforin changes its conformation due to high concentrations of calcium and creates pores in the membrane of the target cell upon polymerization [202]. These pores allow serine-esterase granzymes to enter in the target cell cytoplasm and cleave Bid protein, resulting in mitochondrial cytochrome C release and activation of caspase-dependent apoptosis [203]. The killing of a target cell only takes a few minutes, and an individual CTL is capable of carrying out multiple killing by polarizing lytic granules toward different cells, without discrimination regarding antigenic potential [204]. In addition, Fas ligand is expressed on CD8+ T cells and its ligation by Fas receptors on target cells activates death domains, leading to activation of endonucleases and target-cell DNA fragmentation [205] (**Figure 17**).

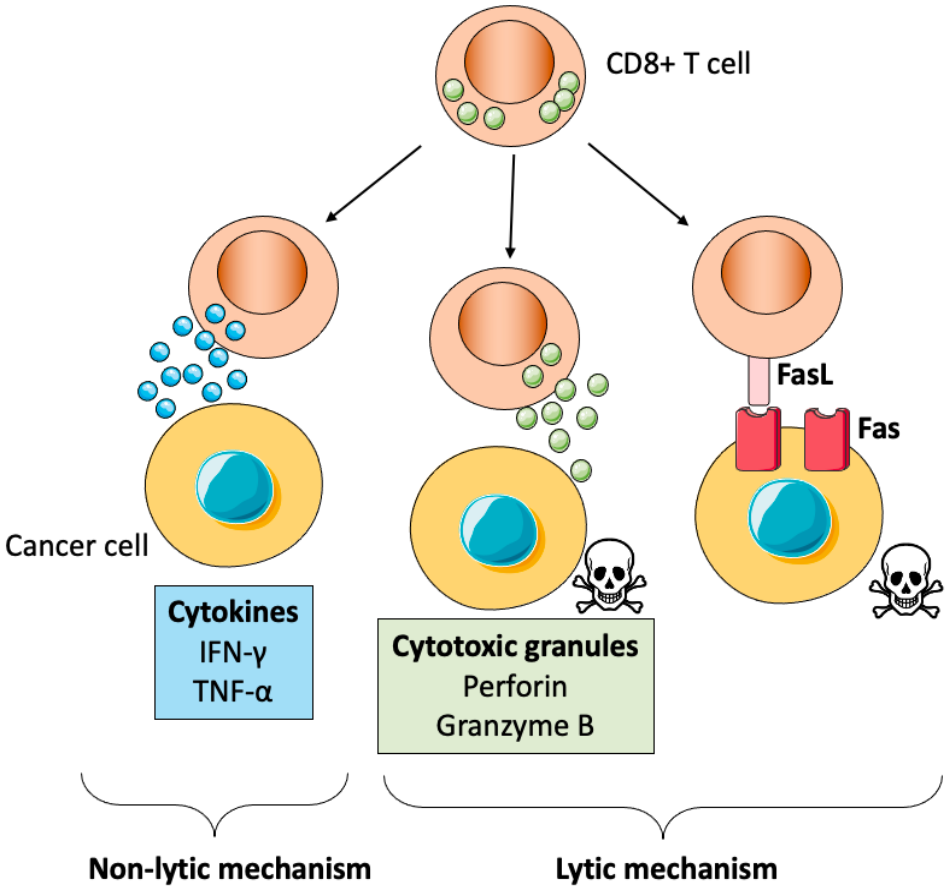

Figure 17: CD8+ T cell cytotoxicity mechanisms against cancer cells.
Activated CD8+ T cells have the ability to induce apoptosis of targeted malignant cells by secretion of cytotoxic enzymes and molecules. The secretion of granules containing perforin and granzymes leads to target cell death through cleavage of cellular protein involved in cell maintenance. CD8+ T cells can also induce apoptosis through Fas-Fas ligand (FasL) interactions leading to the activation of caspase proteases. In addition to apoptosis, CD8+ T cells can kill target cells indirectly through the release of cytokine factors. For instance, interferon (IFN)-γ inhibits viral replication and enhances the presentation of specific antigens. Abbreviations: TNF-α, tissue necrosis factor α. Adapted from [206].

5.1.2.3 Key cytokines for CD8+ cytotoxic T cells

Cytokines are proteins from 10 to 40 kDa, secreted by multiple cell types in response to injurious stimuli (*e.g.* recognition of an antigen by the TCR). The said stimulus induces the temporary transcription of short-life mRNA that do not exist in a pre-formed state in the cell [207]. Secreted cytokines act via specific high-affinity surface receptors located on the membrane of the producer cell (*i.e.* autocrine signaling), a neighbor cell (*i.e.* paracrine signaling) or a distant cell (*i.e.* endocrine signaling). They are involved in a variety of biological functions, including hematopoiesis, inflammation, cellular immunity and antibody production. Immune cells can be divided into different subsets, which all possess distinct cytokine profiles [208]. Typical cytotoxic CD8+ T cell (*i.e.* Tc1 subset) induction is mediated by IL-12 produced by antigen-presenting cells including macrophages and dendritic cells, upon exposure to maturation stimuli [209]. After naive T cell priming, IL-2 signals optimize both effector T cell generation and differentiation into memory T cells [210]. Interestingly, IL-2 elicits a unique pattern of signaling associated with strong activation of PI3K/Akt pathway under TCR-independent conditions, further inducing marked proliferation [211]. Functionally, cytotoxic CD8+ T cells are defined by their high levels of perforin, granzyme B, interferon-gamma (IFN-γ) and TNF-α (**Figure 17**). IFN-γ production has been reported to be dependent on T-bet transcription factor, downstream of IL-12/signal transducer and activator of transcription (STAT) 4 signaling [212]. Of note, some CD8+ subsets such as Tc9 and Tc17 secreting IL-9 and IL-17/22 respectively, exhibit poor cytotoxic functions and low IFN-γ expression and are thought to be implicated in the progression of

several diseases (*e.g.* atopic dermatitis lesions, asthma, multiple sclerosis and response to graft versus host disease) [208].

5.1.2.4 Immune-checkpoints

In order to maintain immune homeostasis and to dampen excessive immune responses, immune-checkpoint molecules are expressed at the surface of immune cells (**Figure 18**). Immune-checkpoints display high diversity in expression, structure and function [213]. The most prominent are programmed cell death receptor 1 (PD-1) and cytotoxic T lymphocyte-associated protein 4 (CTLA-4) expressed by T cells, NK cells and activated macrophages [194]. PD-1 signals are effective during the effector phase and mostly occur within peripheral tissues whereas CTLA-4 signals regulate the priming phase of naive T cells and primary occur in lymphatic tissues.

PD-1 receptor mediates T-cell inactivation upon binding to its ligands PD-L1 and PD-L2, both frequently expressed on the surface of cancer cells. These interactions actually antagonize CD28-CD80/86 co-stimulatory signals, even at very low PD-1 expression levels [214]. As a result, PD-1 leads to T cell anergy and abrogates cytokine production. Moreover, PD-1 was found to promote a switch from glycolysis to FAO (of endogenous lipids) in CD8+ T cell, by increasing the expression of CPT1A and promoting lipolysis as documented by elevation of the adipose triglyceride lipase [215].

CTLA-4 receptors are bound by the same ligands as CD28, but with a 20-time higher affinity, and thus outcompete CD28 for ligands. Schneider et al. showed that CTLA-4 increases T cell motility and overrides the TCR-

induced stop signal required for stable interaction between T cells and antigen-presenting cells, thus reducing the contact time between cells [216]. Other co-inhibitory receptors such as T cell immunoglobulin-3 (Tim-3), lymphocyte-activation gene 3 (LAG-3) and T cell immunoglobulin and ITIM domain (TIGIT) are also reported to regulate T cell functions, autoimmunity and antitumor responses [213].

In the context of chronic infections and cancer, an upregulation of co-inhibitory receptors is frequently documented to counterbalance the persistent antigenic stimulation, which can further lead to T cell dysfunction and/or exhaustion. Exhausted T cells lose robust effector functions (*i.e.* cytokine production and cytotoxic capacities), express multiple inhibitory receptors and are defined by an altered transcriptional program [217]. Of note, co-inhibitory receptors also contribute to enhance immune suppression by acting on regulatory T cells (Tregs) (*i.e.* a subpopulation of T cells that modulate the immune system by suppressing or downregulating the induction and proliferation of effector T cells) [218]. Taken together, enhanced expression of co-inhibitory receptors directly dampens the antitumor response by impairing effector T cell activity and enhancing suppression by Tregs present in the tumor tissue.

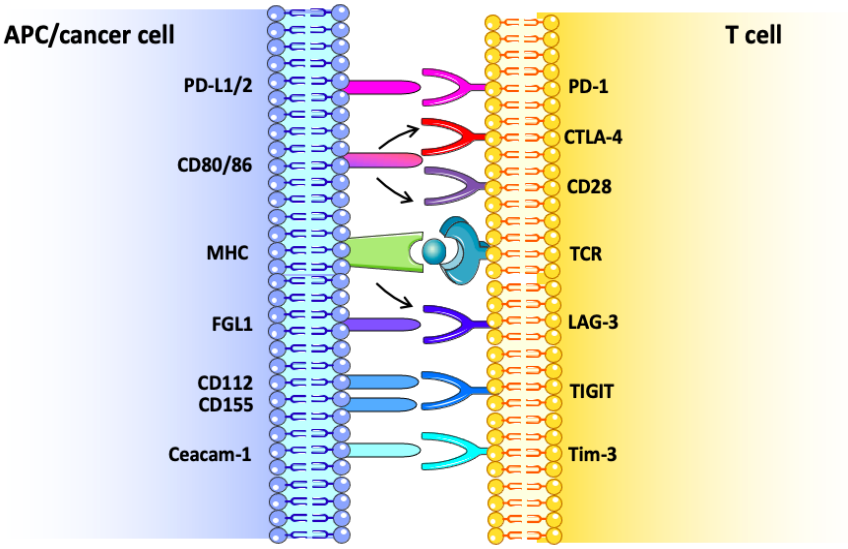

Figure 18: Immune checkpoint receptors and their respective ligands.
Immune checkpoint molecules are negative regulators of immune responses to avoid immune injury. Various immune checkpoint receptors expressed on T cells trigger a negative signal to T cell responses when bound to their corresponding ligands on the surface of antigen presenting cell (APC) or cancer cells. Abbreviations: Ceacam-1, carcinoembryonic antigen-related cell adhesion molecule-1; CTLA-4, cytotoxic T lymphocyte-associated protein 4; FGL1, fibrinogen-like protein 1; LAG-3, lymphocyte-activation gene 3; MHC, major histocompatibility complex; PD-1, programmed cell death protein 1; PD-L1/2, programmed death-ligand ½; TCR, T cell receptor; TIGIT, T cell immunoglobulin and ITIM domain; Tim-3, T cell immunoglobulin-3.

5.1.3 Metabolism drives the life cycle of T cells

Along their normal development, lymphocytes undergo a dramatic metabolic remodeling process, which is controlled by key receptor signaling events and growth factor cytokines, as well as availability of nutrients. Diverse metabolic pathways and metabolites were found to regulate

lymphocyte signaling and influence their differentiation, function and fate [219] (**Figure 19**). Nowadays, the significance of bioenergetic requirements for anticancer effector functions but also memory responses are increasingly elucidated and exploited to improve immunotherapies.

5.1.3.1 Naive T cell metabolism

Naive T cells exhibit extremely long lifetime and can remain alive for the entire duration of the host's life [220]. The survival of naive T cells requires metabolic quiescence, which are largely regulated by IL-7 in concert with tonic TCR signaling [221]. IL-7 in turn promotes glucose uptake via STAT5/Akt-dependent regulation of GLUT1 trafficking and glucose uptake [222] (**Figure 19**). Naive T cells exhibit low proliferation rates accompanied with low metabolic demands and are highly dependent on OXPHOS to generate ATP for survival and homeostasis maintenance.

5.1.3.2 Glycolysis in effector T cell function

After naive T cell adequate priming, effector T cells are reported to engage in Warburg metabolism and to break down glucose to pyruvate and lactate to efficiently proliferate and secrete cytokines, instead of relying on the highly energetically favorable OXPHOS pathway [223, 224] (**Figure 19**). Effector cells present mitochondrial fragmentation with poorly efficient electron transport chain but high capacity to buffer calcium and to produce ROS, which are both needed for the expression of nuclear factor of activated

T cells (NFAT), a transcription factor involved in T cell activation [225]. Interestingly, GAPDH and LDHA are critical to regulate cytokine production in CD4+ and CD8+ effector T cells, respectively, independently of their strict role in supporting the glycolytic pathway. While GAPDH directly binds to the mRNA of key cytokines to prevent their translation in the absence of glucose in CD4+ lymphocytes, LDHA maintains high concentrations of acetyl-CoA (by sparing citrate that is no more “burnt” in the TCA cycle and can be exported out of the mitochondria) to enhance histone acetylation and transcription of IFN-γ in CD8+ T cells [223, 226]. A role of ACLY, the enzyme that converts glucose-derived citrate into acetyl-CoA, was previously documented to make the link between induced increase in glucose metabolism and the regulation of gene expression through histone acetylation [227].

Besides glucose, breakdown of amino acids and particularly glutamine is critical for T cell proliferation through the generation of nucleotides, hexosamines and polyamines as well as oxidation in the TCA cycle [228]. In line with these findings, c-MYC, known to regulate different actors of glutamine metabolism including the transporter ASCT2 and glutaminase, is one of the most upregulated transcription factor upon T cell activation [229, 230]. Of note, glutamine is not required for cytokine production by T cells [231]. Other essential amino acids such as arginine, histidine, phenylalanine, tryptophan, valine and methionine are also required for T cell proliferation [232]. In addition, TCR activation triggers *de novo* lipid synthesis in both CD8+ and CD4+ lymphocytes in a mTOR-dependent manner [233].

5.1.3.3 Mitochondrial properties of memory T cells

Memory T cells are a small fraction of T cells that survive the initial antigen clearance and exhibit adaptations allowing self-renewal and long-term survival [234]. To rapidly enhance IFN-γ production after the second antigen exposure, memory T cells are reported to re-organize their mitochondria to tightly associate with the ER. Consecutive recruitment of HK-I to the voltage-dependent anion channel on mitochondria may then promote respiration to support metabolic reprogramming needed for memory CD8+ T cells to rapidly acquire effector function [235]. In contrast to mitochondrial fragmentation described in effector cells, memory T cells adapt their mitochondrial morphology to promote FAO and undergo mitochondrial fusion leading to less ROS production and enhanced OXPHOS metabolism [236, 237] (**Figure 19**). Moreover, memory T cells, but not effector T cells, possess substantial mitochondrial spare respiratory capacity (*i.e.* the ability to produce energy in response to increased stress or energy demand) [236]. Interestingly, AMP-dependent protein kinase (AMPK) activity is a critical regulator of the mitochondrial biogenesis transcription factor peroxisome proliferator-activated coactivator 1α (PGC1α) and has therefore a function in the development of memory T cells [238]. FAO has been documented to be a key pathway for the development of memory [239]. However, CD8+ memory T cells do not increase their uptake of extracellular FAs but instead rely on cell intrinsic lysosomal acid lipase activity to mediate the lipolysis of triacylglycerides (TAGs) to fuel FAO and thus engage in a futile cycle for uncleared reasons. It is speculated that this cycle may be required to maintain a balanced redox state, provide metabolic

intermediates, or maintain healthy mitochondria with sustained activity of the glycolytic and lipogenic machinery [230]. In addition, the expression of aquaporin-9 channel for glycerol uptake and TAG synthesis has been documented to be vital for the long-term survival of CD8+ memory T cells [240].

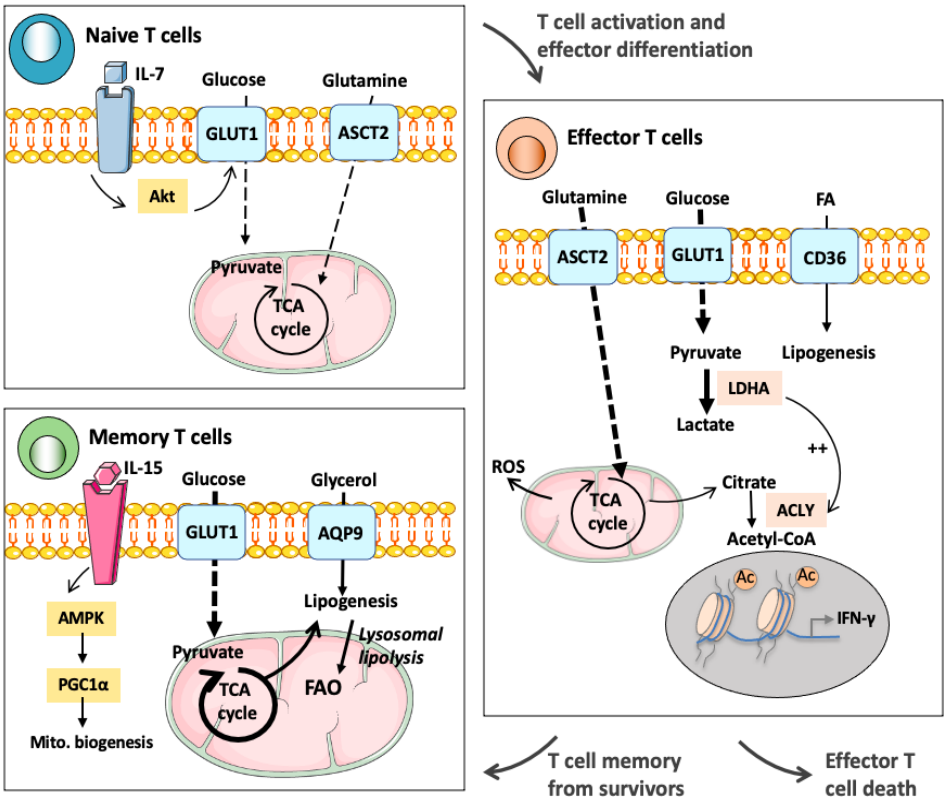

Figure 19: Metabolism drives the life cycle of T cells.

This figure represents different metabolic programs used by naive, effector and memory T cells. Naive T cells rely on the translocation of glucose transporter 1 (GLUT1) through Akt signaling to survive. In the absence of T cell receptor stimulation, resting naive T cells mostly oxidize glucose and glutamine through OXPHOS. Upon T cell stimulation, T cells undergo protein and transcriptional changes resulting in the sustained activity of glycolysis that mediates histone

acetylation to transcription of cytokines. In addition to glucose, effector T cells use amino acids and particularly glutamine to efficiently proliferate. After antigen clearance, most of effector T cells will die but a small population forms memory T cells. Compared to effector T cells, memory T cells possess a metabolic profile dependent on mitochondrial biogenesis. They strongly rely on fatty acid oxidation (FAO), furnished by lysosomal lipolysis of triacylglycerides. Abbreviations: Ac, acetyl groupment; ACLY, ATP-citrate lyase; AQP9, aquaporin 9; AMPK, adenosine monophosphate-activated protein kinase; ASCT2, alanine-serine-cystein transporter 2; IFN, interferon; IL, interleukin; LDHA, lactate dehydrogenase A; PGC1α, peroxisome proliferator-activated receptor gamma coactivator 1 alpha; ROS, reactive oxygen species; TCA, tricarboxylic acid. Adapted from [220].

5.2 Metabolic regulation of the cancer-immunity cycle

The cancer-immunity cycle (CIC) comprises a series of events that are required for immune-mediated control of tumor growth [228] (**Figure 20**). It is today well accepted that tumors develop numerous mechanisms to interrupt one or more steps of this CIC in order to escape immunosurveillance [8]. Immunotherapies aim to restore anti-tumor immunity by reactivating the CIC and although may tumors still fail to respond, recent developments with immune checkpoint inhibitors (ICIs) have renewed the interest for these strategies. Interestingly, recent studies have documented that metabolic reprogramming of tumor-associated immune cells are key contributors to immune evasion and may thus offers a new field of investigation to identify new therapeutic targets.

5.2.1 The cancer-immunity cycle

The first step of CIC relates to the presence of neoantigens resulting from oncogenesis and their capture by dendritic cells for processing [241]. Two major classes of tumor antigens targeted by T cells have been reported: the tumor-specific antigens found on cancer cells only and not on healthy cells (*e.g.* oncoviral antigens or novel peptide sequence arising from oncogenic driver mutations), and the tumor-associated antigens which exhibit elevated levels in tumor cells due to genetic amplification or post-translational modifications but are also expressed in lower amounts by healthy cells [242]. This first step has to be accompanied by immunogenic signals including pro-inflammatory cytokines (*e.g.* TNF-α, IL-1, IFN-α) and factors released by dying tumor cells (*e.g.* CDN, ATP, HMGB1) to yield an efficient anticancer T cell response. Next, dendritic cells present the captured antigens on MHC-I and MHC-II molecules to T cells, resulting in the priming and the activation of effector T cell responses against the antigen. Activated effector T cells traffic to finally reach and infiltrate the tumor site, were they specifically bind to cancer cells through the interaction between the TCR and the cognate antigen bound to MHC-I, and lead to cancer cell apoptosis. The killing of cancer cells will further lead to the release of additional cancer antigens and immunostimulatory molecules, reinforcing the immune response and initiating subsequent revolutions of the cycle [241]. Of note, CD4+ T cells mediate anti-tumor immunity by driving specific anti-immune response and providing help for CD8+ T cells via secretion of effector cytokines such as IFN-γ and TNF-α. By contrast, Tregs, characterized

by the expression of the master transcription factor forkhead box protein p3 can inhibit the activation and differentiation of CD4+ helper T cells and CD8+ cytotoxic T cells.

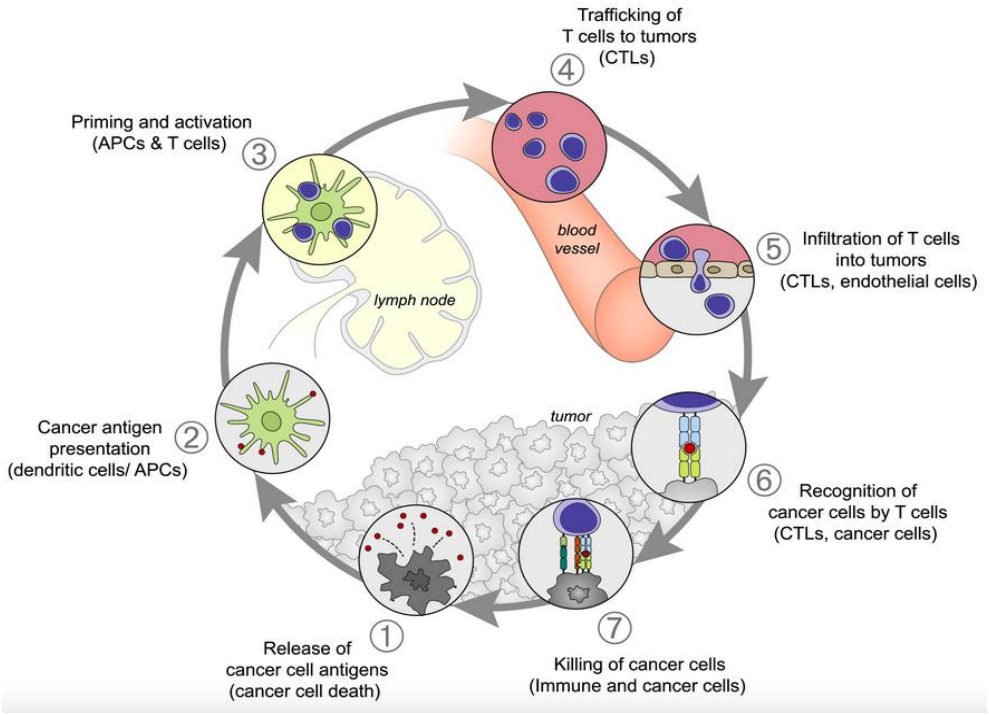

Figure 20: The cancer-immunity cycle.

The generation of immunity to cancer is a cyclic process that can be divided in seven major steps, starting from the release of antigens from the cancer cell and ending with the killing of cancer cells by cytotoxic T lymphocytes (CTLs). This cycle leads to an accumulation of immune-stimulatory factors amplifying and broading T cell reponses. Abbreviations: APC, antigen presenting cell. Reproduced from [241].

5.2.1.1 Goal of cancer immunotherapy

Tumors employ multiple strategies to attenuate the effectiveness of T cell-mediated attack by interfering with almost every step of the CIC, from deregulation of antigen-presenting cells to the establishment of a physical barrier at the vasculature preventing the infiltration of effector T cells and through the recruitment of immunosuppressive cells like MDSCs and Tregs [243]. Immunotherapies aim to initiate or reinitiate a self-sustaining CIC and must therefore be carefully configured to prevent negative feedback mechanisms (*i.e.* inhibitory factors keeping the CIC in check and reducing immune activity and/or prevent autoimmunity, such as immune checkpoints molecules).

Regarding cancer antigen presentation, many efforts have involved the use of therapeutic vaccines to boost the immune system's ability to find and destroy antigen-bearing cancer cells, or to induce an immunogenic cancer cell death [244, 245]. Today, the use of cancer vaccines remains challenging because of uncertainties concerning the identities of antigens to use, their mode of delivery, the types of adjuvants required and the negative signals repressing the anticancer immune response [244].

The identification of immune-checkpoints molecules such as CTLA-4 and PD-1 has led to the development of antibodies to reverse the T cell exhaustion phenotype. ICIs represent one of the most promising approach to activate therapeutic antitumor immunity. CTLA-4 was the first immune-checkpoint receptor to be clinically targeted to potentiate effector T cell priming. The humanized antibody ipilimumab demonstrated a survival

benefit for patients with metastatic melanoma and was approved by the US Food and Drug Administration in 2010 [246]. The interaction between PD-1 on mature lymphocytes and PD-L1/2 on cancer cells has also emerged as a relevant target and several clinical trials have documented that blocking antibodies (*e.g.* nivolumab and pembrolizumab) can exert dramatic antitumor effects mostly in melanoma and NSCLC but also in renal, ovarian, head and neck, bladder, gastric, colon, esophageal, hepatocellular and breast cancers, as well as in Hodgkin's lymphoma [247]. Of note, PD-1 blockade was shown to also enhance NK cell activity and antibody production through direct effects on PD-1^{+}B cells [248].

Finally, the flourishing research field of cell-based therapy also proposes approaches to help the patient's immune system to fight cancer through the transfer of T cells and/or the modification of patient's own immune cells. Adoptive cell transfer mainly refer to tumor-infiltrating lymphocytes and chimeric antigen receptor (CAR) T cell. Recently, anti-CD19 CAR therapy was shown to efficiently treat relapsed/refractory hematologic cancer [249]. Several other surface tumor antigens such as CD20, CD22 and CD30 are currently under scrutiny by pharmaceutical companies to develop new generations of CAR T cells [250-252]. The discovery that all tumors may have potential antigens to attack that can be revealed by tumor genomic sequencing offers a variety of exciting approaches to apply adoptive cell therapy to the majority of cancer types [253], although several challenges such as prioritization of antigen targets, optimization of tumor-specific TCR and costs still need to be faced [254].

5.2.2 T cells versus the tumor microenvironment

Besides deficient antigen recognition, development of resistance and opposing effects of immunosuppressive cells, tumor metabolism rewiring may alter T cell requirements to sustain anticancer activity (**Figure 21**). Indeed, since cancer and T cells share common metabolic programs to survive, and the TME imposes specific gradients (*e.g.*, hypoxia, acidosis, …) that impact on any tumor-associated cells, there is a continuous battle for nutrients (the so-called « tug of war ») [255, 256]. Using a mouse sarcoma model, Chang et al. reported that glucose consumption by tumors metabolically restricts T cells, leading to dampened glycolytic capacity and IFN-γ production, thereby mediating T cell hyporesponsiveness [256]. Similarly, RCC exhibiting accelerated glucose metabolism are associated with a poor infiltration of CD8+ effector T cells [257].

High amounts of lactate and protons secreted by glycolytic cancer cells both support evasion of immune surveillance. Acidic pHe conditions have been reported to decrease T cell proliferation and their capacity to produce a variety of cytokines, including IL-2, IFN-γ, granzyme B and perforin, in a dose-dependent manner [258]. Tumor acidosis also impairs immune system functions by reducing dendritic cell maturation [259], monocyte-derived TNF secretion [260], and NK cell activity [261]. Indeed, tumor-derived H^+ and/or lactate accumulation in the extracellular compartment alter(s) T cell function by inhibiting the glycolytic route [258, 260]. In particular, inhibition of the transcription factor NFAT has been proposed to block IFN-γ production in T cells and NK cells upon intracellular

accumulation of H^+ and lactate [262]. The same authors also proposed a direct role of LDHA for lactate generation and the subsequent inhibition of tumor surveillance by T and NK cells. Furthermore, lactate was also shown to serve as a substrate to promote immunosuppressive population of Tregs [263]. Interestingly, neutralization of tumor acidity with sodium bicarbonate [264], or with proton pump inhibitors [265] can improve the response to antitumor immunotherapy by restoring T cell cytolytic activity and cytokine secretion together with an increased tumor lymphocyte infiltration in mouse models but also in human cancer patients.

This paragraph is derived from "Catherine Vander Linden and Cyril Corbet, Frontiers in Oncology, doi: 10.3389/fonc.2019.00159 ».

5.2.3 Immunosuppressive compounds

Besides the nutrient tug of war between cancer cells and T cells, tumor metabolism adaptation to nutritional stress may also indirectly influence T cell bioenergetics [220]. For example, the accumulation of potassium (K^+) in the tumor interstitial fluids suppresses transporters for amino acids and glucose in T cells, leading to impaired cytokine production (**Figure 21**). Tissue hypoxia reported to establish an immunosuppressive environment *in vivo* by increasing the level of extracellular adenosine, which elicits its deleterious effects on T cells by signaling through A2AR receptor [266] but also recruits Tregs and promotes their immunoregulatory activity [267]. Tumor metabolic byproducts such as cholesterol can induce ER stress in CD8+ T cell, promoting immune-checkpoints transcription by the

cholesterol-induced ER-stress sensor XBP1 and thereby leading to T cell exhaustion [268].

Besides cancer cells, some immune cells can also divert a variety of nutrients from T cells. For instance, the upregulation of arginase-1 in M2 macrophages depletes the arginine pool for NO and protein synthesis in T cells, impairing TCR function and T cell differentiation [269, 270]. Furthermore, indoleamine 2,3 dioxygenase (IDO1) strongly expressed in M2 macrophages catalyzes the conversion of the essential amino acid tryptophan (Trp) into kynurenines, thereby limiting tryptophan availability for T cells.

Interestingly, other Trp catabolic enzymes including tryptophan 2,3-dioxygenase (TDO2) and more recently interleukin-4-induced protein 1 (IL4I1) represent key actors in cancer immunosuppression [228]. IDO1/TDO2-mediated depletion of tryptophan and IL4I1-mediated depletion of all aromatic amino acids inhibit proliferation of CD8+ T cells while promoting Tregs activity in a GCN2 kinase-dependent way [271]. IL4I1-derived H_2O_2 also inhibits CD4+ and CD8+ T cell proliferation and effector function through decreased TCR signaling [272]. Interestingly, IFN-γ was shown to induce the expression of IDO1 gene in human cells via the IFN-γ receptor JAK/STAT1 signaling pathway [273]. For all these reasons, tryptophan catabolism appears to constitute a powerful immunosuppressive mechanism in the TME.

5.2.4 Metabolic regulation of immune checkpoints

PD-L1 expression is known to be activated by nearly every oncogenic signaling pathways promoting tumor cell growth and proliferation (*e.g.* EGFR, KRAS, MAPK, MYC and Hippo pathways) [228]. However, increasing evidence suggests that PD-L1 expression is also activated by metabolic consequences of this oncogenic growth (**Figure 21**). For instance, high metabolic activity triggers ROS production, which can activate NRF2 and HIF-α pathways in mouse and human cells [274]. Both NRF2 and HIF-α are able to promote PD-L1 expression through direct transcriptional mechanisms [275, 276]. Recently, aryl hydrocarbon receptor activation by IDO1/TDO2/IL4I2-derived catabolites was also reported to suppress anti-tumor immunity through the upregulation of PD-L1 expression in CD8+ T cells [277].

Immune-checkpoint receptors can also impair T cell responses by perturbing their metabolism (**Figure 21**). PD-1 is reported to disturb effector function by increasing the FAO enzyme CPT1A and consequently downregulating glycolysis activity [215]. At the opposite, PD-L1 expression on tumor cells enhances glucose uptake and leads to higher glucose deprivation for T cells [256]. CTLA-4 activation on T cells suppresses their function and nutrient acquisition, in particular glutamine and glucose [215].

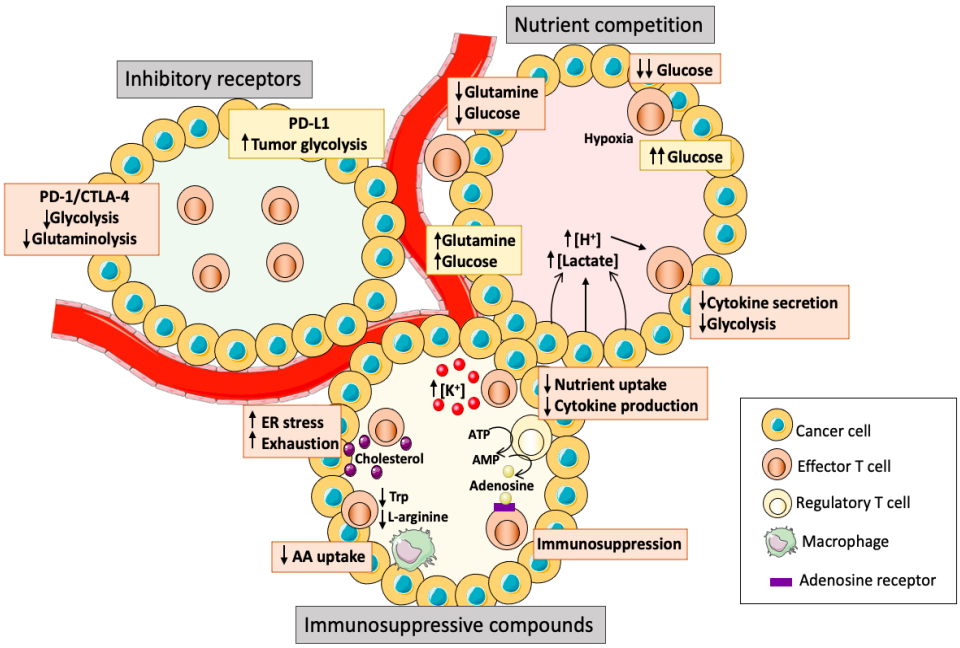

Figure 21: Metabolism-related mechanisms suppressing tumor immunity. *Metabolic activity of tumor cells compete and scavenge T cells for glucose and amino acids, leading to the suppression of T cell bioenergetics and cytokine secretion. Moreover, some tumor metabolites, metabolic enzymes and tumor microenvironment peculiarities can also have immunosuppressive properties. Finally, the expression of immune checkpoint receptors molecules such as PD-1/PD-L1 and CTLA-4 leads to negative metabolic function in T cells. Abbreviations: AA, amino acid; AMP, adenosine monophosphate; ATP, adenosine triphosphate; CTLA-4, cytotoxic T lymphocyte-associated protein 4; ER, endoplasmic reticulum; PD-1, programmed cell death protein 1; PD-L1, programmed death-ligand 1. Adapted from [220].*

Scope and Aims

---

1. Rationale and general aim

The deregulation of energetics and in particular the metabolic plasticity of cancer cells offer them the ability to adapt their substrate dependencies under harsh TME conditions and make very challenging the use of metabolism-interfering drugs as monotherapy. Although tumor metabolism is becoming a major source of inspiration to develop new anticancer drugs, the current number of breakthrough discoveries under clinical evaluation is so far limited and numerous examples where tumors adapt their metabolic preferences to counteract a specific pathway inhibition have been reported. Direct consequences of metabolic adaptation are the progressive loss of drug activity and *in fine* the development of resistance. To take advantage of this adaptation and even to force it in order to create a vulnerability was at the origin of the first part of my thesis work.

Besides metabolism-targeting treatments, the increasing interest for immunotherapy in the last decade and the evidence that metabolism drives the life cycle of a T cell led us to dedicate the second part of my thesis project to the immuno-oncology field. Despite remarkable outcomes obtained with immunotherapy (in particular to eliminate tumors non-responding to conventional chemo- and/or radiotherapy), many metabolic alterations occurring in tumors may actually represent an immunosuppressive

microenvironment. Moreover, the use of metabolism-targeting drugs as anticancer treatments will not only affect cancer cells, but also healthy cells from the TME including immune cells and thereby might abrogate efforts to develop new metabolism-targeting drugs.

Altogether, the main questions we aimed to address in this thesis are the following: how to optimize the use of metabolism-targeting treatments to kill plastic cancer cells and how to simultaneously stimulate (or not to anihilate) anticancer immune response.

2. Specific aims

The first part of my thesis project aims to identify and validate an optimal combination of metabolism-targeting drugs, in order to prevent a possible escape for cancer cells. The rationale behind our work is, with a first drug, to force cancer cells to become addicted to specific bioenergetic fuels/pathways in order to exploit such drug-induced metabolic rewiring in cancer cells and render a second drug lethal (*i.e.* collateral lethality). For the proof of principle, we used the glycolysis-inhibitor 3-bromopyruvate (3-BrPA) as a first drug and the emergence of new metabolic addictions of the 3-BrPA-resistant (3-BrPA-R) was closely investigated in the quest to identify an adequate second metabolism-targeting treatment (see Results, chapter 1).

The second part of my thesis aims to bring new insights on the capacity of metabolism-targeting treatments to enhance cytolytic activity of CD8+ T cells, and thereby to improve immunotherapy efficacy. More

precisely, the effects of three compounds blocking the activity of ETC complex I, MCT and CPT1 transporters will be used to assess the effects of inhibiting mitochondrial OXPHOS, glycolysis and fatty acid oxidation, respectively, on T cell phenotype. Treatments will be used either to directly affect T cell metabolism or to pre-challenge cancer cells in order to find the best treatment combination (see Results, chapter 2).

Table 2: Chemical structures, affinity values and working concentrations of key compounds used in this thesis.

This table summarizes the chemical structures, the affinity values (half-maximal inhibitory concentration (IC_{50}) or inhibitory constant (K_i)) and working concentrations used in the Results chapter.

	Structure	Affinity values	Working concentrations
3-bromopyruvate	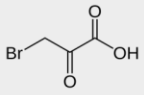	K_i GAPDH ~25 µM K_i hexokinase 2.4 mM	25 µM or 50 µM
Diclofenac	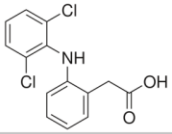	IC_{50} MCT1/4 1.45-0.14 µM* IC_{50} MCT1/4 0.1-0.2 mM** IC_{50} COX2 42.2 µM	0.1-0.2 mM in cancer cells 0.1 mM in CD8+ T cells
CIM203070	Unknown	IC_{50} 97.57 nM	100 nM in CD8+ T cells
Etomoxir	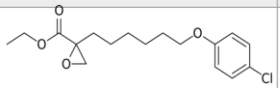	K_i CPT1 8 µM	3 µM in CD8+ T cells

References for 3-bromopyruvate K_i GAPDH value: [278], determined in cultured cancer cells; K_i hexokinase value: [279], determined in isolated liver implanted tumors;

*Reference for diclofenac MCT1/4 IC_{50} values: [142], *determined in Xenopus laevis oocytes transduced to express either MCT1 or MCT4; of note, aspirin 1 mM has no impact on lactate transport in the same oocyte models; **determined in cultured cancer cells; IC_{50} COX2 value: [280], determined in cultured cancer cells stably transfected to overexpress COX2;*

CIM203070 IC_{50} value determined in our laboratory in cancer cells cultured in galactose-containing medium;

Reference for etomoxir K_i CPT1 value: [281], determined in isolated rat myocytes.

Results

1. Therapy-induced DNA methylation inactivates MCT1 and renders tumor cells vulnerable to MCT4 inhibition

Catherine Vander Linden[1,3], Cyril Corbet[1,3,*], Estelle Bastien[1], Ruben Martherus[1], Céline Guilbaud[1], Laurenne Petit[1], Loris Wauthier[1], Axelle Loriot[2], Charles De Smet[2], Olivier Feron[1,4,*]

Cell Reports 2021 June 21;35(9):109202.

[1]Pole of Pharmacology and Therapeutics (FATH), Institut de Recherche Expérimentale et Clinique (IREC), UCLouvain, 57 Avenue Hippocrate B1.57.04, 1200 Brussels, Belgium.
[2] Group of Genetics and Epigenetics, de Duve Institute, UCLouvain, 75 Avenue Hippocrate B1.75.04, 1200 Brussels, Belgium.
[3] These authors contributed equally
[4] Lead contact
[*] Correspondance cyril.corbet@uclouvain.be, olivier.feron@uclouvain.be

Keywords: tumor metabolism, 3-bromopyruvate, monocarboxylate transporter, metabolic plasticity, drug repurposing, diclofenac, methylation, epigenetic.

This study was published in Cell Reports in June 2021. I share the first authorship with the Pr. Cyril Corbet and I will mention my personal contribution to this work at the end of each figure legend in the Results section.

1.1 Summary

Metabolic plasticity in cancer cells makes very challenging the use of metabolism-targeting agents. Drug-induced metabolic rewiring may however uncover vulnerabilities that can be exploited. We report that resistance to glycolysis inhibitor 3-bromopyruvate (3-BrPA) arises from DNA methylation in treated cancer cells and consecutive silencing of monocarboxylate transporter MCT1. We observe that unexpectedly 3-BrPA-resistant cancer cells mostly rely on glycolysis to sustain their growth, with MCT4 as an essential player to support lactate flux. This shift makes cancer cells particularly suited to adapt to hypoxic conditions and resist to OXPHOS inhibitors and anti-proliferative chemotherapy. By contrast, blockade of MCT4 activity in 3-BrPA-exposed cancer cells, either by diclofenac or genetic knock-out, leads to inhibition of the growth of derived spheroids and tumors in mice. This study supports a new mode of collateral lethality according to which metabolic adaptation of tumor cells to a first-line therapy makes them more responsive to a second-line treatment.

1.2 Introduction

Although tumor metabolism has become a major source of inspiration to develop new anticancer drugs, the current number of breakthrough discoveries under clinical evaluation is so far limited [282]. One explanation besides the usual pharmacokinetic and pharmacodynamic issues that stop drug candidates during their development is the metabolic

plasticity of tumor cells. In particular, when a metabolic pathway is pharmacologically inhibited, accumulation of metabolites upstream the enzymatic blockade or a deficit in intermediates down the route may foster cancer cells to shift their metabolic preferences to survive and/or keep growing. Limiting the options of metabolic adaptations in response to a pharmacological intervention is thus increasingly considered to identify the most efficient metabolism-based anticancer modalities. The concept of metabolic synthetic lethality emphasizes how some oncogenic mutations by reprogramming cancer cell metabolism [283-285] may actually offer opportunities to develop selective therapies that would target cancer cells without affecting healthy tissues [286]. Besides oncogene-driven metabolic rewiring, tumor microenvironment peculiarities also shape cancer cell metabolic phenotypes [31]. Metabolic preferences driven by the local tumor milieu may actually support *de novo* drug resistance or contribute to the progressive loss of activity of a given drug when its own effects have induced alterations in the tumor microenvironment. This may however also represent an Achilles heel for cancer cells that are or become dependent on external conditions that prevent them to get access to some nutrients or to transform them into biosynthetic intermediates and ATP [287].

It has been proposed that application of evolutionary (Darwinian) principles to cancer therapy may help circumvent the resistance to anticancer drugs in human cancer patients [288]. Indeed, evolution-based approaches termed “double bind” [289] or “sucker’s gambit” [290] aim to apply combination therapies, in which the phenotypic adaptation of cancer cells to a first-line treatment makes them more susceptible (than the original

population) to a second-line therapy. For instance, in lung cancer patients who received a p53 vaccine and standard chemotherapy, it was shown that the sequence of treatments substantially impacted on the overall treatment efficacy [291, 292]. Here, we reasoned that a similar strategy could be applied to metabolism-targeting drugs with one of the two drugs used as an inducer of metabolic addiction to a given pathway, instead of contributing to major direct anticancer effects. For this approach to be realistic, it should involve a drug that profoundly and stably reprograms cancer cell metabolism, and if possible, after a transient exposure, to allow the second agent to rapidly be used to express its full therapeutic potency. We postulated that 3-bromopyruvate (3-BrPA) could fulfil this role of the pre-challenging drug since the alkylating potential of this small compound may rapidly induce lasting changes in a variety of targets including glycolytic enzymes. We actually found that long-lasting metabolic rewiring induced by 3-BrPA exposure was instead associated with an epigenetic mechanism consisting of hypermethylation of *SLC16A1* (MCT1) gene promoter and a consecutive dramatic MCT1 downregulation in various cancer cells. We further documented that the lack of MCT1 led to a deficit for cancer cells to use lactate as an energy fuel and to a strict dependence on MCT4 to support lactate release. We also took advantage of the epigenetic inactivation of MCT1 to document how a brief pre-challenge with 3-BrPA may stimulate the antitumor effects of MCT4 inhibition both *in vitro* and *in vivo*.

1.3 Results

1.3.1 Resistance to 3-BrPA in cancer cells is associated with MCT1 downregulation

To study the metabolic adaptation of cancer cells to a treatment with a metabolism-interfering drug, three different human cancer cell lines derived from cervix, bladder and colorectal carcinoma (SiHa, UM-UC-3 and HCT-116 respectively) were exposed for several weeks to increasing concentrations (from 10 to 100 µM, *i.e.* range of concentrations demonstrating cytotoxic effects on the three cell lines) of 3-bromopyruvate (3-BrPA) (**Figures 22A-B and S1A-E**). Surprisingly, we found that each cancer cell line developed a complete resistance to 3-BrPA even in the presence of high concentrations of the drug. This led us to hypothesize that the acquired resistance to 3-BrPA could be due to a blockade of drug import. In a previous study, a genome-wide haploid genetic screen actually identified the monocarboxylate transporter 1 (MCT1 or *SLC16A1* gene product) as the main 3-BrPA entry path into tumor cells [115]. We actually observed a dramatic decrease in both mRNA (**Figure 22C**) and protein expression for MCT1 (**Figures 22D and S1F-G**) in 3-BrPA-resistant (3-BrPA-R) cancer cells.

We then wondered whether MCT1 downregulation was an early or late event occurring upon 3-BrPA exposure. Thus, we evaluated MCT1 expression at the mRNA (**Figure 22E**) and protein (**Figure 22F**) levels in native UM-UC-3 treated with 25 µM 3-BrPA (close to the IC_{50} value) for different periods of time, from 16 to 96 hours. A decrease in MCT1 transcripts of

about 40% was observed after 24h treatment, reaching 80% when 3-BrPA was present for 96h (**Figure 22E**). Moreover, a net decrease in MCT1 protein expression was observed after 72h of treatment, followed by a complete extinction after 96h (**Figure 22F**).

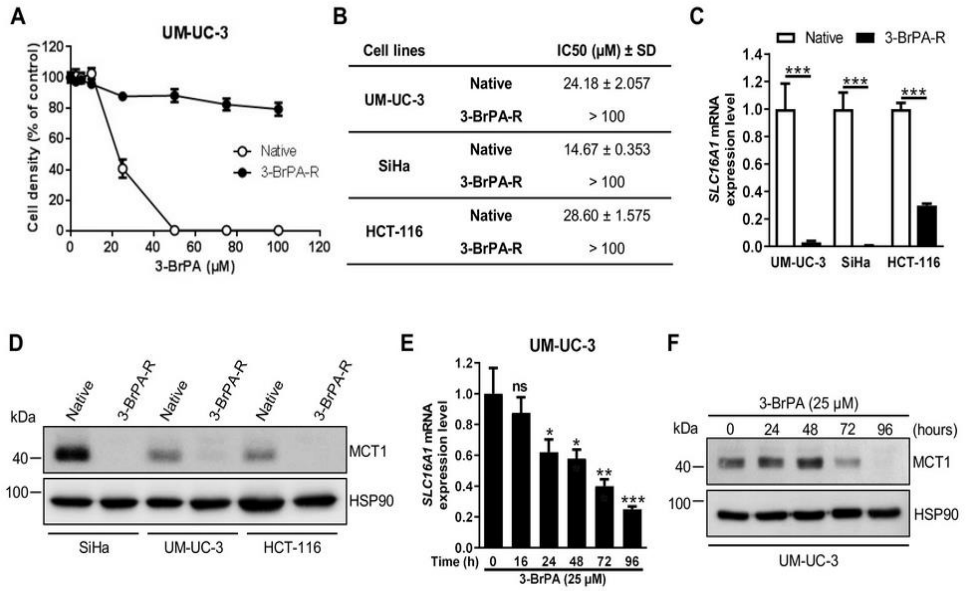

Figure 22: MCT1 is downregulated in 3-BrPA-R cancer cells.

*(**A-B**) Cell growth of native and 3-BrPA-R UM-UC-3 cells (**A**) and calculated IC_{50} for 3-BrPA in native and 3-BrPA-R cancer cells (**B**) after 3-BrPA treatment for 72h. (**C-D**) mRNA expression (**C**) and representative immunoblotting (**D**) for MCT1 in native and 3-BrPA-R cancer cells. (**E-F**) mRNA expression (**E**) and representative immunoblotting (**F**) for MCT1 in native UM-UC-3 cells treated with 25 µM 3-BrPA at different timings. Data are represented as mean ±SEM of three independent experiments (with ≥6 technical replicates). Significance was determined by one-way ANOVA (**E**) or two-way ANOVA (**C**) with Bonferroni multiple-comparison analysis. *p<0.05; **p<0.01; ***p<0.001; ns, not significant. I have directly contributed to the panel D.*

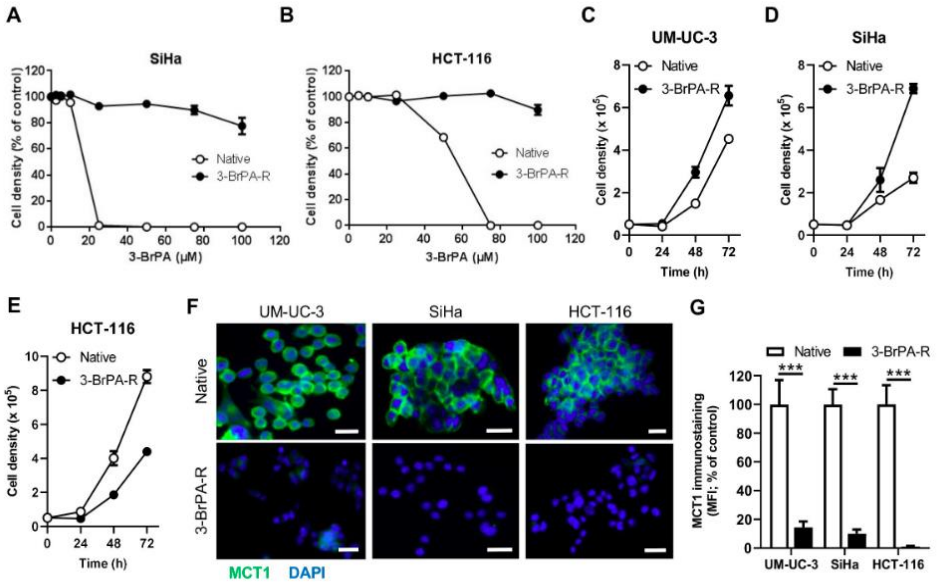

Supplementary Figure 1: MCT1 is downregulated in 3-BrPA-R cancer cells, Related to Figure 22.

*(**A-B**) Dose-dependent effects of 3-BrPA treatment (72h) on the growth of native and 3-BrPA-R SiHa (**A**) and HCT-116 (**B**) cancer cells. (**C-E**) Time course of the growth of native and 3-BrPA-R UM-UC-3 (**C**), SiHa (**D**) and HCT-116 cancer cells (**E**). (**F-G**) Representative pictures (**F**) and quantification (**G**) for MCT1 immunostaining in native and 3-BrPA-R cancer cells. Scale bar: 25 µm. Data are represented as mean ±SEM of three independent experiments (with ≥3 technical replicates). Significance was determined by two-way ANOVA (**G**) with Bonferroni multiple-comparison analysis. ***p<0.001. I have directly contributed to the panels F and G.*

1.3.2 DNA hypermethylation in *SLC16A1* gene promoter triggers MCT1 downregulation and subsequent 3-BrPA resistance

Since MCT1 downregulation, upon 3-BrPA treatment, was shared by cancer cells of distinct tissue origins (*i.e*. cervix, bladder and colon), we excluded a clonal selection of cells harboring specific mutation patterns but rather focused on epigenetic alterations, including DNA methylation, which are frequently associated with drug resistance [293]. Bisulfite genomic sequencing analysis actually revealed a hypermethylation of *SLC16A1* gene promoter in 3-BrPA-R UM-UC-3 cells in comparison to native counterparts (**Figure 23A**). Hypermethylation of CpG islands within the *SLC16A1* gene promoter was also detected in a genome-wide methylation analysis in 3-BrPA-R UM-UC-3 cancer cells (*vs* native cells) (**Table S1**). Importantly, we found that *SLC16A1* gene hypermethylation was not resulting from a global increase in 5-methylcytosine levels in 3-BrPA-R cell genome as revealed by either dot blot (**Figure 23B**) or the genome-wide methylation analysis (**Figure S2A**). Methylated DNA immunoprecipitation (MeDIP) allowed to show that *SLC16A1* gene hypermethylation was already detectable after 16-24h of treatment with 3-BrPA in native cancer cells (**Figure 23C**). Importantly, treatment of 3-BrPA-R cancer cells with 5-aza-2'-deoxycytidine (5-aza-dC), a hypomethylating agent (**Figure S2B**), induced a re-expression of *SLC16A1* mRNA (**Figures 23D and S2C-D**) and even restored sensitivity to 3-BrPA treatment **(Figure 23E**).

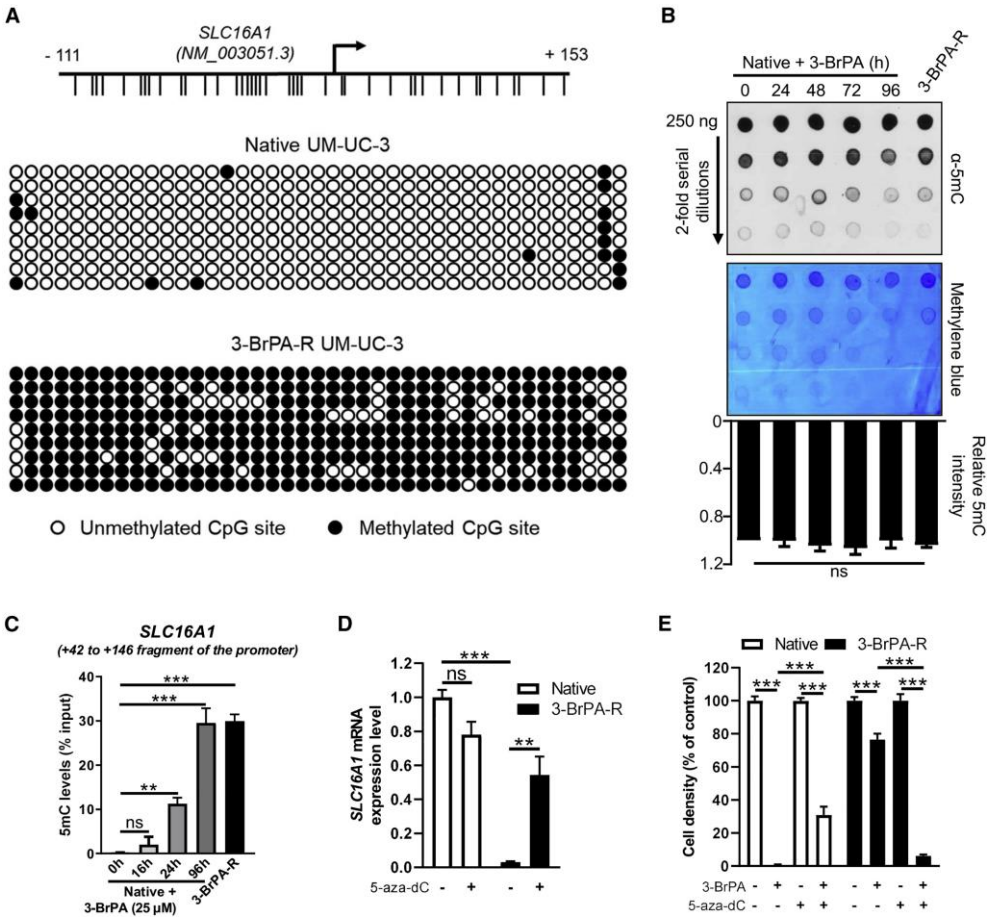

Figure 23: 3-BrPA resistance in cancer cells is associated with DNA hypermethylation in SLC16A1 gene promoter.

*(**A**) Methylation status of 41 CpG sites located within the SLC16A1 gene promoter (region spanning from -111 to +153), as determined by bisulfite sequencing analysis of genomic DNA from native and 3-BrPA-R UM-UC-3 cells. Each row represents an individual subclone. Methylated and unmethylated CpG sites are shown as black and white circles, respectively. (**B**) Representative dot-blot and quantification for 5mC levels in serial dilutions of genomic DNA extracted from native UM-UC-3 cells treated with 25 µM 3-BrPA for the indicated timings and 3-BrPA-R UM-UC-3 cells. Methylene blue staining was used as a loading control for genomic DNA. (**C**) Level of 5mC in the SLC16A1 gene promoter (region spanning from +42 to +146) from native UM-UC-3 cells treated with 25 µM 3-BrPA for the indicated timings and 3-*

*BrPA-R UM-UC-3 cells. (**D**) mRNA expression for SLC16A1 in native and 3-BrPA-R UM-UC-3 cells treated or not with 1 µM 5-aza-dC for 96h. (**E**) Cell growth extent for native and 3-BrPA-R UM-UC-3 cells treated or not with 1 µM 5-aza-dC for 96h and then incubated with 100 µM 3-BrPA for 72h. Data are represented as mean ±SEM of three independent experiments (with ≥3 technical replicates). Significance was determined by one-way ANOVA (**B-C**) or two-way ANOVA (**D-E**) with Bonferroni multiple-comparison analysis. **p<0.01; ***p<0.001; ns, not significant. I have directly contributed to the panels C, D and E.*

				Native UM-UC-3 (β-values)			3-BrPA-R UM-UC-3 (β-values)		
Map Info	Target ID	Gene region	Relation to CpG island	Sample #1	Sample #2	Sample #3	Sample #1	Sample #2	Sample #3
113486135	cg07967176	5'UTR		0,7811272	0,8221753	0,8294837	0,8121827	0,8060743	0,8118019
113467640	cg07572909	Body		0,7720162	0,8156894	0,7862034	0,8591189	0,7982169	0,8198919
113456650	cg24347098	Body		0,8079306	0,826317	0,8577765	0,6197161	0,6472906	0,5965848
113454575	cg18130079	3'UTR		0,8608495	0,8800131	0,8990213	0,8792385	0,8703759	0,8887461
113494852	cg18383124	5'UTR	N_Shelf	0,8360713	0,798995	0,8501308	0,4907808	0,5056119	0,4864716
113497932	cg16251079	5'UTR	N_Shore	0,1218921	0,1359904	0,1248415	0,895394	0,8176747	0,8418375
113499149	cg00963079	TSS200	Island	0,5290548	0,5410122	0,5383182	0,6548285	0,5831227	0,647546
113499109	cg03386556	TSS200	Island	0,04454545	0,04849	0,04853284	0,6638021	0,6562241	0,6659797
113499074	cg25128803	TSS200	Island	0,05784697	0,05739021	0,07214132	0,7935107	0,8299725	0,8177001
113499045	cg06854391	TSS200	Island	0,03209352	0,04228351	0,03371667	0,9549138	0,8990347	0,9632639
113498174	cg17020695	5'UTR	Island	0,1283636	0,1578027	0,1857765	0,6508	0,6551827	0,6249498
113498761	cg00502533	1stExon	Island	0,07607207	0,08009222	0,08312621	0,62401	0,6411011	0,6058092
113498193	cg00058299	5'UTR	Island	0.1615611	0.173691	0.2364249	0.9194608	0.9385607	0.9398947
113498742	cg16163697	1stExon	Island	0,1391245	0,1486643	0,1164489	0,619805	0,5913538	0,6304806
113498438	cg20614262	5'UTR	Island	0,0917592	0,1057082	0,09999374	0,6857528	0,6878024	0,6900913
113498382	cg11717506	5'UTR	Island	0,02196332	0,02746417	0,04394895	0,8255821	0,8198854	0,8591306
113497999	cg07423363	5'UTR	Island	0,07726269	0,08382066	0,07912727	0,8656909	0,8899528	0,8718388
113498799	cg08491025	1stExon	Island	0,05637864	0,06826802	0,07465228	0,6411369	0,6454289	0,6318172
113498106	cg12551029	5'UTR	Island	0,06864487	0,0923031	0,09544373	0,8737226	0,875627	0,8676797
113500384	cg19645639	TSS1500	S_Shore	0,1273661	0,1675912	0,1528079	0,8482763	0,8477861	0,8231998
113500329	cg07176692	TSS1500	S_Shore	0,06965348	0,08703503	0,08418729	0,5231712	0,5793037	0,557514
113499849	cg01328949	TSS1500	S_Shore	0,4089324	0,4804121	0,4615189	0,6243663	0,6244442	0,6335197
113499731	cg26162147	TSS1500	S_Shore	0,1492201	0,1674998	0,173913	0,4912865	0,4817425	0,4897403
113499528	cg02569658	TSS1500	S_Shore	0,3369282	0,3690048	0,3651741	0,540563	0,5489488	0,5368378
113499526	cg09226792	TSS1500	S_Shore	0,3119335	0,3485877	0,3244807	0,5072379	0,5264472	0,5238962

Supplementary Table 1: Methylation levels of CpG sites located in different regions of SLC16A1 gene in native and 3-BrPA-R UM-UC-3 cancer cells, Related to Figure 23.

TSS1500/TSS200 = region located 1500 bp or 200 bp from transcriptional start site, respectively; 5′/3′UTR = 5′/3′untranslated region. β-values are calculated as follows: methylated allele intensity/ (unmethylated allele intensity + methylated allele intensity +100); from 0 (unmethylated) to 1 (fully methylated). <0.3 ; 0.3-0.5 ; 0.5-0.7 ; >0.7

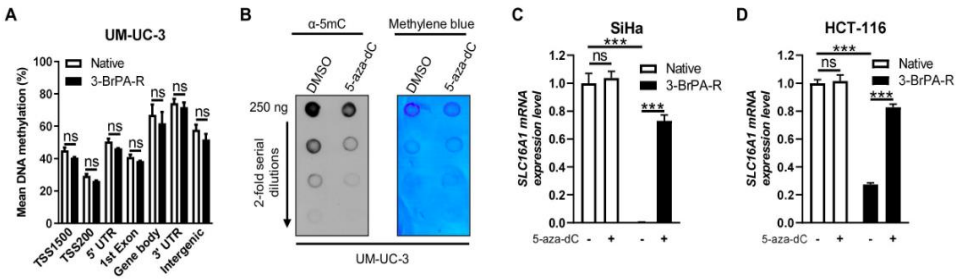

Supplementary Figure 2: 3-BrPA resistance in cancer cells is associated with DNA hypermethylation in SLC16A1 gene promoter, Related to Figure 23.

*(**A**) Methylation levels (as determined in a genome-wide methylation analysis) of CpG sites located in different gene regions from DNA samples extracted from native and 3-BrPA-R UM-UC-3 cancer cells. TSS1500 = region located 1500 bp from transcriptional start site; TSS200 = region located 200 bp from transcriptional start site; 5'UTR = 5' untranslated region; 3'UTR = 3' untranslated region. (**B**) Representative dot-blot for 5mC levels in serial dilutions of genomic DNA extracted from 3-BrPA-R UM-UC-3 cells treated or not with 1 µM 5-aza-dC for 96h. Methylene blue staining was used as a loading control for genomic DNA. (**C-D**) mRNA expression for SLC16A1 in native and 3-BrPA-R SiHa (**C**) and HCT-116 (**D**) cells treated or not with 1 µM 5-aza-dC for 96h. Data are represented as mean ±SEM of three independent experiments (with ≥3 technical replicates). Significance was determined by two-way ANOVA (**A, C-D**) with Bonferroni multiple-comparison analysis. ***p<0.001; ns, not significant. I have directly contributed to the panels C and D.*

1.3.3 MCT1 downregulation in 3-BrPA-resistant cells impairs lactate-fueled respiration

As MCT1 has been reported to transport monocarboxylates and to be a major actor in the lactate-based metabolic symbiosis in tumors [99], we decided to investigate the metabolic consequences of MCT1 downregulation in 3-BrPA-R cancer cells. First, using a Seahorse analyzer, we found that oxygen consumption rate (OCR) in 3-BrPA-R cells was limitedly influenced upon full access to glucose, glutamine and fatty acids (*vs.* native cells) (**Figures 24A and S3A-B**), with however a small but significant reduction in basal and maximal respiration (**Figures 24B-C**) as well as in respiration-dependent contribution to ATP production (**Figure S3C**). We next examined how the two cell populations behaved when restricting the nutrient access to single substrate. While there was no major difference in OCR between native and 3-BrPA-R cells when using glucose or glutamine as an energetic fuel, lactate-fueled mitochondrial respiration was blunted in 3-BrPA-R cells (**Figures 24D and S3D-E**). In native cancer cells, lactate used as a single nutrient supported OCR (to a larger extent than glucose) (**Figures 24D and S3D-E**) and the MPC inhibitor UK-5099 prevented its contribution to OCR proving the capacity of lactate, upon oxidation into pyruvate, to fuel oxidative metabolism (**Figures 24E and S3F-G**); no significant difference in the expression of LDH isoforms involved in the pyruvate and lactate interconversion was identified (**Figure S3H**). We further showed that lactate uptake was almost completely inhibited in 3-BrPA-R cancer cells incubated in a medium with only lactate as an energetic substrate (*vs*. native cells)

(**Figures 24F and S3I**), leading to dramatic cell growth inhibition (**Figures 24G and S3J-K**); cell viability in a glucose- or glutamine-containing medium was not altered (**Figures 24G and S3J-K**). Altogether the above data confirm that the epigenetic MCT1 downregulation resulting from 3-BrPA cell exposure may have dramatic consequences according to the availability of different substrates in the tumor microenvironment.

Since glucose was less prominently fueling respiration than glutamine but similarly supporting cell growth (**Figures 24G and S3J-K**), we next examined whether aerobic glycolysis (*i.e.* glucose conversion into lactate) was maintained in 3-BrPA-R cancer cells despite the well-described capacity of an acute treatment with 3-BrPA to inhibit HKII and GAPDH [294, 295]. We did not observe any change of expression for these two enzymes in 3-BrPA-R cancer cells (*vs* native cells) (**Figure S3L**). Interestingly, however, while basal glycolysis (probed by measuring extracellular acidification rate (ECAR) was unaltered in 3-BrPA-R cells (**Figures 24H-I and S3M-N**), the glycolytic reserve was significantly increased (**Figure 24J**), suggesting an increased capacity to generate ATP from glucose when oxidative metabolism is inhibited or less effective.

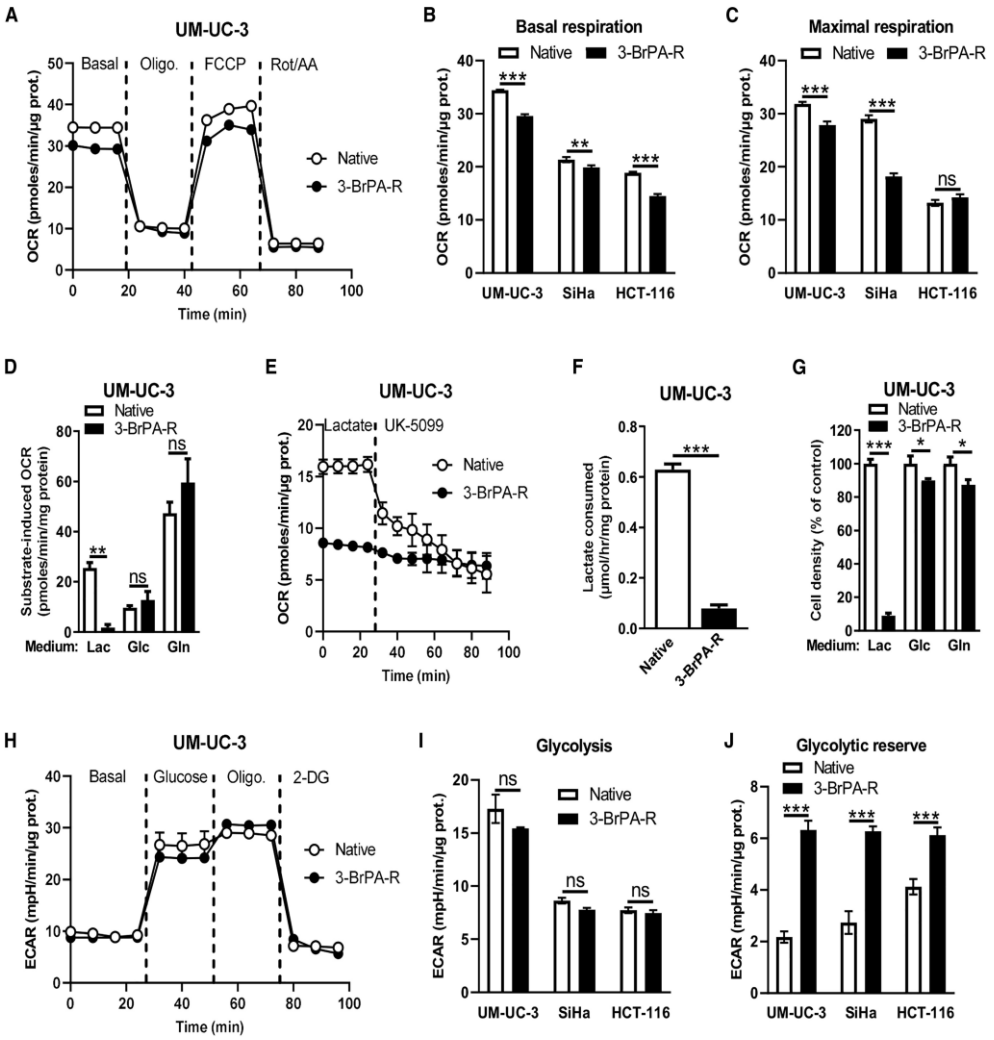

Figure 24: Lactate utilization is impaired in 3-BrPA-R tumor cells.

*(**A**) Representative OCR profiles in native and 3-BrPA-R UM-UC-3 cells following sequential treatment with oligomycin, FCCP and rotenone/antimycin A in a glucose- and glutamine-containing medium. (**B-C**) Basal (**B**) and maximal (**C**) respiration rates in native and 3-BrPA-R cancer cells. (**D**) Substrate-dependent OCR of native and 3-BrPA-R UM-UC-3 cancer cells in media containing lactate (Lac), glucose (Glc) or glutamine (Gln). (**E**) Representative OCR profiles in native and 3-BrPA-R UM-UC-3 cells before and after treatment with 10 µM UK-5099 in a lactate-containing medium. (**F**) Lactate consumption by native and 3-BrPA-R UM-UC-3 cancer cells for*

*24h in a lactate-containing medium. (**G**) Cell growth extent (72h) of native and 3-BrPA-R UM-UC-3 cancer cells in media containing lactate (Lac), glucose (Glc) or glutamine (Gln). (**H**) Representative ECAR profiles in native and 3-BrPA-R UM-UC-3 cells following sequential treatment with glucose, oligomycin and 2-DG in a glutamine-containing medium. (**I-J**) Glucose-dependent ECAR (**I**) and glycolytic reserve (**J**) in native and 3-BrPA-R cancer cells. Data are represented as mean ±SEM of three independent experiments (with ≥3 technical replicates). Significance was determined by Student's t-test (**F**) or two-way ANOVA (**B-D, G** and **I-J**) with Bonferroni multiple-comparison analysis. *p<0.05; **p<0.01; ***p<0.001; ns, not significant. I have directly contributed to the panels A, B, C, E, H, I and J.*

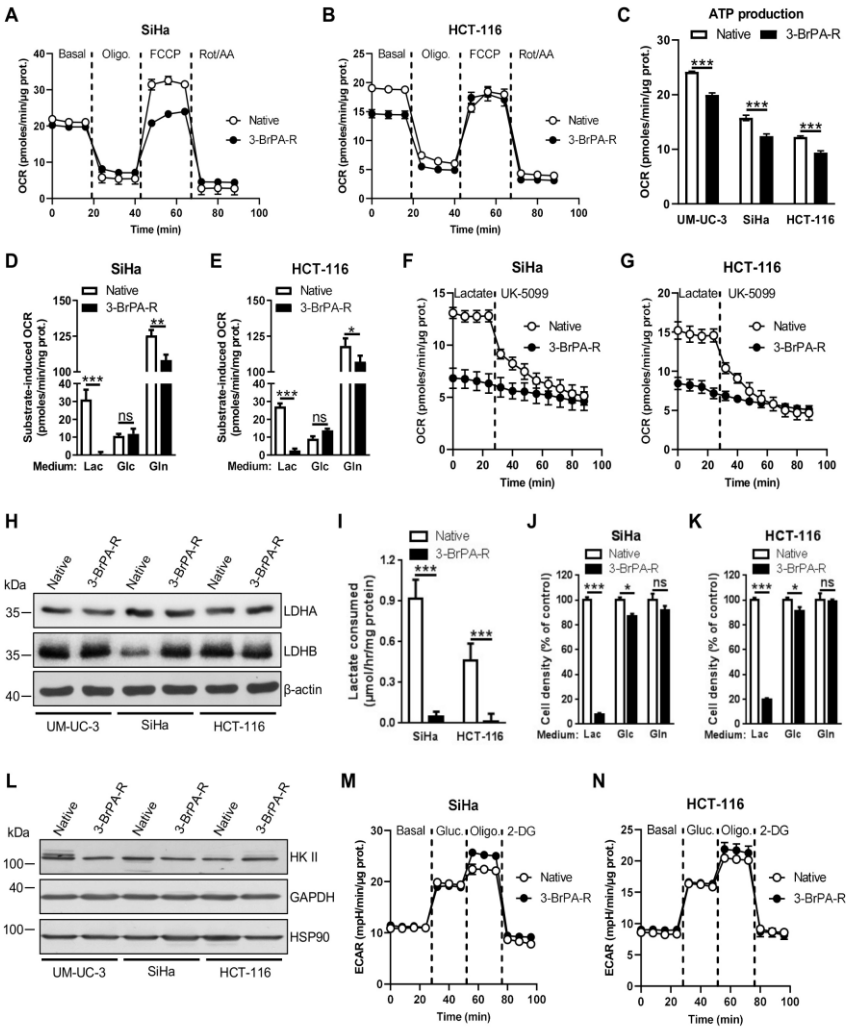

Supplementary Figure 3: Lactate utilization is impaired in 3-BrPA-R tumor cells, Related to Figure 24.

*(**A-B**) Representative OCR profiles in native and 3-BrPA-R SiHa (**A**) and HCT-116 (**B**) cells following sequential treatment with oligomycin, FCCP and rotenone/antimycin A in a glucose- and glutamine-containing medium. (**C**) ATP production-related OCR in native and 3-BrPA-R cancer cells. (**D-E**) Substrate-dependent OCR of native and 3-BrPA-R SiHa (**D**) and HCT-116 (**E**) cancer cells in media containing lactate (Lac), glucose (Glc) or glutamine (Gln). (**F-G**) Representative OCR profiles in native and 3-*

*BrPA-R SiHa (**F**) and HCT-116 (**G**) cancer cells before and after treatment with 10 µM UK-5099 in a lactate-containing medium. (**H**) Representative immunoblotting for lactate dehydrogenases A (LDHA) and B (LDHB) in native and 3-BrPA-R cancer cells. (**I**) Lactate consumption by native and 3-BrPA-R SiHa and HCT-116 cancer cells for 24h in a lactate-containing medium. (**J-K**) Cell growth extent (72h) of native and 3-BrPA-R SiHa (**J**) and HCT-116 (**K**) cancer cells in media containing lactate (Lac), glucose (Glc) or glutamine (Gln). (**L**) Representative immunoblotting for hexokinase II (HK II) and glyceraldehyde-3-phosphate dehydrogenase (GAPDH) in native and 3-BrPA-R cancer cells. (**M-N**) Representative ECAR profiles in native and 3-BrPA-R SiHa (**M**) and HCT-116 (**N**) cancer cells following sequential treatment with glucose, oligomycin and 2-DG in a glutamine-containing medium. Data are represented as mean ±SEM of three independent experiments (with ≥3 technical replicates). Significance was determined by two-way ANOVA (**C-E and I-K**) with Bonferroni multiple-comparison analysis. *p<0.05; **p<0.01; ***p<0.001; ns, not significant. I have directly contributed to the panels A, B, C, F, G, H, M and N.*

1.3.4 3-BrPA-R cancer cells rely on glycolysis in a MCT4-dependent manner

Lactate efflux by cancer cells is mainly mediated by MCT transporters, through which monocarboxylates are co-transported with protons [107]. As MCT1 expression is epigenetically inactivated in 3-BrPA-R cells, we investigated the role of MCT4, another monocarboxylate transporter. Interestingly, we could document a net increase in MCT4 protein expression in 3-BrPA-R SiHa and UM-UC-3 cells (**Figures 25A and S4A-B**). This was particularly striking in UM-UC-3 cells that do not express MCT4 in native conditions (**Figures 25A and S4A-B**). Native HCT-116 cells already expressed large amounts of the MCT4 transporter (**Figure 25A**) but still, immunofluorescence studies revealed a significant increase in the

expression of this transporter (**Figures S4A-B**). Of note, a role for HIF-1α in driving MCT4 upregulation could be excluded in experiments where HIF-1α was silenced (**Figures S4C-D**).

Although MCT1 and MCT4 are two lactate transporters, the latter is usually more largely involved in lactate efflux, in particular under hypoxia and when mitochondrial respiration is blocked [113, 296, 297]. To further examine potential consequences of this shift, we exposed native and 3-BrPA-R cells to rotenone, an inhibitor of complex I from the mitochondrial respiratory chain, and measured time-dependent lactate release. We found that lactate efflux was consistently increased in 3-BrPA-R cancer cells (**Figures 25B and S4E**). We actually found that 3-BrPA-R UM-UC-3 cells were resistant to rotenone but also to other respiration inhibitors such as IACS-010759, metformin and antimycin A (**Figures 25C-D and S4F-G**).

Altogether, the above data pointed MCT4 as an attractive target to render cancer cells less able to adapt to 3-BrPA exposure. We therefore examined the consequences of MCT4 silencing (using a pool of 4 specific siRNA sequences) (**Figure S4H**) and found that glycolysis (determined by measuring lactate release) was dramatically inhibited in 3-BrPA-R UM-UC-3 cells (**Figure 25E**), leading to significant cell growth inhibition (**Figure 25F**) (*vs.* native UM-UC-3 cancer cells). Interestingly, we also showed that CRISPR/Cas9-mediated MCT4 silencing partially restored sensitivity to OXPHOS inhibition in 3-BrPA-R cancer cells (**Figures 25G and S4I**), suggesting that MCT4 upregulation dictates -above all other adaptations- the metabolic preferences of 3-BrPA-R cells. We also documented that the interplay between MCT1 and MCT4 could be recapitulated by exposing native cancer

cells to MCT1 inhibitor AZD3965 or upon MCT1 silencing (**Figures 25H-J and S4J**).

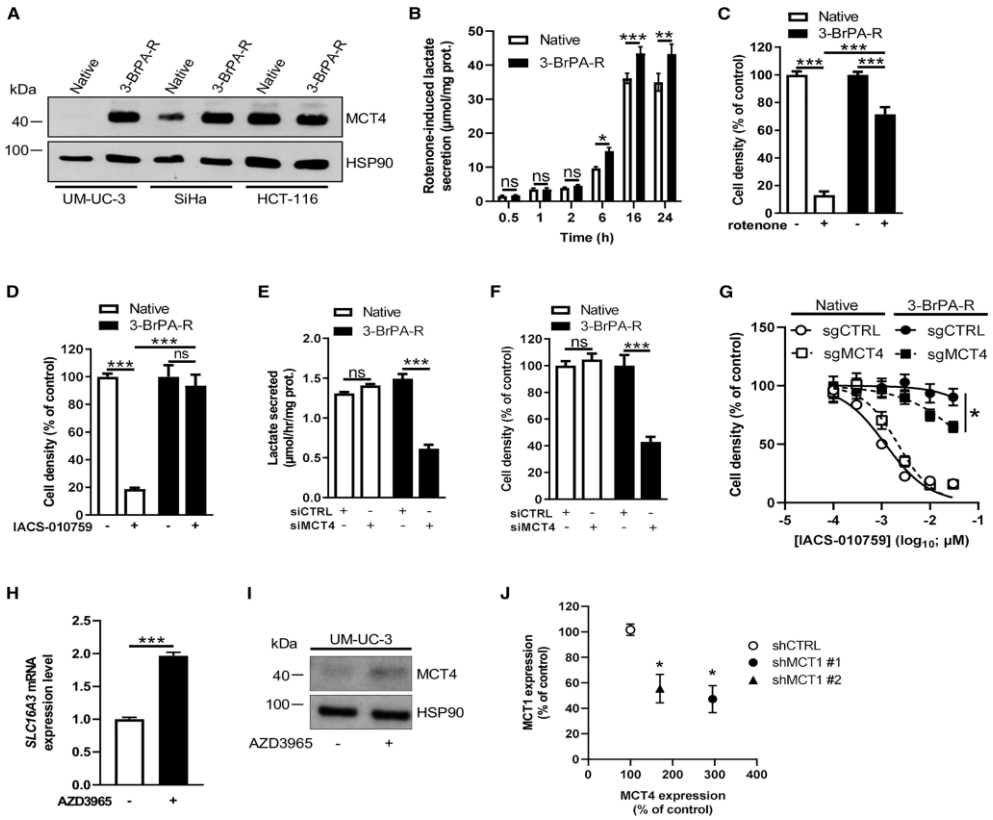

Figure 25: 3-BrPA-R cancer cells rely on glycolysis in a MCT4-dependent manner. *(**A**) Representative immunoblotting for MCT4 in native and 3-BrPA-R cancer cells. (**B**) Lactate secretion in native and 3-BrPA-R UM-UC-3 cancer cells following treatment with 100 nM rotenone for increasing timings in glucose-containing medium. (**C-D**) Cell growth extent (72h) of native and 3-BrPA-R UM-UC-3 cancer cells following treatment with 100 nM rotenone (**C**) or 100 nM IACS-010759 (**D**). (**E-F**) Lactate secretion (**E**) and growth extent (**F**) of native and 3-BrPA-R UM-UC-3 cancer cells following transfection of MCT4-targeting (or control) siRNA for 72h in glucose-containing medium. (**G**) Cell growth extent (72h) of native and 3-BrPA-R UM-UC-3 cells stably expressing Cas9 either with control or MCT4-targeting sgRNA upon treatment with IACS-010759. (**H-I**) mRNA expression (**H**) and representative*

*immunoblotting (**I**) for MCT4 in native UM-UC-3 cells following treatment with 10 µM AZD3965 for 72h. (**J**) Protein expression for MCT1 and MCT4 in FAC-sorted native UM-UC-3 cells stably expressing control or MCT1-targeting shRNA. Data are represented as mean ±SEM of three independent experiments (with ≥3 technical replicates). Significance was determined by Student's t-test (**H**), one-way ANOVA (**J**) or two-way ANOVA (**B-F**) with Bonferroni multiple-comparison analysis. *p<0.05; **p<0.01; ***p<0.001; ns, not significant. I have directly contributed to the panels A, B, H, I and J.*

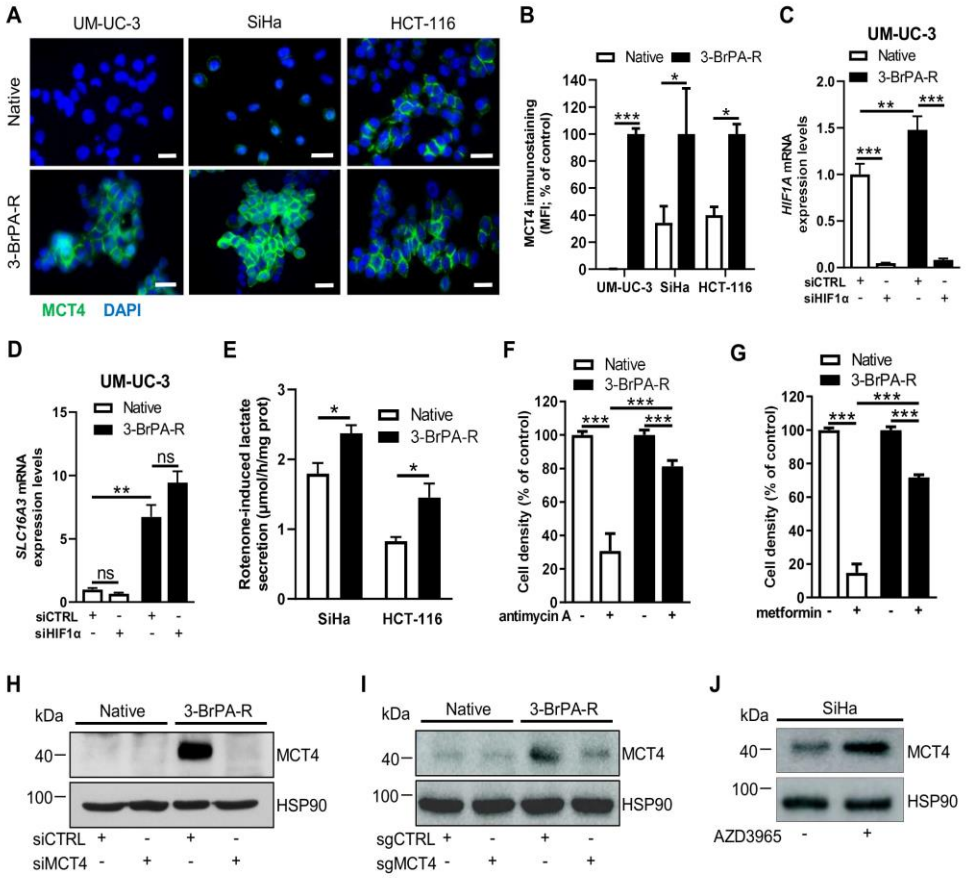

Supplementary Figure 4: 3-BrPA-R cancer cells rely on glycolysis in a MCT4-dependent manner, Related to Figure 25. *(**A-B**) Representative pictures (**A**) and quantification (**B**) for MCT4 immunostaining in native and 3-BrPA-R cancer cells. Scale bar: 25 µm. (**C-D**) mRNA expression for HIF1A (**C**) and SLC16A3 (MCT4) (**D**) in native and 3-BrPA-R UM-UC-3 cells following transfection of HIF1A-targeting (or control) siRNA for 72h. (**E**) Lactate secretion in native and 3-BrPA-R SiHa and HCT-116 cancer cells following treatment with 100 nM rotenone for 24h in glucose-containing medium. (**F-G**) Cell growth extent (72h) of native and 3-BrPA-R UM-UC-3 cancer cells following treatment with 100 nM antimycin A (**F**) or 10 mM metformin (**G**). (**H-J**) Representative immunoblotting for MCT4 in native and 3-BrPA-R UM-UC-3 cancer cells following transfection of MCT4-targeting (or control) siRNA for 72h (**H**) or stable expression of Cas9 with either control or MCT4-targeting sgRNA (**I**) and*

*in native SiHa cells following treatment with 10 µM AZD3965 for 72h (**J**). Data are represented as mean ±SEM of three independent experiments (with ≥3 technical replicates). Significance was determined by two-way ANOVA (**B-G**) with Bonferroni multiple-comparison analysis. *p<0.05; **p<0.01; ***p<0.001; ns, not significant. I have directly contributed to the panels A, B, C, D, E, I and J.*

1.3.5 3-BrPA-R cancer cells exhibit a phenotype that supports a growth advantage under hypoxic conditions

In our attempt to prove that MCT4 activity became critical to support cancer cell fitness upon MCT1 silencing resulting from 3-BrPA pre-challenge, we further focused on hypoxic conditions that are known to induce MCT4 expression to get rid of excess lactate production [296]. We examined whether MCT4 (over)expression in 3-BrPA-R cancer cells could give them an advantage of proliferation under low oxygen conditions. We first found higher growth capacities for 3-BrPA-R cancer cells (*vs* native cells) when exposed for 96h in hypoxia (1% O_2) (**Figure S5A**). Under these hypoxic conditions, MCT4 expression was also higher in 3-BrPA-R SiHa and HCT-116 cancer cells (than in corresponding native cells) and expressed in very large amounts in both native and 3-BrPA-R UM-UC-3 cancer cells (**Figure S5B**). Of note, 3-BrPA-R cancer cells still exhibited MCT1 downregulation as observed under normoxia (**Figure S5B**). These results led us to examine the behaviour of 3-BrPA-R cancer cells by using 3D spheroid models in which a natural hypoxic core develops. We therefore generated tumor spheroids by mixing GFP-labelled native and mCherry-labelled 3-BrPA-R HCT-116 cancer cells. We observed a preferential location for 3-BrPA-R cancer cells at the centre

of the spheroids, while native cancer cells formed a surrounding layer at the rim of the 3D structures (**Figures 26A-B**). Pimonidazole staining also confirmed that hypoxic zones barely overlapped with native (GFP-labelled) cancer cells (**Figure 26C**) while the distribution of hypoxia staining in the spheroid depth was very similar to that of mCherry-labelled 3-BrPA-R cancer cells (**Figure 26D**). Finally, we showed that 3-BrPA-R cancer cells exhibited a low-proliferating state, as indicated with a non-overlap between Ki67 staining and mCherry fluorescent signal (**Figures 26E-F**). This reduced proliferation capacity of 3-BrPA-R cells (*vs* native cells) was also reflected in a reduced proportion of resistant cells in large spheroids despite a similar amount of the two cell populations at the initiation (see untreated condition in **Figure 26G**). A lack of sensitivity to the anti-proliferating drug 5-fluorouracil (5-FU) was also unravelled by documenting the dose-dependent enrichment in 3-BrPA-R cell population (*vs* native cells) in 3D spheroids (**Figure 26G**); this differential sensitivity was lost when both cell populations (native and 3-BrPA-R) were exposed to 5-FU in 2D conditions (**Figure S5C**).

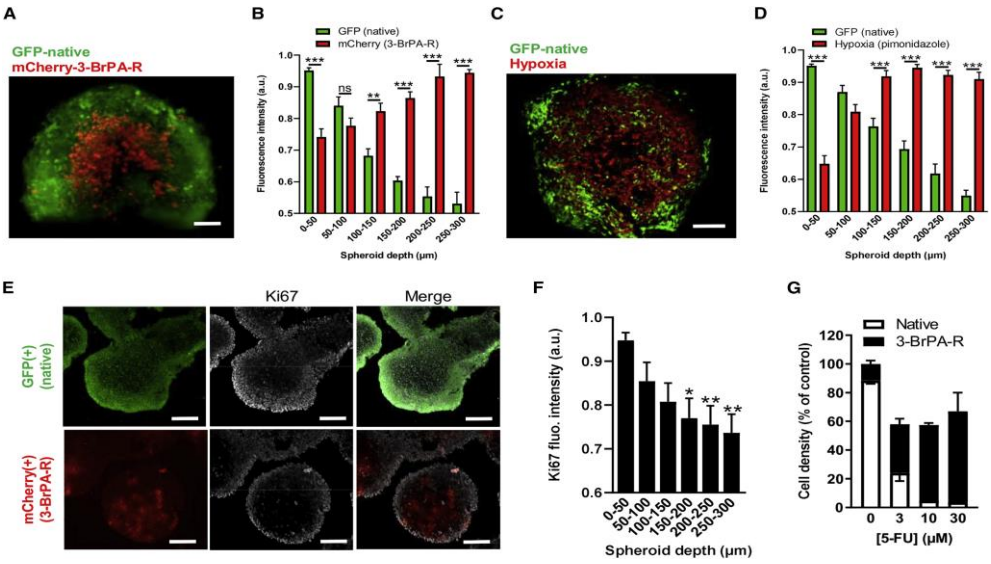

Figure 26: 3-BrPA-R cancer cells exhibit a phenotype that supports a growth advantage under hypoxic conditions.

*(**A-B**) Representative light-sheet microscopy fluorescence pictures (**A**) and distribution from the periphery to the core of GFP and mCherry fluorescent markers (labelling native and 3-BrPA-R HCT116 cancer cells, respectively) (**B**) in 10-day-old 3D mixed spheroids. Scale bar: 150 µm. (**C-D**) Representative fluorescence pictures (**C**) and distribution from the periphery to the core of GFP and pimonidazole (labelling native cancer cells and hypoxic areas, respectively) (**D**) in 10-day-old 3D mixed tumor spheroids composed of GFP-labelled native and unlabelled 3-BrPA-R HCT-116 cells. Scale bar: 200 µm. (**E-F**) Representative fluorescence pictures (**E**) and distribution from the periphery to the core of Ki-67 staining (proliferation marker) (**F**) in 10-day-old 3D mixed HCT-116 spheroids. Scale bar: 200 µm. (**G**) Respective cell abundance within 3D mixed spheroids composed of GFP- and mCherry-labelled native and 3-BrPA-R HCT-116 cancer cells after treatment with increasing concentrations of 5-FU for 5 days (starting 5 days after spheroid initiation). Data are represented as mean ±SEM of three independent experiments (with ≥3 technical replicates). Significance was determined by one-way ANOVA (**F**) or two-way ANOVA (**B, D**) with Bonferroni multiple-comparison analysis. *p<0.05; **p<0.01; ***p<0.001; ns, not significant. I have directly contributed to the panels A, B, C, D, E, F and G.*

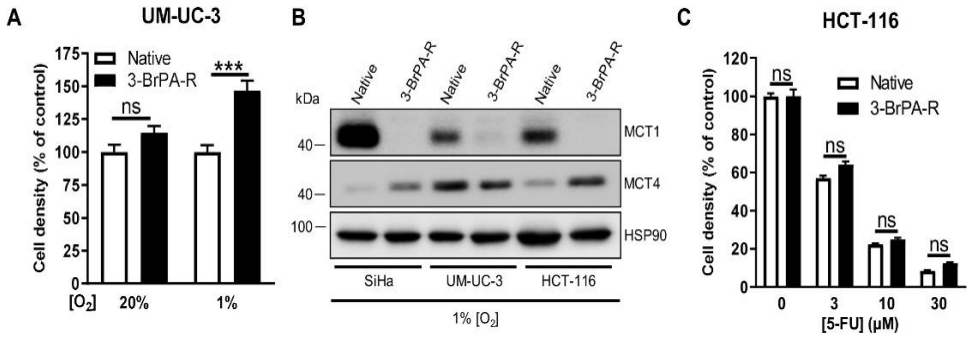

Supplementary Figure 5: 3-BrPA-R cancer cells exhibit a phenotype that supports a growth advantage under hypoxic conditions, Related to Figure 26.

*(**A**) Growth of native and 3-BrPA-R UM-UC-3 cancer cells incubated under normoxic (20% O_2) or hypoxic (1% O_2) conditions for 48h. (**B**) Representative immunoblotting for MCT1 and MCT4 in native and 3-BrPA-R cancer cells incubated under hypoxic (1% O_2) conditions for 48h. (**C**) Growth of native and 3-BrPA-R HCT-116 cancer cells cultured in 2D following treatment with increasing concentrations of 5-FU for 72h. Data are represented as mean ±SEM of three independent experiments (with ≥6 technical replicates). Significance was determined by two-way ANOVA (A, C) with Bonferroni multiple-comparison analysis. ***p<0.001; ns, not significant. I have directly contributed to the panels A, B and C*

1.3.6 MCT4 activity blockade prevents 3-BrPA resistance establishment in 2D and 3D tumor models

To prove that MCT4 expression represented a vulnerability for cancer cells pre-challenged with 3-BrPA, we examined the combination of 3-BrPA with MCT4 gene silencing but also pharmacological inhibition using diclofenac, a nonsteroidal anti-inflammatory drug recently shown to

interfere with lactate efflux through MCT4 inhibition [142]. We first generated tumor spheroids from either native or 3-BrPA-R HCT-116 cancer cells and showed that growth of the latter was more affected by diclofenac treatment (**Figure 27A**), with induction of cytotoxicity as revealed by the occurrence of a halo of dead cells around the spheroids (**Figures 27B-C**). Similar effects were observed with spheroids derived from 3-BrPA-R UM-UC-3 cancer cells (**Figures 27D-E**). Of note, native UM-UC-3 cells could not be tested in 3D conditions since they did not spontaneously form spheroids. Still, we showed that growth inhibitory effects of diclofenac in native UM-UC-3 cancer cells could only be observed upon concomitant MCT1 pharmacological inhibition (**Figure 27F**) and were interestingly more pronounced when administered after 3-BrPA treatment (than the opposite) (**Figure 27G**). Importantly, using spheroids made of mixed native and 3-BrPA-R HCT-116 cells, we could validate a preferential cytotoxic effect of diclofenac toward 3-BrPA-R cancer cells since propidium iodide staining (to label dead cells) was mostly located in the spheroid centre (**Figures 27H-I and S6A**). Finally, we wondered whether MCT4 silencing or blockade could synergize with acute 3-BrPA treatment *in vivo*. To do so, Cas9-expressing HCT-116 native cells were infected with either control or MCT4-targeting guide RNA sequences. Combination of 3-BrPA treatment with genetic invalidation of MCT4 led *in vitro* to a dramatic decrease in HCT-116 cancer cell growth (**Figure 27J**). In mice, the growth of MCT4 knock-out HCT-116 tumors was also significantly delayed in response to a tolerated dose of 3-BrPA (*vs.* sgCTRL HCT-116 tumors) (**Figure 27K**). Finally, to avoid any interference resulting from long-term MCT4 genetic silencing, we acutely

exposed tumor-bearing mice to 3-BrPA and diclofenac either in a combined or sequential mode. A significant increase in mouse survival was observed upon co-treatment with 3-BrPA and diclofenac regardless of the chronology of administration (**Figure 27L**). In the different *in vivo* settings, single treatment had no significant growth inhibitory effects as observed *in vitro* (**Figures 27G and 27J-K**), and neither gross toxicity nor body weight changes were observed (**Figures S6B-C**).

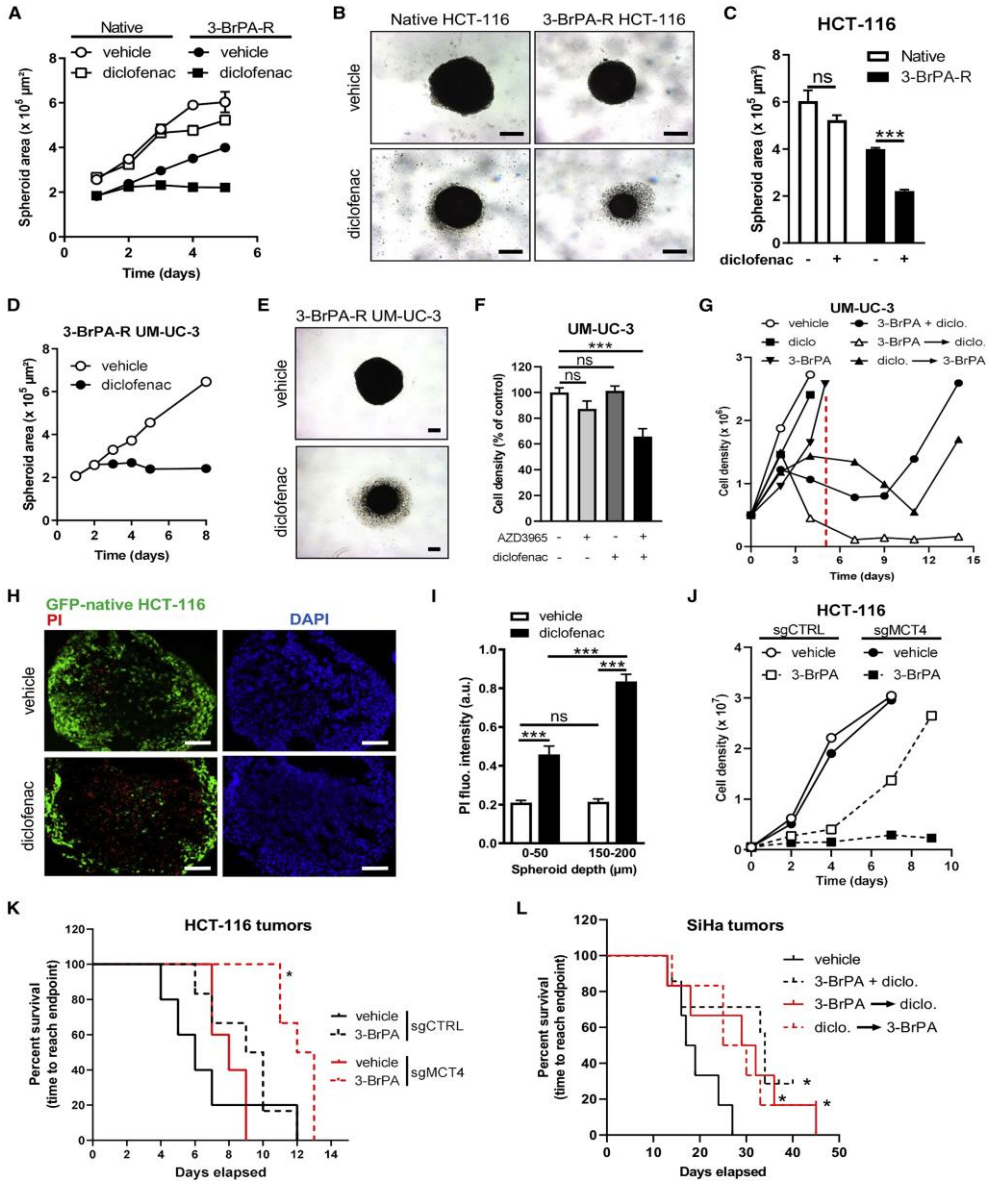

Figure 27: Pre-challenge with 3-BrPA potentiates antitumor effects of MCT4 activity blockade.

*(**A-C**) Time-dependent growth (**A**), representative pictures at day 5 (**B**) and quantification of spheroid area (**C**) of native and 3-BrPA-R HCT-116 spheroids upon treatment with 0.2 mM diclofenac for 5 days (starting 3 days after spheroid*

*initiation). Scale bar: 100 µm. (**D-E**) Time-dependent growth (**D**) and representative pictures at day 8 (**E**) of 3-BrPA-R UM-UC-3 spheroids upon treatment with 0.2 mM diclofenac for 8 days (starting 3 days after spheroid initiation). Scale bar: 100 µm. (**F**) Cell growth of native UM-UC-3 cells following treatment with 10 µM AZD3965 and/or 0.1 mM diclofenac for 72h. (**G**) Cell growth of native UM-UC-3 cells upon single, combinatory or sequential treatment with 25 µM 3-BrPA and 0.1 mM diclofenac. Sequential treatments were switched at day 5 (as indicated with the red dashed line). (**H-I**) Representative fluorescence pictures (**H**) and distribution from the periphery to the core of propidium iodide staining (labelling dead cells) (**I**) in 3D mixed tumor spheroids, composed of GFP-labelled native and unlabelled 3-BrPA-R HCT-116 cells upon treatment with 0.2 mM diclofenac for 4 days (starting one week after spheroid initiation). Scale bar: 200 µm. (**J**) Cell growth of native HCT-116 cells stably expressing Cas9 either with control or MCT4-targeting sgRNA upon treatment with 50 µM 3-BrPA. (**K**) Kaplan-Meier survival curves of nude mice bearing tumors from native HCT-116 cells stably expressing Cas9 either with control or MCT4-targeting sgRNA and daily treated with 2 mg/kg 3-BrPA or saline solution. Endpoint was defined when tumors reached a volume > 250 mm³. (**L**) Kaplan-Meier survival curves of nude mice bearing tumors from native SiHa cells daily administered with combinatory or sequential treatment of 2 mg/kg 3-BrPA, 7.5 mg/kg diclofenac or saline solution. Sequential treatments were changed at day 20. Endpoint was defined when tumors reached a volume > 500 mm³. Data are represented as mean ±SEM of three independent experiments (with ≥3 technical replicates). Significance was determined by one-way ANOVA (**F**), two-way ANOVA (**C** and **I**) with Bonferroni multiple-comparison analysis or log-rank test (**K-L**). *p<0.05; ***p<0.001; ns, not significant. I have directly contributed to the panels A, B, C, D, E, F, G, H, I, J, K and L.*

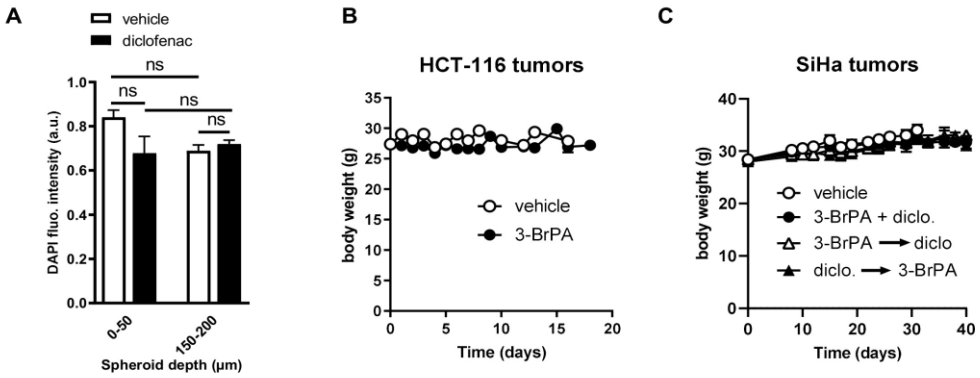

Supplementary Figure 6: Evaluation of 3-BrPA- and diclofenac-induced overall toxicity in vitro and in vivo, Related to Figure 27.

*(**A**) Distribution from the periphery to the core of DAPI nuclear staining in 3D mixed tumor spheroids, composed of GFP-labelled native and unlabelled 3-BrPA-R HCT-116 cells upon treatment with 0.2 mM diclofenac for 4 days. (**B-C**) Body weight for nude mice bearing either HCT-116 tumors daily treated with 2 mg/kg 3-BrPA or saline solution (vehicle) (**B**) or SiHa tumors daily administered with combinatory or sequential treatment of 2 mg/kg 3-BrPA and 7.5 mg/kg diclofenac (**C**). Data are represented as mean ±SEM of three independent experiments (with ≥6 technical replicates). Significance was determined by two-way ANOVA (A) with Bonferroni multiple-comparison analysis. ns, not significant. I have directly contributed to the panels A, B and C.*

1.4 Discussion

Metabolic plasticity allows tumor cells to adapt their bioenergetic and/or biosynthetic preferences in order to grow and survive in harsh local environmental conditions [83, 88]. In this study, we aimed to identify a treatment that could drive a cancer cell metabolic phenotype towards a direction that could be highly efficiently tackled by a second treatment. Although we reached this goal, the mechanism was different from the one

initially anticipated. Indeed, we used an alkylating agent known to preferentially alter the activity of metabolic enzymes because of its structural analogy with pyruvate [298]. While we were expecting, from the use of 3-BrPA, a rapid covalent-based alteration in glycolytic enzymes such as GAPDH and HK [298], we ended up with an epigenetic adaptation to the cytotoxic effects of 3-BrPA leading to the silencing of monocarboxylate transporter MCT1. This response that prevented further entry of the drug into cancer cells was rapid and long-lasting even in the absence of a continuous exposure to 3-BrPA. Although we cannot exclude that a large-scale DNA methylation response to 3-BrPA led to a selection of cancer cells wherein MCT1 was among the many silenced genes, the possibility of a non-random process is supported by several studies [299-301]. DNA methylation changes in response to external stress conditions (*e.g.* drug exposure) can indeed result from gene-specific phenomena that involve sequence-specific binding motifs and rapidly provide cancer cells with a phenotypic advantage [302]. In our study, it is noteworthy that a short pre-challenge with 3-BrPA was already sufficient to induce DNA hypermethylation in MCT1-encoding gene promoter and subsequent protein downregulation, thereby positioning MCT1 loss as a primary event in acquired resistance to 3-BrPA. This hypermethylation-induced inhibition of drug influx in 3-BrPA-R cancer cells is actually reminiscent of epigenetic alterations observed in methotrexate-resistant lymphomas, with an aberrant methylation of the folate carrier-encoding *SLC19A1* gene promoter that led to a reduced drug uptake [303].

A second unexpected finding from our study was the dependence of 3-BrPA-R cancer cells for glycolysis that was even exacerbated in the presence of OXPHOS inhibitors. 3-BrPA was previously identified in a genomic study to exert strong inhibitory effects on GAPDH, with an accumulation of upstream glycolytic metabolites and a dramatic fall in intermediates located downstream from the enzyme [298]. Thus, our work stands out from the mechanistic studies that aim to identify the preferred targets of 3-BrPA and instead leads us to shed light on the subtle equilibrium between the roles of MCT1 and MCT4 in cancer cells. The co-expression of these two monocarboxylate transporters in the same cancer cell or the induction of MCT4 in MCT1-expressing cancer cells generally relies on K_m values that account for a low affinity of MCT4 for pyruvate making this transporter more prone to support lactate efflux in highly glycolytic cells. By contrast, the lower K_m of MCT1 for lactate makes this transporter able to transport lactate the other way around (*i.e*. into the cell) [80, 99, 100]. Here, we found that because of the induced loss of MCT1 expression (and despite the presence of MCT4), 3-BrPA-R cancer cells are not able to take up extracellular lactate anymore and use it as a substrate to fuel mitochondrial respiration when other nutrients are scarce. These data are reminiscent of studies with *bona fide* MCT1 inhibitors documenting how by preventing the symbiotic exchange between lactate-generating and lactate-producing cells, tumor growth inhibitory effects can be observed [99, 304]. Our study provides evidence that MCT1 epigenetic silencing may actually promote addiction to MCT4 activity, the blockade of which leading to profound anticancer effects. We found indeed that upon 3-BrPA treatment, cancer

cells become highly dependent on the expression of MCT4. That MCT1 replacement by MCT4 dictates the metabolic phenotype of 3-BrPA-R cells is further revealed by the exposure of cancer cells to OXPHOS inhibitors but also hypoxia. We showed indeed that 3-BrPA-R cells are less dependent on mitochondrial respiration and preferentially accumulate in the hypoxic core of 3D spheroids. These data indicate that MCT4 becomes a major driver of 3-BrPA-R cell phenotype that may actually support tumor aggressiveness through an increased capacity of adaptation to hypoxic conditions and a lesser response to anti-proliferative drugs. In this study, we took advantage of the recent demonstration of diclofenac, a nonsteroidal inflammatory drug, being a MCT inhibitor with a 10-fold higher potency for MCT4 than for MCT1 [142]. We showed the capacity of diclofenac, but also CRISPR-based genetic MCT4 knockout strategy, to synergize with 3-BrPA treatment to trigger inhibition of cancer cell growth in 2D and 3D conditions as well as *in vivo*.

More generally, our study is part of the ongoing quest for best combinations of treatments targeting tumor metabolism such as the association of a LDH inhibitor with IACS-010759 complex I inhibitor [305] or metformin with MCT1 inhibitor AZD3965 [306]. Yet, we propose a specific angle to reach this goal with the demonstration that stress-induced hypermethylation, as obtained upon exposure to a cytotoxic compound, may represent an attractive modality to knock-down the expression of genes encoding for proteins critically involved in tumor metabolism. To some extent, this strategy can be related to the co-deletion of tumor suppressor genes together with neighbor passenger genes playing diverse functions in

cell homeostasis [185]. In the field of tumor metabolism, this notion of collateral lethality is consistent with the identification of mutations in specific metabolic enzymes giving rise to druggable cancer cell vulnerabilities [282, 307-309]. We propose here that such addiction can also be induced by drug treatment, including by drugs that *per se* do not exert major cytotoxic effects and are even associated with resistance. This allows to envision an evolution-based therapeutic approach according to which the metabolic rewiring in cancer cells upon a first-line treatment makes them more vulnerable to a second-line antimetabolic therapy. Moreover, with the use of diclofenac recently identified as a MCT inhibitor, our study supports the interest of drug repurposing. This may be particularly relevant to speed up time to market of the combination of drugs that need to face the complicated issues of evaluating toxicity of concomitantly administered compounds [310].

In conclusion, we provide evidence that administration of 3-BrPA can lead to epigenetic-driven loss of MCT1 making MCT4 more critical for cancer cells and thus a druggable attractive target. This may be particularly suited to treat cancers in which these transporters play critical roles such as metastatic melanoma [104]. More generally, a short 3-BrPA pulse exposure could advantageously complement a treatment with MCT4 inhibitors that are currently under development [311, 312]. The primary aim before the onset of the MCT4 inhibitor treatment would thus consist in shaping a more vulnerable metabolic phenotype.

1.5 Methods

Animal strains

Rj:NMRI-*Foxn1*$^{nu/nu}$ mice (female 7-week-old) were purchased from Janvier Labs. Studies using mice were performed after approval of the UCLouvain ethic committee (approval ID 2016/UCL/MD/018 and 2020/UCL/MD/032) and were carried out according to national care regulations. All mice were housed in the facility of the Institut de Recherche Expérimentale et Clinique (IREC) at UCLouvain.

Cell lines

All human cancer cell lines were acquired in the last three years from ATCC where they are regularly authenticated by short tandem repeat profiling. Cells were stored according to the supplier's instructions and used within 6 months after resuscitation of frozen aliquots. SiHa cervix cancer cells, UM-UC-3 bladder cancer cells and HCT-116 colon cancer cells were maintained in DMEM containing 25 mM D-glucose, 2 mM L-glutamine and supplemented with 10% heat-inactivated FBS in a humidified atmosphere at 37°C and 5% CO_2. 3-BrPA-resistant cancer cells were established by incubating cells with increasing concentrations of 3-BrPA (from 10 to 100 µM) until no cell death was observed. All cell lines were tested for mycoplasma contamination with the MycoAlert™ Mycoplasma Detection kit (Lonza) before being used. GFP-expressing native and mCherry-expressing 3-BrPA-R HCT-116 cancer cells were established by infection with eGFP

Lentifect™ (#LPP-EGFP-LV105-025; GeneCopoeia) and mCherry Lentifect™ (LPP-MCHR-LV105-025; GeneCopoeia) purified lentiviral particles, according to manufacturer's instructions and further selection with 2 µg/ml puromycin (#ant-pr-1; InvivoGen) for 1 week.

Cell treatment and transfection

Cell treatment was performed in a full culture medium with 2-deoxy-D-glucose (2-DG; #D8375), 3-bromopyruvate (#16490), 5-aza-2'-deoxycytidine (#A3656), antimycin A (#A8674), diclofenac (#S0765000), metformin (#D150959) and rotenone (#R8875), all purchased from Sigma-Aldrich, at different timings and concentrations, as indicated in the figure legends. 5-fluorouracil was purchased from Teva Pharma Belgium while IACS-010759 was synthesized and purified in our lab. In some conditions, cells were maintained at 37°C in normoxic conditions (20% O_2, 5% CO_2) or exposed to hypoxia (1% O_2, 5% CO_2) in an Invivo2 300 hypoxia chamber (Ruskinn). Cell growth was assessed either by direct cell counting on a hemocytometer with Trypan Blue exclusion dye or by using the Presto Blue reagent (#A13262; Thermo Fisher Scientific) according to manufacturer's instructions. Cell transfection with a pool of 4 non-targeting siRNA sequences (D-001810-10-05) or a pool of 4 siRNA sequences targeting the human *SLC16A3* gene (#L-019204-01), both from Dharmacon, was carried out with Lipofectamine™ RNAiMAX transfection reagent (#13778150; Thermo Fisher Scientific) at 50 nM, according to manufacturer's instructions. Native UM-UC-3 cells were transfected with 1 µg of either one of two

plasmids encoding for human *SLC16A1*-targeting shRNA sequences or one non-effective scrambled shRNA plasmid (#TL309405; Origene) with Turbofectin 8.0 transfection reagent (#TF81001; Origene) (ratio Turbofectin:DNA 3:1), according to manufacturer's instructions. For CRISPR-Cas9 system, HCT-116 and UM-UC-3 cancer cells were first infected with an Edit-R Lentiviral hEF1α-Blast-Cas9 Nuclease vector (VCAS10126; Dharmacon). Cas9-expressing cells, selected after one-week exposure to 8-12 µg/ml blasticidin (#ant-bl-05; InvivoGen), were then secondly infected with either a non-targeting single guide (sg) RNA (VSGC10215; Dharmacon), or a *SLC16A3*-targeting sgRNA (VSGH10142-246491301; Dharmacon). Final selection of sgRNA-expressing cells was done with 2 µg/ml puromycin for 1 week.

Western blot analysis

Subconfluent cancer cells were washed twice with ice-cold PBS and lysed in a RIPA buffer supplemented with a protease inhibitor cocktail (Sigma-Aldrich). Cell lysates were then cleared by centrifugation (6,000 rcf, 10 min, 4°C) and stored at −80°C until analysis. After determination of protein concentration using a bicinchoninic acid-based assay (Thermo Fisher Scientific), samples were denatured (5 min, 95°C) with Laemmli sample buffer containing 100 mM dithiothreitol. Samples (20 µg per well) were then separated by SDS-PAGE (8 to 15% acrylamide/bis-acrylamide gels) and transferred to PVDF membranes. Membranes were blocked with 5% skimmed milk or bovine serum albumin (BSA) in TBS-0.1% Tween 20 (TBS-T)

and subsequently immunoblotted overnight at 4°C with specific primary antibodies against β-actin (#A5441; Sigma-Aldrich), GAPDH (#2118; Cell Signaling Technology), hexokinase II (#2867; Cell Signaling Technology), HSP90 (#610419; BD Biosciences), LDHA (#3582; Cell Signaling Technology), LDHB (#H00003945-M01; Novus Biologicals), MCT1 (home-made) or MCT4 (#sc-376101; Santa Cruz Biotechnology). After several washes with TTBS, membranes were then incubated (1h, room temperature) with horseradish peroxidase (HRP)-conjugated secondary antibodies (Jackson Immunoresearch) and chemoluminescent signals were revealed by using Amersham ECL Western Blotting Detection Kit (GE Healthcare) on X-ray films in a dark chamber.

RNA extraction and RT-qPCR

Samples were collected from an equal amount of intact subconfluent cells in Tri-Reagent (Molecular Research Center). RNA was recovered after separation in 1-bromo-3-chloropropane and precipitation with isopropanol, washed with ethanol (70%), resuspended in RNAse-free water, and then quantified by spectrophotometry (Nanodrop 1000, Thermo Fisher Scientific). After reverse transcription on 1 µg of total RNA with the RevertAid Reverse-Transcriptase and random hexamers (Thermo Fisher Scientific), quantitative PCR amplification was performed on a ViiA™ 7 real-time PCR system (Applied Biosystems) using SYBR® select master mix for cfx (Thermo Fisher Scientific) and gene-specific primer sequences. Data were analyzed according to ddCt method using human *GTF2B* as reference gene.

Methylated DNA immunoprecipitation (MeDIP)

Methylated DNA was immunoprecipitated by using the MeDIP kit (C02010010; Diagenode) according to manufacturer's recommendations. Immunoprecipitated DNA was analyzed by qPCR using specific primer pairs for the human *SLC16A1* promoter (region spanning from +42 to +146) (Table S2). MeDIP-qPCR data were normalized by using the percent input method in order to include normalization for both background levels and input chromatin going into the MeDIP.

Dot blot analysis

Genomic DNA was isolated using the AllPrep DNA/RNA mini kit (Qiagen) according to manufacturer's instructions, and then denatured with 0.4 M NaOH, 10 mM EDTA (95°C, 10 min) before being neutralized with ice-cold 2 M ammonium acetate (pH 7.0). Two-fold serial dilutions of DNA were spotted on a nitrocellulose membrane (Bio-Rad). Membranes were washed, air-dried, UV-crosslinked, blocked with 5% half-skimmed milk in PBS-Tween 20 for 1h, and then incubated overnight with an anti-5mC primary antibody (1:500; BI-MECY-0100, Eurogentec). After washes and incubation with HRP-conjugated secondary antibodies (Jackson Immunoresearch), chemoluminescent signals were revealed by using Amersham ECL Western Blotting Detection Kit (GE Healthcare) on X-ray films in a dark chamber. To

ensure equal spotting of total DNA on the membrane, the same blot was stained with 0.02% methylene blue in 0.3 M sodium acetate (pH 5.2).

Bisulfite genomic sequencing

Genomic DNA was extracted using the AllPrep DNA/RNA mini kit (Qiagen) according to manufacturer's instructions, denatured in 0.4 N NaOH and then treated with 4.5 M sodium bisulfite and 0.5 mM hydroquinone (pH 5.0) (for 4h at 50°C with 5 min at 95°C after 3h). Bisulfite-treated DNA was desalted, concentrated on a silica matrix (GeneClean Glassmilk; MP Biomedicals), and then incubated in 0.3 N NaOH (10 min, at room temperature), before being neutralized with 1.9 M ammonium acetate, and precipitated with ethanol 100%. Amplification of the 5 'region of *SLC16A1* (from -111 to +153) from bisulfite-modified DNA was performed by nested PCR using 1/500 of the first PCR product in the second PCR. Primer sequences were designed to recognize the human *SLC16A1* promoter sequence reported elsewhere (Cuff and Shirazi-Beechey, 2002) and are described in Table S2. Amplification products were purified by using the Qiaquick PCR purification kit (Qiagen), cloned into the pCR4-TOPO vector using the TOPO TA cloning kit for sequencing (Life Technologies), and transformed into electrocompetent *Escherichia coli* TOP10 (Life Technologies), according to manufacturer's recommendations. Ampicillin-resistant colonies were screened by direct PCR amplification and then analyzed by using the BigDye Terminator v1.1 cycle sequencing kit (Applied Biosystems) with the -21 M13 forward or M13 reverse primers. Sequences

were resolved on an ABI 3100 genetic analyzer (Applied Biosystems) and analyzed with the FinchTV v1.4.0 software.

Genome-wide methylome analysis

Genomic DNA was extracted using the AllPrep DNA/RNA mini kit (Qiagen) according to manufacturer's instructions. Methylation analysis of bisulfite-treated DNA was carried out at the Genome Centre from Queen Mary University of London, by using the Infinium Human Methylation 450K BeadChip (Illumina) according to a previously published array design (Bibikova et al., 2011). The Illumina Infinium Human Methylation 450K BeadChip allowed to assess the DNA methylation status of 482,421 CpG sites, covering 99% of RefSeq genes and intergenic regions. The DNA methylation level for each interrogated CpG site was reported as a beta value, ranging from 0 (not methylated) to 1 (fully methylated) by using GenomeStudio Methylation module v1.8 (Illumina).

Dosage of extracellular lactate

For lactate dosage, cells ($2x10^5$ cells/well; 3 wells/condition) were seeded in 12-well plates with 2 mL of their routine culture medium. After 24h, medium was replaced by 500 µL of DMEM containing 10 mM L-lactate, 2 mM L-glutamine and supplemented with 10% dialyzed FBS (Sigma-Aldrich). Initial concentration of lactate in the experimental medium was also assessed by including control wells containing only cell culture medium (no

cells) on each plate. After incubation for 24h, extracellular media were collected and deproteinized by centrifugation (15 min, 10,000 rpm, 4°C) in 10 kDa cut-off filter tubes (VWR). Lactate concentrations were measured in the samples (50 µl) by using enzymatic assays (CMA Microdialysis AB) and a CMA 600 analyzer (Aurora Borealis). Data analysis was done by calculating the difference in lactate concentrations between the control wells and the experimental wells. Data were then normalized by the protein content in each well and expressed in µmol/hr/µg protein.

Seahorse analysis

Oxygen consumption rate (OCR) and extracellular acidification rate were measured by using the Seahorse XF96 plate reader. All assays were carried out using a seeding density of 30,000 cells/well in non-buffered DMEM, adjusted at pH 7.4 and supplemented with specified metabolic substrates. Mitochondrial respiration and glycolytic capacities were assessed by using the XF Cell Mito Stress Test and XF Glycolysis Stress Test, respectively, according to manufacturer's recommendations. Briefly, mitochondrial function parameters (*i.e.* basal and maximal respirations and ATP production-linked OCR) were evaluated in a DMEM medium containing 10 mM glucose and 2 mM glutamine and after sequential treatment with 1 µM oligomycin, 1 µM carbonyl cyanide-4 (trifluoromethoxy)phenylhydrazone (FCCP) and 0.5 µM rotenone/antimycin A. Glycolytic function (*i.e.* basal glycolysis and glycolytic reserve) was assessed in a DMEM medium containing 2 mM glutamine and after

sequential treatment with 10 mM glucose, 1 µM oligomycin and 50 mM 2-DG. To evaluate their capacity to use specific single substrates, cells were pre-challenged in a substrate-free DMEM medium for 16h before starting the experiment. OCR values were assessed before (3 cycles of 3 min mixing/4 min measuring) and after (6 cycles of 3 min mixing/4 min measuring) the injection of 10 mM glucose, lactate or glutamine (as indicated in the figure legends). In some experiments, 10 µM UK-5099 was injected after lactate treatment and OCR was assessed for 8 cycles of 3 min mixing/4 min measuring. Substrate-dependent OCR were calculated by comparing the values before and after addition of the substrates.

Immunocytochemistry

Cells grown on coverslips were fixed with 4% PFA for 5 min. After blocking with 5% BSA for 1h, cells were incubated overnight at 4°C with an anti-MCT1 antibody (1/200; home-made) or with an anti-MCT4 antibody (1/400; #ab244385; Abcam). Cells were then incubated with an Alexa Fluor 488-conjugated anti-rabbit secondary antibody (#A11034; Thermo Fisher Scientific) for 1h and nuclei were counterstained with DAPI (#D9542; Sigma-Aldrich). Slides were prepared with a fluorescence mounting medium (Dako) and staining was visualized with a Zeiss Imager 1.0 Apotome microscope.

3D spheroid cultures

Spheroids were prepared with native and 3-BrPA-R tumor cells by seeding 1,500 cells/well in Ultra-Low Attachment 96-well plates (Corning) in

DMEM supplemented with 10% heat-inactivated FBS, 25 mM D-glucose and 2 mM L-glutamine. For mixed spheroids, 750 cells of each GFP-expressing native and mCherry-expressing 3-BrPA-R HCT-116 cell population were seeded into the wells. Treatments (5-FU and diclofenac) (mean diameter of spheroids: 300 µm) are renewed every 2-3 days (as indicated in the figure legends) by adding fresh drug-containing medium after the removal of the old one. Spheroid growth was monitored using live-cell phase contrast microscope (Axio Observer, Zeiss); spheroid area was manually measured using ImageJ software by tracing spheroid contours.

For immunofluorescence studies, spheroids were first incubated with 1 µM pimonidazole (overnight at 37°C; #N1165; Sigma-Aldrich) or with 1 mg/mL propidium iodide (PI; 15 min at room temperature; #P4170; Sigma-Aldrich) to label hypoxic areas or dead cells, respectively. Spheroids were then washed twice in PBS, harvested, PFA-fixed and embedded in OCT. PI staining, as well as GFP and mCherry fluorescence intensity, were measured on cryosections (5 µm) with a Zeiss Imager 1.0 Apotome microscope. To stain proliferating cells and hypoxic areas respectively, cryosections were incubated with either anti-Ki67 antibody (#556003, BD Biosciences), or anti-pimonidazole antibody (#PAb2627AP; Hypoxyprobe). Sections were then incubated with Alexa Fluor 488-conjugated anti-mouse (#A11029; Thermo Fisher Scientific) or Alexa Fluor 568-conjugated anti-rabbit secondary antibodies (#A11036; Thermo Fisher Scientific) for 1h at RT; nuclei were counterstained with DAPI (#D9542; Sigma-Aldrich). Slides were prepared with fluorescence mounting medium (Dako), and staining was visualized with a Zeiss Imager 1.0 Apotome microscope. All spheroid samples from a

same experiment were imaged by using the same gain and exposure settings.

Clear, Unobstructed Brain/body Imaging Cocktails and Computational analysis (CUBIC) method was also used for clearing and imaging of 10-day-old mixed HCT-116 spheroids. Briefly, PFA-fixed spheroids were first incubated in CUBIC1 solution (N, N, N', N'-tetrakis (2-hydroxypropyl) ethylenediamine 25%, urea 25%, Triton X-100 15%, H_2O 35%; for 6h at room temperature) and then in CUBIC2 solution (sucrose 50%, urea 25%, 2,2',2'-nitrilotriethanol 10%, H_2O 15%; for overnight at room temperature) before image acquisition using a Lightsheet Z.1 fluorescence microscope (Zeiss).

Flow cytometry

After 72h of treatment with 5-fluorouracil (5-FU), spheroids were collected in round-bottom test tubes (VWR; 734-0000) and washed twice with PBS. Spheroid dissociation was done after addition of trypsin-EDTA (0.05%) and mechanical pipetting and vortexing. GFP- and mCherry-positive cells in suspension were then centrifuged 5 min at 1,500 rpm and the supernatant was replaced by 300 µl flow cytometry buffer (PBS supplemented with 1 mM EDTA and 2% Bovine Serum Albumin (BSA)) for analysis. For each experimental condition, native GFP- and 3-BrPA-R mCherry-labeled cells were separated and quantified as a percentage of the total number of cells with the FACSAria™ II (BD Biosciences). 2D-cultured native UM-UC-3 cells stably expressing either shCTRL or shMCT1 sequences

were detached with trypsin-EDTA (0.05%), collected in round-bottom test tubes (VWR; 734-0000) and washed with PBS. Cells were then incubated for 20 min at 4°C with 200 µl of Cytofix/Cytoperm fixation and permeabilization solution (#554722; BD Biosciences), washed twice with PBS, and incubated 15 min at room temperature with primary antibodies anti-MCT1 (1/200; home-made) or anti-MCT4 (1/200; #ab244385; Abcam). After two washes, cells were finally incubated 15 min in the dark at room temperature with a goat anti-rabbit Alexa Fluor 647-conjugated secondary antibody (1/200; #A-21245; Thermo Fisher Scientific), washed again twice with PBS and resuspended in 200-400 µl of flow cytometry buffer. MCT1 and MCT4 expression was quantified in GFP-positive population of shMCT1-transfected cells and expressed as a percentage of shCTRL-transfected cells.

In vivo mouse experiments

All experiments were performed with 7-week-old female Rj:NMRI-*Foxn1*$^{nu/nu}$ mice from Janvier Labs. Before injection, native HCT-116 (sgCTRL- and sgMCT4-expressing) or SiHa cancer cells were washed twice with PBS, resuspended in 0.9% NaCl (1 x 10^6 cells/100 µl for HCT-116 and 2 x 10^6 cells/100 µl for SiHa) and then injected subcutaneously into the right flank of the animals. When tumors reached a mean diameter of 5 mm, 3-bromopyruvate (2 mg/kg, corresponding to the dose delaying tumor growth without inducing general toxicity in a preliminary *in vivo* pilot study) and/or diclofenac (7.5 mg/kg, dose determined by Renner et al. showing no effect

on mouse tumor growth *in vivo* when diclofenac is administrated alone [142]), both freshly prepared in PBS, were injected intraperitoneally daily.

Quantification and statistical analysis

When applicable (*i.e*, more than 2 biological replicates), data are presented as mean ±SEM. Statistical analyses were computed with GraphPad Prism 8 software by using one-sample t test, one-way or two-way ANOVA (Bonferroni's post-hoc test) and log-rank test, where appropriate, as indicated in the figure legends. Statistical significance is indicated in the figures as follows: *, $p < 0.05$; **, $p < 0.01$; ***, $p < 0.001$. Non-statistically significant data ($p>0.05$) are referred to as "n.s".

2. Insights on the capacity of metabolism-targeting treatments to enhance cytolytic activity of T cells

Catherine Vander Linden[1], Davide Brusa[2], Céline Guilbaud[1], Cyril Corbet[1], Olivier Feron[1,3,*]

[1] Pole of Pharmacology and Therapeutics (FATH), Institut de Recherche Expérimentale et Clinique (IREC), UCLouvain, 57 Avenue Hippocrate B1.57.04, 1200 Brussels, Belgium.
[2] Flow Cytometry Platform, Institute of Experimental and Clinical Research (IREC), Université Catholique de Louvain (UCLouvain), 1200 Brussels, Belgium.
[3] Lead contact
[*] Correspondence olivier.feron@uclouvain.be

The data detailed in the first Results chapter have provided the proof of concept that the sequential administration of two different metabolism-targeting drugs may represent an innovative strategy to overcome treatment resistance resulting from cancer cell metabolic plasticity. While this approach paves the way for further studies exploring the combination of various metabolism-targeting drugs, another critical issue to transpose these results in the clinic is related to the effects of these treatments on non-cancer cells present in tumors. In particular, with the flourishing field of immunotherapy and adoptive T cell therapy in the last few years, one cannot make the economy of a fine dissection of the effects of metabolism-targeting drugs on immune cells and more specifically CD8+ T cells. Whether

additive/synergistic or instead counterproductive effects can result from the exposure of cancer cells and T cells to a same drug interfering with key metabolic routes requires systematic studies. In this second part of the thesis, we therefore aimed to examine the direct effects of three anti-metabolic compounds on CD8+ T cell phenotype but also on changes in the T cell response when cancer cells are first pre-challenged by these drugs. Both sets of information could be particularly relevant in the context of anticancer adoptive cell therapy.

2.1 Introduction

The deregulation of cellular energetics is nowadays well accepted as a phenotypic alteration sustaining malignant cell growth [8]. Cancer cell metabolism is rewired throughout disease progression under the influence of mutations in oncogenes and tumor suppressor genes, and in response to external constraints from the TME (*e.g.* hypoxia, acidosis or nutrient deprivation) [313]. Since Otto Warburg's seminal discovery of aerobic glycolysis in 1930, numerous studies have focused on targeting cancer cell energy metabolism to unravel innovative anticancer strategies [314]. In this context, a bunch of pharmacological drugs inhibiting the uptake of important metabolic substrates for tumor growth or interfering with the activity of specific metabolic enzymes have been developed, and potential good candidates are currently tested in clinical trials on human patients [315].

On the other hand, immunotherapies have recently brought new hopes for cancer treatment. Central players of the immune system to fight against cancer are the CD8+ T lymphocytes by virtue of their capacity for antigen-directed cytotoxicity [316]. Accordingly, so called « hot tumors » infiltrated by T cells (*e.g.* melanoma and lung cancers) typically demonstrate high response rates to immune checkpoint inhibitors [317]. As cancer cells, T cells have their own metabolic preferences which actually evolve with their differentiation state [220]. After the first antigen exposure, naive T cells become effector T cells (T_{EFF}) and switch from an oxidative metabolism towards the preferential use of aerobic glycolysis to efficiently proliferate and produce cytokines. After antigen clearance, most of T_{EFF} die, but a small fraction of survival T cells give rise to memory T cells (T_{MEM}). T_{MEM} mostly rely on FAO and exhibit mitochondrial biogenesis. Due to their self-renewal and long-term survival capacities, T_{MEM} play a crucial role to avoid cancer relapse [318].

Common metabolic pathways between tumor and immune cells account for a continuous competition for nutrients [319-321]. For instance, the glycolytic activity of cancer cells outcompetes T cells for glucose availability, thereby leading to diminished cytokine production by the latter and tumor progression [256]. Furthermore, high lactate concentrations in the TME associated with low pH values disturb T cell metabolism by inhibiting glycolysis and directly impeding cytotoxic activities [258, 260].

This study aims to bring new insights on the capacity of metabolism-targeting treatments to enhance cytolytic activity of T cells, and consequently to improve response to immunotherapy. More precisely, the

effects of three compounds blocking either OXPHOS, glycolysis or FAO will be used to assess the effects of these metabolic routes on T cell phenotype. As an inhibitor of OXPHOS, we have used CIM203070, of which the structure cannot be revealed for patent issue. Our laboratory has worked for two years on this compound and has validated it as a *bona fide* ETC complex I inhibitor based on a variety of assays including Seahorse measurements on isolated mitochondria. As a glycolysis inhibitor, we have used diclofenac, an NSAID recently identified with potent inhibitory effects on MCT1/4, the main transporters involved in lactate transport [142]. Finally, we have used etomoxir, a compound validated in numerous studies as an inhibitor of CPT1, a key protein involved in the uptake of acyl-CoA in the mitochondria and thus of consecutive β-oxidation [146, 322-325].

2.2 Results and Discussion

2.2.1 FAO inhibition increases glucose consumption and stimulates *in vitro* CD8 T cell proliferation

We have first investigated the effects of 100 nM CIM203070 (OXPHOSi), 100 µM diclofenac (MCTi) and 3µM etomoxir (FAOi) on CD8+ T cell glycolysis and after 36 h incubation. These concentrations were chosen based on the literature and previous experience documenting these concentrations as the lowest giving rise to maximal inhibition of the targeted metabolic paths. For these experiments, we have used CD8+ T cells collected from spleen of C57BL/6 OT-1 mice. OT-1 mice have transgenic T cell receptor

designed to recognize ovalbumin peptide residues 257-264 (OVA257-264/SIINFEKL) in the context of H2-Kb (CD8 co-receptor interaction with MHC class I). OT-1 CD8+ T cells thus primarily recognize the SIINFEKL peptide when presented by the MHC-I molecule. CD8+ T cells were first activated 72 hrs with SIINFEKL peptide and IL-2 before the administration of different metabolic treatments.

As expected, the inhibition of MCT transporter activity with diclofenac significantly reduced glucose consumption and lactate secretion whereas the blockade of OXPHOS complex I significantly increased both parameters (**Figures 28A-B**). Inhibition of FAO induced an increase of glucose consumption but barely altered lactate secretion. We have next examined the effects of the above 3 metabolism-targeting compounds on T cell proliferation using carboxyfluorescein succinimidyl ester (CFSE) dilution assay. We have found that blocking OXPHOS with CIM203070 was detrimental for T cell proliferation (vs. vehicle treatment) contrary to FAOi etomoxir which revealed a highly significant increase in T cell proliferation (as depicted by a global shift toward less-intense CFSE staining) (**Figure 28C**). Treatment with 0.1 mM diclofenac for 48 hrs strongly impacted T cell viability (**Figure 28D**) preventing us to examine the effects of the drug on proliferation. These findings are at odd with the results of Renner et al. who have reported a slightly diminished proliferation of activated T cells upon incubation with 0.2 mM diclofenac for 7 days together with a preserved effector functions [142]. The reasons for these differences are unknown but considering the well documented stimulation of the glycolytic turnover upon

T cell activation, diclofenac cytotoxicity can be explained by the detrimental effects of lactate accumulating into the cytosol.

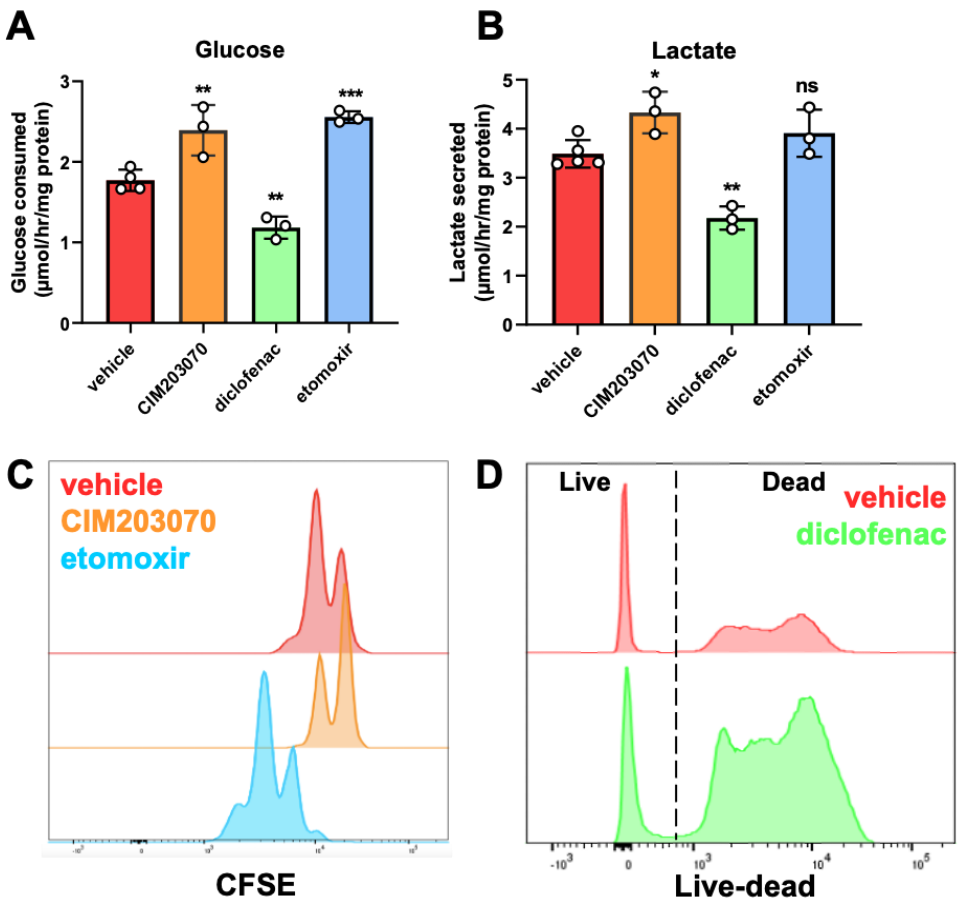

Figure 28: Effects of metabolism-targeting drugs on T cell metabolism and proliferation.

(A-B) *Glucose consumption* ***(A)*** *and lactate secretion* ***(B)*** *of activated T cells upon treatment with 100 nM CIM203070, 0.1 mM diclofenac, 3 µM etomoxir for 36 hrs in glucose and glutamine-containing medium.* ***(C)*** *Proliferation profile of CFSE-loaded activated T cells treated 72 hrs with 100 nM CIM203070 or 3 µM etomoxir.* ***(D)*** *Representative histogram of live and dead T cells after activation and treatment with 0.1 mM diclofenac for 48 hrs. Data are represented as mean ±*

*SD of one experiment with at least three technical replicates. Significance was determined by one-way ANOVA **(A-B)** with Bonferroni multiple-comparison analysis. *p<0.05; **p<0.01; ***p<0.001; ns, not significant.*

2.2.2 Acute treatment of T cells with etomoxir increases cytolytic capacity of CD8+ T cells

We have next examined whether the observed changes in terms of glycolytic activity and proliferation rates induced by OXPHOSi, MCTi and FAOi could alter the cytolytic capacity of CD8+ T cells towards cancer cells. To study this parameter, we have co-cultured *in vitro* murine melanoma cells YUMM1.7 pre-pulsed with SIINFEKL (OVA) peptide together with activated OT-1 T cells (**Figure 29A**). After 6h YUMM1.7 incubation with SIINFEKL peptide, SIINFEKL presentation on H2-Kb could be detected using a dedicated antibody (**Figure 29B**). Using this validated model for specific OT-1 TCR recognition, we have examined whether YUMM1.7 cell integrity was differently influenced upon exposure to OT-1 T cells pre-challenged for 48 hours with either CIM203070, diclofenac or etomoxir. While a trend toward a reduction in the extent of OVA-dependent cell death was observed in the presence of CIM203070 and diclofenac, blocking FAO in T cells with etomoxir led to a significant increase in YUMM1.7 OVA-dependent mortality as revealed by propidium iodide (PI) measurements (**Figures 29C-D)**. This higher cytolytic capacity of etomoxir-treated OT-1 T cells might be explained by a more efficient engagement in glucose (and glutamine) metabolism, since both substrates are required for proliferation and cytolytic activity of

effector T cells [220]. The failure of OXPHOSi to increase cytotoxic effects of OT-1 T cells while the same drug significantly stimulated glycolysis indicate that mitochondrial activity is needed to support the activity of effector T cells.

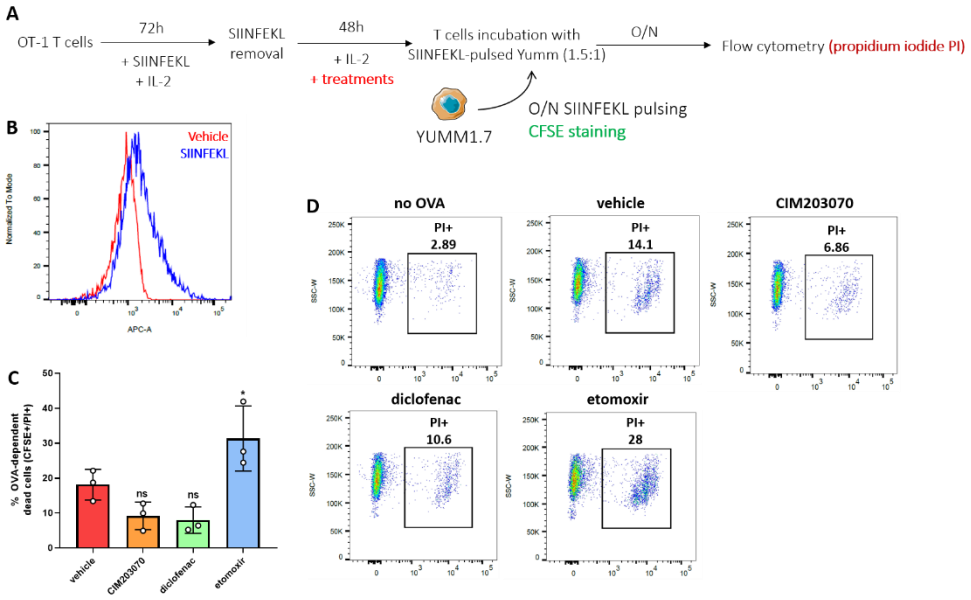

Figure 29: Blocking FAO with etomoxir in T cells increases their cytolytic capacity in vitro.

(A) *To generate OVA-specific CD8+ T cells, OT-1 splenocytes were activated with SIINFEKL peptide and IL-2 (25 U/ml) and expanded for 72 hrs, followed by 48 hrs of exposure to metabolism-targeting treatments. CD8+ T cells were then co-incubated overnight (O/N) with YUMM1.7 cancer cells, previously pulsed with SIINFEKL peptide and stained with CFSE. YUMM1.7 cell death determination was finally carried out by flow cytometry with propidium iodide (PI) staining.* ***(B)*** *SIINFEKL bound to H2-Kb fluorescence intensity in YUMM1.7 cancer cells incubated for 6 hrs with 1 µg/ml SIINFEKL peptide.* ***(C-D)*** *Representative flow cytometry analysis of PI-positive dead YUMM1.7 cells* ***(C)*** *and percentages of OVA-dependent dead cells ("no OVA" values substracted from total percentages)* ***(D)*** *after co-incubation with activated T cells treated for 48 hrs with 100 nM CIM203070, 0.1 mM diclofenac or 3 µM etomoxir. Data are represented as mean ±SD of one experiment with at least*

*three technical replicates. Significance was determined by one-way ANOVA **(D)** with Bonferroni multiple-comparison analysis. *p<0.05; **p<0.01; ***p<0.001; ns, not significant.*

2.2.3 Treatment of cancer cells with OXPHOSi potentiates T cell cytolytic activity

While adoptive T cell transfer offers the possibility to pharmacologically treat CD8+ T cells *in vitro* to increase their effector function (see above), metabolism-targeting drugs can also be used to pre-challenge tumors before administration of T cells (in an environment more favorable to let them exert their cytolytic activity). We have therefore evaluated the impact of the above same three drugs on YUMM1.7 cancer cells before co-incubation with OT-1 T cells (**Figure 30A**). Of note, none of the three drugs significantly altered cancer cell viability, the proportion of dead cells ranging between 8 and 13% of the total YUMM1.7 cell population (**Figure 30B**). Although T cell-induced OVA-dependent cell death was not significantly altered by YUMM1.7 pre-treatment with diclofenac and etomoxir, a net increase in cell death was observed in cancer cells pre-challenged with CIM203070 (**Figures 30C-D**). Since high lactate concentrations associated with acidic pH could impair T cell glycolytic metabolism, cytokine secretion and cytolytic activity [258, 326], we have next examined whether YUMM1.7 treatments led to changes in extracellular lactate concentrations. Changes in lactate release were similar to the measurements performed in T cells (**Figure 28C**) with extracellular lactate

levels being increased by both CIM203070 and etomoxir, and reduced upon diclofenac exposure (**Figure 30E**). As expected, the beneficial effects of OXPHOS inhibition in cancer cells before T cell exposure could therefore not be explained by a reduced glycolytic turnover and lesser lactate/H^+ concentrations in the extracellular medium. An alternative hypothesis is the possibility that inhibiting OXPHOS has led to a reduction in metabolic hypoxia (*i.e.*, less O_2 being consumed because of the interruption of ETC) which could in turn reduce the expression of PD-L1 inhibitory receptor (known to be a direct target of HIF-1α protein) [275]. Tumor cell oxidative metabolism has also been linked to the resistance to PD-1 blockade immunotherapy in melanoma [327]. More work is needed to examine whether less PD-1/PD-L1 inhibitory signaling is dampened upon OXPHOS complex I inhibition. Interestingly, tumor re-oxygenation upon exposure to OXPHOS complex I inhibitor IACS-010759 was recently shown to increase the efficacy of radiotherapy in PD-1-resistant NSCLC adenocarcinoma mouse models [328]. In a pilot study, we have therefore examined the effects of the MPC inhibitor 7ACC2 that our lab previously documented to radiosensitize tumors through a similar reoxygenation process [161]. A non-significant trend toward an increase in the capacity of OT-1 T cell to kill 7ACC2-pretreated YUMM1.7 cancer cells was observed, further supporting the hypothesis of an increase in tumor O_2 availability being favorable for T cell activity (**Figure 30F**).

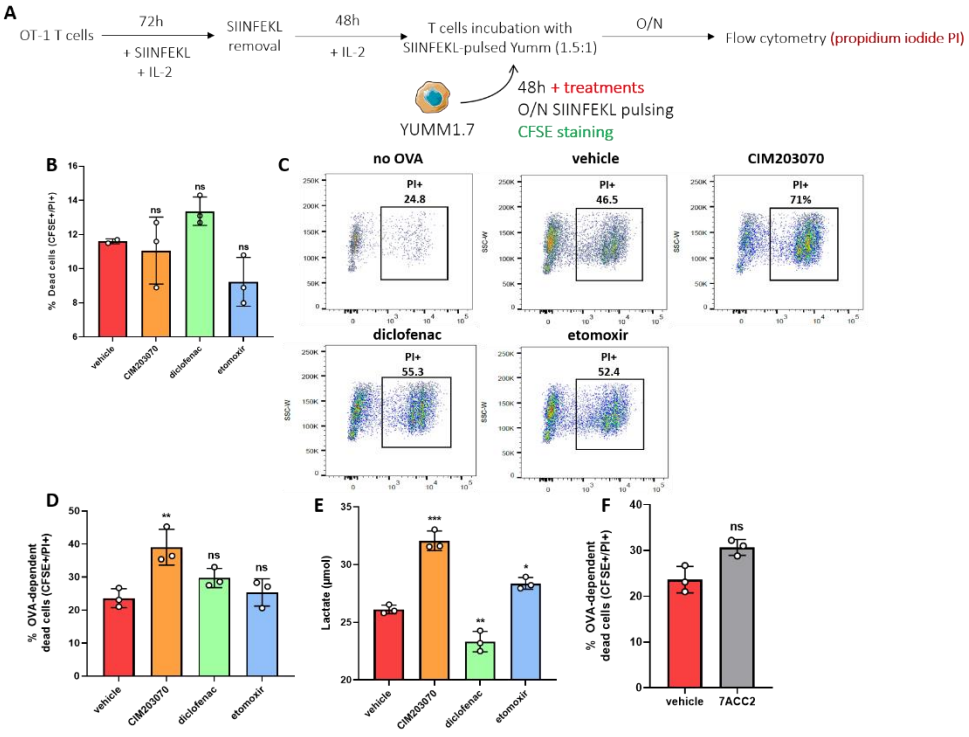

Figure 30: Blocking OXPHOS in cancer cells potentiates T cell cytolytic activity. ***(A)*** *To generate OVA-specific CD8+ T cells, OT-1 splenocytes were activated with SIINFEKL peptide and IL-2 (25 U/ml) and expanded for 72 hrs, followed by 48 hrs without peptide. CD8+ T cells were then co-incubated overnight (O/N) with YUMM1.7 cancer cells, previously pulsed with SIINFEKL peptide, stained with CFSE and exposed for 48 hrs to metabolism-targeting treatments. YUMM1.7 cell death determination was finally carried out by flow cytometry with propidium iodide (PI) staining.* ***(B)*** *Percentage of YUMM1.7 dead cells after 48 hrs of treatment with 100 nM CIM203070, 0.1 mM diclofenac or 10 µM etomoxir in RPMI medium.* ***(C-D)*** *Representative flow cytometry analysis of PI-positive dead YUMM1.7 cells treated for 48 hrs with 100 nM CIM203070, 0.1 mM diclofenac or 10 µM etomoxir* ***(C)*** *and percentages of OVA-dependent dead cells ("no OVA" values substracted from total percentages)* ***(D)*** *after co-incubation with activated T cells.* ***(E)*** *Quantification of lactate in the extracellular medium of YUMM1.7 cells treated for 48 hrs with 100 nM CIM203070, 0.1 mM diclofenac or 10 µM etomoxir in RPMI medium.* ***(F)*** *Percentages of OVA-dependent dead YUMM1.7 cells ("no*

*OVA" values substracted from total percentages) treated for 48 hrs with 10 µM 7ACC2 after co-incubation with activated T cells. Data are represented as mean ±SD of one experiment with at least three technical replicates. Significance was determined by one-way ANOVA **(B-D-E-F)** with Bonferroni multiple-comparison analysis. *p<0.05; **p<0.01; ***p<0.001; ns, not significant.*

2.2.4 Blocking OXPHOS complex I promotes T cell memory phenotype

A key aspect for T_{MEM} efficient formation is the complete absence of antigen stimulation after the effector phase. However, in the context of chronic viral infections and cancer, continuous antigen exposure leads to a state of T cell dysfunction named T cell exhaustion [217]. Exhausted T cells (T_{EXH}) are characterized by poor effector functions dictated by loss of cytokine production, low proliferation, expression of inhibitory receptors such as PD-1, LAG-3 and TIM-3 and dysregulated metabolism [329]. We have therefore pursued our analysis of the effects of metabolism-targeting drugs on the memory and exhaustion phenotypes of T cells. To recapitulate T cell exhaustion *in vitro*, we have repeatedly stimulated isolated CD8+ T cells every 48-72 hrs for 10 days with anti-CD3/CD28 beads, in the presence of CIM203070 or etomoxir. Of note, the effects of the glycolysis inhibitor diclofenac on T_{MEM} and T_{EXH} could not be determined because of the high toxicity of this compound on T cells.

We have found that blocking OXPHOS complex I with CIM203070 led to an increase of CD62-L^+/$CD44^+$ T_{MEM} proportion while treatment with FAOi etomoxir had no significant effects (*vs.* vehicle) (**Figure 31**). Since T_{MEM} are

known to mostly rely on long-chain-FAO for survival [330], the results obtained with etomoxir were anticipated. The beneficial effects obtained with CIM203070 may be interpreted by considering that blocking OXPHOS complex I may favor complex II to get fueled by $FADH_2$ generated by FAO. As a first insight to support this hypothesis, we have used the MPC inhibitor 7ACC2 and found that blocking the mitochondrial respiration component supported by pyruvate (but not by acetyl-CoA generated by FAO) led to a significant increase in the T_{MEM} proportion reaching the same extent than that obtained with CIM203070 (**Figure 30**). Further investigation is warranted to determine whether the increased use of fatty acids to sustain mitochondrial respiration accounts for this beneficial effect[180].

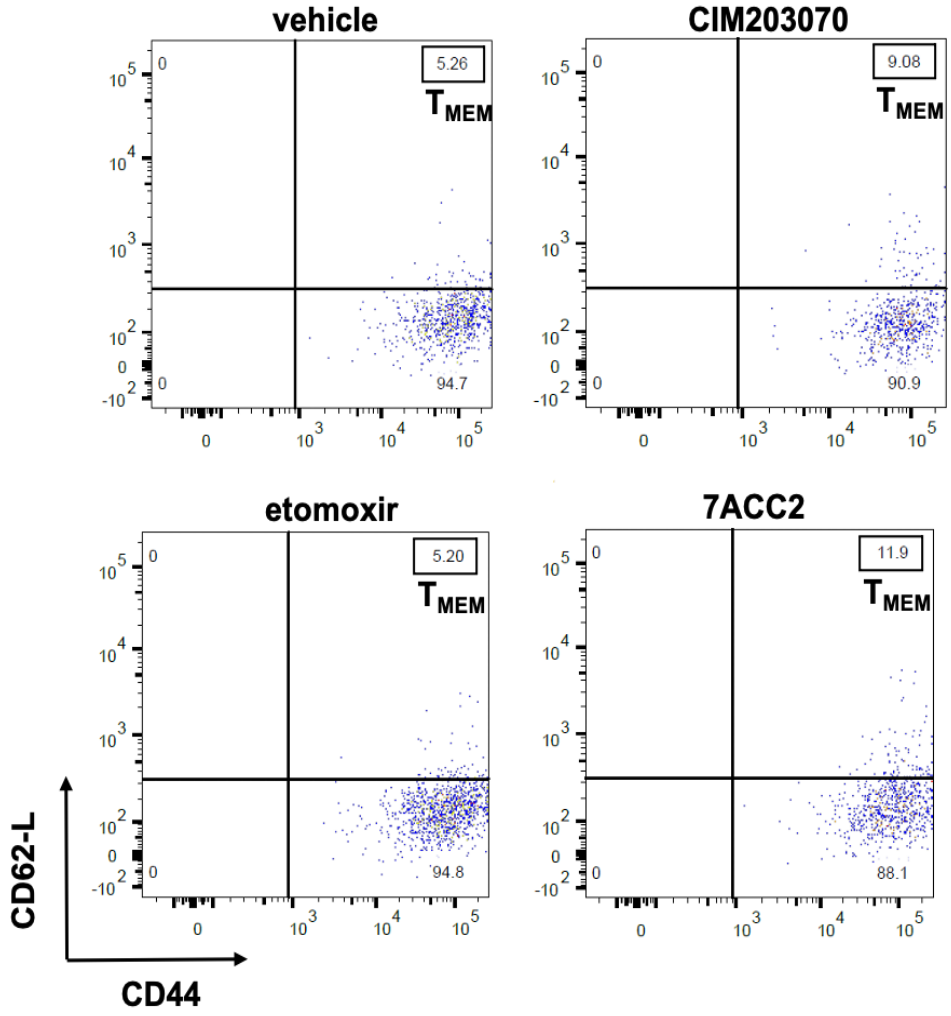

Figure 31: Blocking OXPHOS complex I promotes T cell memory phenotype. *Representative flow cytometry analysis of CD62-L and CD44 staining in activated T cells after 48 hrs of treatment with 100 nM CIM203070, 3 µM etomoxir or 10 µM 7ACC2. This experiment was carried out with 3 technical replicates showing similar results.*

2.2.5 OXPHOSi CIM203070 increases PD-1 expression in exhausted T cells

Finally, using the same protocol of multiple stimulations with anti-CD3/CD28 dynabeads (**Figure 32A**), we have examined if the different metabolism-targeting drugs could lead to changes in the expression of the inhibitory receptors PD-1 and LAG-3 on the surface of T cells. PD-1 represents the historically most described target for ICIs (*i.e.*, pembrolizumab, nivolumab, cemiplimab and dostarlimab) while the interest for LAG-3 is more recent with Relatlimab as the first LAG-3 blocking antibody; the latter recently showed promising response in first-line advanced melanoma in combination with anti-PD-1 nivolumab in a phase III clinical trial (RELATIVITY-047) [331]. We have found a significant increase in PD-1 expression upon treatment with OXPHOS complex I inhibitor CIM203070 but not with FAOi etomoxir (**Figures 32B-C**), and no additional modification in LAG-3 expression in response to either treatment (**Figures 32D-E**). Interestingly, Scharping et al. showed that a loss of mitochondrial mass correlates with an increase of co-inhibitory molecules and that the most exhausted T cells exhibit the lower mitochondrial activity [332]. We can therefore suggest a parallel with our observations related to the increase in PD-1 expression in response to the mitochondrial OXPHOS inhibitor CIM203070. In line with the above results, we have observed a significant higher percentage of OVA-dependent YUMM1.7 cell death in response to CD8+ T cells that undergo the exhaustion protocol in the presence of etomoxir but not CIM203070 (**Figures 32F-G**). Nevertheless,

conclusions regarding these results should be drawn with caution since inhibitory receptors have to be ligated to their corresponding ligands on cancer cells (namely PD-L1 and MHC-II for PD-1 and LAG-3, respectively) to negatively impact on the immune response. Therefore, it would be relevant to study the status of these ligands on cancer cells, alone and in co-culture with T cells. In addition, other parameters such as cytokine production or cell proliferation index should be assessed to further characterize the exhaustion phenotype of the CD8+ T cells in our *in vitro* stimulation model.

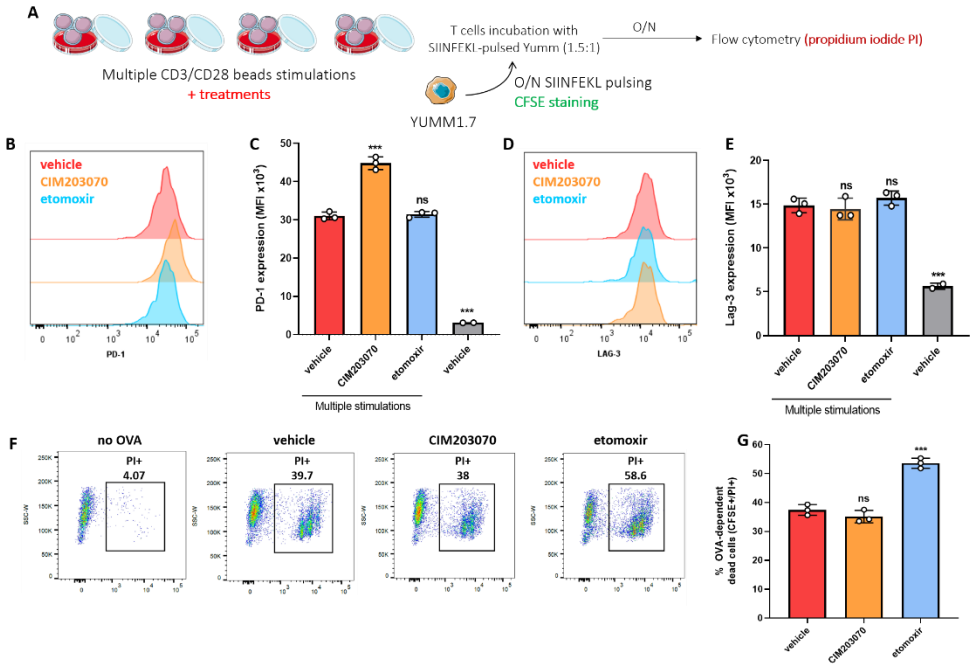

Figure 32: Blocking OXPHOS complex I increases PD-1 expression in T cells in our exhaustion in vitro model.

(A) *To generate T exhausted cells, CD8+ T cells were repeatedly stimulated with anti-CD3/CD28 dynabeads concomitantly with metabolism-targeting treatments. CD8+ T cells were then co-incubated overnight (O/N) with YUMM1.7 cancer cells, previously pulsed with SIINFEKL peptide and stained with CFSE. YUMM1.7 cell death*

determination was finally carried out by flow cytometry with propidium iodide (PI) staining. ***(B-C)*** *Representative flow cytometry analysis of PD-1 staining* ***(B)*** *and relative mean fluorescence intensity values* ***(C)*** *of T cells after multiple stimulations with anti-CD3/CD28 dynabeads every 48-72 hrs concomitantly with 100 nM CIM203070 or 3 µM etomoxir for 10 days.* ***(D-E)*** *Representative flow cytometry analysis of LAG-3 staining* ***(D)*** *and relative mean fluorescence intensity values* ***(E)*** *of T cells after multiple stimulations with anti-CD3/CD28 dynabeads every 48-72 hrs concomitantly with 100 nM CIM203070 or 3 µM etomoxir for 10 days.* ***(F-G)*** *Representative flow cytometry analysis of PI-positive dead YUMM1.7 cells* ***(F)*** *and percentages of OVA-dependent dead cells ("no OVA" values substracted from total percentages)* ***(G)*** *after co-incubation with T cells stimulated with anti-CD3/CD28 dynabeads every 48-72 hrs concomitantly with 100 nM CIM203070 or 3 µM etomoxir for 10 days. Data are represented as mean ±SD of one experiment with at least three technical replicates. Significance was determined by one-way ANOVA* ***(C-E-G)*** *with Bonferroni multiple-comparison analysis. *p<0.05; **p<0.01; ***p<0.001; ns, not significant.*

2.3 Conclusions and perspectives

In the last few years, adoptive cell therapy (ACT) has emerged as a therapeutic option for patients with advanced cancers [333]. ACT is a type of immunotherapy consisting in taking patient's own T cells from blood or from tumor tissue, and giving the T cells back to the patient after a large expansion phase in the laboratory. T cells may be modified *in vitro* before the growing phase to more efficiently target the patient's cancer cells. For instance, the insertion of a CAR (*i.e.* artificial engineered receptor combining both antigen-binding and T cell activating functions into a single receptor) results in genetically modified T cells called « CAR-T cells » ; high efficacy of CAR T cells were documented in patients with relapsed or refractory B-cell

acute lymphoblastic leukemia [334]. ACT treatment is of particular interest in the context of the use of metabolism-targeting drugs since it allows T cells to be treated *in vitro*, without any leakage of the drug towards cancer cells or other healthy cells from the TME. Inversely, cancer cells may be treated in parallel with drugs targeting other metabolic pathways before the adoptive transfer of T cells. Interestingly, Klein Geltink et al. have recently showed that transient glucose restriction in activated CD8+ T_{EFF} cells enhanced effector functions (*i.e.* cytokine and granzyme B production) and that the consequent ACT in murine lymphoma model could lead to complete tumor clearance [335]. These results further support the relevance of *in vitro* T cell metabolic conditioning to synergize with immunotherapy benefits.

The main findings of this work are the identification of distinct benefits (in terms of immune response) resulting from the treatment with the OXPHOSi CIM203070 and the FAOi etomoxir. First, we have shown that acute treatment of activated T cells with etomoxir leads to an increase of their proliferation rates *in vitro*, and to higher cytotoxic capacities towards YUMM1.7 melanoma cancer cells. We have also documented that the concomitant long-term administration of etomoxir to multiple stimulations of CD8+ T cells in an *in vitro* exhaustion model does not lead to additional PD-1 surface expression while increasing the extent of OVA-dependent cancer cell death. Second, we identified the OXPHOS complex I inhibitor CIM203070 as a potential candidate to favor the T_{MEM} over T_{EXH} phenotype acquisition, probably in response to $FADH_2$ production from FAO to sustain OXPHOS complex II activity. We have also shown that pre-treatment of cancer cells for 48 hrs with CIM203070 before co-incubation with activated

T cells potentiates T cell cytotoxic activity. By contrast, we found highly detrimental effects of the glycolytic flux inhibitor diclofenac on T cell viability and proliferation, already detectable after 48 hrs but even more dramatically after long-term treatment.

As a perspective, an *in vivo* model of ACT to treat melanoma-bearing mice could thus take advantage of T cell *in vitro* treatment with etomoxir whilst OXPHOSi would be administered *in vivo*. Etomoxir should contribute to enhance the cytotoxic potential of T cells and to stimulate *in vitro* T cell proliferation. The latter is crucial since the growing phase of T cells before re-injection to the patient is often rate-limiting for a successful ACT procedure. In parallel, tumor-bearing mice would be treated with an inhibitor of mitochondrial complex I in an attempt to recapitulate the increased cytotoxic activity of T cells put in contact with cancer cells pre-challenged with such inhibitor. Although the above situation would represent our priority, other combinations remain attractive. The advantages in terms of T_{MEM} phenotype conferred by CIM203070 treatment could be particularly relevant in a model of tumor relapse (as possibly obtained after primary tumor removal). Etomoxir treatment of tumor-bearing mice could also be relevant since we recently reported that cancer cells located in the acidic environment of primary tumors were among the most metastasis-prone cancer cells but also highly dependent of FAO to provide energy to sustain invasiveness (upon lipid droplet lipolysis) [97].

2.4 Methods

Animal strains

Genetically engineered immunodeficient C57BL/6-Tg(TcraTcrb)1100Mjb/Crl OT I Mice (male) were purchased from Charles River. Splenocyte isolation is performed when mice are between 6 and 12-week old. Studies using mice were performed after approval of the UCLouvain ethic committee (approval ID 2020/UCL/MD/032) and were carried out according to national care regulations. All mice were housed in the facility of the Institute de Duve (DDUV) at UCLouvain.

Cell lines

The murine skin melanoma cell line YUMM1.7 (CRL-3362) was acquired in the last three years from ATCC and was kindly provided from Prof. Bénédicte Jordan's REMA pole from UCLouvain. Cells were stored according to the supplier's instructions and used within 6 months after resuscitation of frozen aliquots. YUMM1.7 cells were maintained in DMEM/F-12 GlutaMAX™ containing 25 mM D-glucose and supplemented with 10% heat-inactivated FBS and 1% P/S in a humidified atmosphere at 37°C and 5% CO_2. Cells were tested for mycoplasma contamination with the MycoAlert™ Mycoplasma Detection kit (Lonza) before being used.

T cell isolation, stimulation and culture

Spleens of OT-I mice were isolated, washed twice in PBS and gently scratched out through a 40 µm strainer to obtain single cell suspension. Erythrocytes were removed with RBC lysis buffer (Roche). Splenocytes were resuspended at 10^6 cells/ml in RPMI-GlutaMAX™ medium containing 25 mM glucose and supplemented with 10% heat-inactivated FBS, 1% P/S, 1 mM sodium pyruvate (#11360070; ThermoFisher Scientific) and 50 µM 2-mercaptoethanol. For CD8 T cell activation, OT-I splenocytes were incubated for 72 hrs in a 24-well plate under humidified atmosphere at 37°C and 5% CO2 with 1 µg/ml of SIINFEKL peptide (#HY-P1489; MedChemExpress), 1 µg/ml anti-CD28 antibody (#553294; BD Biosciences) and 25 U/ml mouse recombinant IL-2 (#78081; Stemcell technologies).

For T cell exhaustion model, CD8-positive lymphocyte population was first negatively isolated from total splenocytes with CD8a+ T cell Isolation Kit (#130-104-075; Miltenyi Biotec) and subsequently seeded at 10^6 cells/ml in RPMI medium with Dynabeads™ Mouse T-Activator CD3/CD28 (#11452; ThermoFisher Scientific) and 30 U/ml IL-2 at 1:1 ratio according to supplier's instructions. Every 2-3 days, dynabeads were magnetically removed, and CD8 lymphocytes were resuspended at 10^6 cells/ml in RPMI medium with fresh dynabeads for 10 days.

Cell treatment

YUMM1.7 cell treatment for cytotoxic assay was performed in full RPMI culture medium for 48 hrs with 100 nM CIM203070, 0.1 mM diclofenac

(#S0765000; Sigma-Aldrich), 10 µM etomoxir (Tocris) or 10 µM 7ACC2. CIM203070 and 7ACC2 were synthesized and purified at Centre for Drug design and Discovery (Heverlee; Belgium).

For T cell treatment, cells were carefully collected after 72 hrs of SIINFEKL-mediated activation, reseeded at $2x10^6$ cells/ml in a 24-well plate and incubated 48 additional hours in RPMI supplemented with 100 nM CIM203070, 0.1 mM diclofenac, 3 µM etomoxir or 10 µM 7ACC2 and 25 U/ml IL-2. Finally, live cells were isolated with Ficoll-Paque™ (#17-5442; VWR) and washed twice in PBS before being used. In T cell exhaustion model, same concentrations of treatments were administrated to CD8 T cells concomitantly with anti-CD3/CD28 dynabeads.

CD8 T cell proliferation assay

To assess T cell proliferation, CD8 naive T cell population was negatively isolated from OT-I splenocytes and subsequently stained with CellTrace™ CFSE Proliferation Kit (#C34554; ThermoFisher Scientific) for 20 min at 37°C protected from light, according to supplier's instructions. 10^5 T cells were stimulated with anti-CD3e (coated, 0.5 µg/ml) (#100201; BioLegend) in combination with anti-CD28 antibody (soluble, 0.7 µg/well) and cultured for 72 hrs in 200 µl of RPMI medium in a 96-well flat bottom plate concomitantly with 100 nM CIM203070 or 3 µM etomoxir under humidified atmosphere at 37°C and 5% CO_2. CFSE intensity staining was measured with flow cytometry and histograms were obtained using the Proliferation Tool of FlowJo v10 program.

T cell proliferation with diclofenac was determined by staining SIINFEKL-stimulated OT-I cells with CellTrace™ CFSE Proliferation Kit prior 48 hrs of incubation with 100 µM diclofenac and 25 U/ml IL-2. Proliferation is reflected by CFSE mean fluorescence intensity among CD8 positive T cell population, as determined by flow cytometry analysis.

Dosage of extracellular glucose and lactate

For glucose and lactate dosage, OT-I cells were carefully collected after 72 hrs of SIINFEKL-mediated activation and CD8 positive T cells were subsequently negatively isolated with CD8a+ T cell Isolation Kit (#130-104-075; Miltenyi Biotec). CD8 T cells were then seeded at 400,000 cells/ml in DMEM containing 10 mM glucose, 2 mM glutamine and supplemented with 10% dialyzed FBS (Sigma-Aldrich) and adequate treatments. Initial concentration of glucose in the experimental medium was also assessed by including control wells containing only cell culture medium (no cells) on each plate. After incubation for 36 hrs, extracellular media were collected and deproteinized by centrifugation (15 min, 10,000 RPM, 4°C) in 10 kDa cut-off filter tubes (VWR). Glucose and lactate concentrations were measured in the samples (75 µl) by using enzymatic assays (CMA Microdialysis AB) and a CMA 600 analyzer (Aurora Borealis). Data analysis was done by calculating the difference in glucose and lactate concentrations between the control wells and the experimental wells. Data were then normalized by the protein content in each well and expressed in µmol/hr/mg protein.

Cytotoxic assay

Before incubation with isolated live CD8 T cells, YUMM1.7 cells were pulsed overnight with SIINFEKL peptide, washed twice with PBS and stained with CellTrace™ CFSE Proliferation kit for 20 min at 37°C protected from light, according to supplier's instructions. YUMMM1.7 cells were then plated at 40,000 cells/well in a 96-well plate, before adding 60,000 activated T cells (ratio 1:1.5) 3 hrs later. After overnight co-incubation in a humidified atmosphere at 37°C and 5% CO2, YUMM1.7 cells and T cells were carefully collected by mechanical pipetting or upon addition of 30 µl trypsin-EDTA (0.05%) (#25300054; Gibco) respectively in round-bottom test tubes (734-0000; VWR). YUMM1.7 population was determined by CFSE-positivity and mortality was subsequently assessed with flow cytometry by adding 3 µl of propidium iodide (PI) (#P4170; Sigma-Aldrich, 1 mg/ml) in every test tubes.

Flow cytometry

Fluorochrome-conjugated anti-mouse monoclonal antibodies anti-SIINFEKL bound to H2-Kb (#141603), anti-CD62-L (#161202), anti-CD44 (#156002), anti-PD-1 (#114101) and anti-LAG-3 (#125209) were purchased from BioLegend. Staining was performed in flow cytometry buffer (PBS supplemented with 1 mM EDTA and 2% Bovine Serum Albumine) for 20 min at room temperature in the dark. Dead cells were excluded with the Fixable Viability Dye eFluorTM 780 (#65-0865-14; ThermoFisher Scientific) and T cell

purity was determined by CD8 expression (#162302; BioLegend). Data were analyzed with FlowJo v10 program.

Quantification and statistical analysis

When applicable (*i.e.*, more than 3 technical replicates or 2 biological replicates), data are presented as mean ± SD. Statistical analyses were performed with GraphPad Prism 8 software y using on-way ANOVA (Bonferroni's post-hoc test) when appropriated, as indicated in the figure legends. Statistical significance is indicated in the figures as follows: *, $p < 0.05$; **, $p < 0.01$; ***, $p < 0.001$. Non-statistically significant data ($p>0.05$) are referred to as "n.s".

General discussion

1. Achievements and significance

Metabolic inhibitors aim to interfere with bioenergetic and biosynthetic processes and are increasingly investigated as innovative anticancer treatments. Although they often exhibit promising antitumor effects in preclinical studies, the clinical applicability of metabolism-interfering strategies is hampered by the capacities of cancer cells to reprogram their metabolic preferences, thereby leading to the occurrence of resistance mechanisms and long-term therapeutic failure. Several cases of tumor relapse were indeed described after monotherapy with the few metabolic inhibitors that reached the clinics. For instance, although the IDH1 inhibitor Ivosidenib (AG-120) has initially shown progression-free survival improvements compared with placebo in cholangiocarcinoma patients bearing IDH1 mutations in an international phase III clinical study [336], receptor tyrosine kinase pathway mutations, second-site IDH1 mutations and IDH2 mutations were further identified to contribute to primary resistance to Ivosidenib [337]. In parallel, Enasidenib (AG-221), a selective small molecule inhibitor of mutant IDH2, has been reported to produce a clinical response in 40% of treated patients with relapsed/refractory AML [338] but therapy resistance was also described, with the emergence of second-site IDH2 mutations that restore the production of the oncometabolite 2-hydroxyglutarate [339]. These examples are actually

recapitulating the conventional mechanism leading to the failure of targeted therapies such as TKIs, and often the need to use a second generation TKI to restore a therapeutic blockade (until a new occurrence of mutation-based resistance). There are however examples where the resistance to antimetabolic anticancer drugs doe not involves mutation-based mode of resistance but an adaptation of the metabolic preference of the treated cancer cells. For instance, endogenously produced pyruvate secreted by TNBC cells was recently documented to act in a paracrine manner to significantly decrease the sensitivity to Telaglenastat (CB-839), a potent, selective and orally bioavailable inhibitor of GLS [340]. To consider the occurrence of such metabolic adaptation to drugs as a source of vulnerability instead of a relentless failure of metabolism-targeting strategies was the aim of the first part of my thesis.

Since cancer cells exhibit increased energy requirements in comparison to normal cells, the use of metabolic inhibitors has been commonly thought to restrictively affect cancer cells. However, such statement is only partially true and a second issue for most anticancer metabolic inhibitors resides in their low therapeutic index (*i.e.* their capacity to spare healthy cells/tissues). In particular, altering metabolic pathways in immune cells can disturb anticancer immune response including those facilitated by the new generation of ICIs. Metabolic reprogramming of T cells to acquire their effector function upon TCR engagement represents a paradigmatic example of a critical path that may suffer from a systemic interference with cell metabolism. The second part of my thesis aimed to bring new insights to rationalize the choice of metabolism-targeting

treatments able to impact cancer cells while enhancing or at least maintaining the activity of CD8+ effector T cells.

In the first part of this thesis, we have documented that cancer cells exposed to a first anti-metabolic drug develop stable new metabolic addictions, allowing the use of a second metabolism-targeting treatment to be lethal. As a first treatment, we have used 3-BrPA, a drug known to exert inhibitory effects on glycolysis, either resulting from hypoxia or from tumor specificities (*i.e.*, Warburg effect). This halogenated derivative of pyruvate has the reputation to be a potent anticancer agent, able to cause rapid toxicity to cancer cells without affecting normal tissues due to the high glucose turnover in cancer cells but also to have off-targets because of its alkylating properties (described in paragraph « 3. Limitations) [341]. The induction of apoptosis after a rapid ATP depletion (the so-called « metabolic catastrophe ») by 3-BrPA was documented in multiple tumor models, both *in vitro* and *in vivo* [279, 294, 342, 343]. However, the clinical use of 3-BrPA has been limited due to side effects and drug resistance establishment [344]. To overcome the issue of systemic toxicity (in particular in erythrocytes), Hanafy et al. have demonstrated that encapsulating 3-BrPA in a structure coated with folic acid and bovine serum albumin may avoid deleterious leakage of 3-BrPA out of vehicle when circulating in the bloodstream [345].

In our study, we have shown that resistance to 3-BrPA in three different cancer cell lines is mediated by an almost complete downregulation of protein and mRNA expression of MCT1 (**Figure 33**), previously identified by Birsoy et al. as the protein responsible for 3-BrPA

uptake by cancer cells [115]. We have next documented that *SLC16A1*/MCT1 gene silencing is the direct consequence of an epigenetic adaptation of the cancer cells, with hypermethylation in the gene promoter upon 3-BrPA treatment. While the mechanisms remain poorly understood, alterations in DNA methylation in response to anticancer drugs are nowadays well documented [302]. Increasing evidence actually shows that promoter hypermethylation and consequent gene silencing are epigenetic hallmarks of multidrug resistance. For instance, in line with our findings, DNA hypermethylation has been shown to play a major role in generating drug-resistant cancer cell phenotypes by inactivating genes that are required for cisplatin cytotoxicity [346]. Reduced folate carrier gene promoter hypermethylation has also been associated with a lower complete remission rate in patients with primary central nervous system lymphoma treated with high dose of methotrexate-based chemotherapy due to reduced drug uptake [303]. More generally, it is proposed that in response to various environmental stresses including drug exposure, cancer cells trigger various mechanisms driving alterations in gene expression programs [347]. A similar phenomenon was actually reported in plants under stress, with the caveat that some of the stress-driven changes are temporary while other are inheritable to allow the next cell generations to cope with similar stress challenges in the future [348]. In tumors, a combination of genetic and/or epigenetic changes created during the period of stress is also though to result in an altered cellular « memory » that consecutively drives disease progression [349].

In our study, we may interprete the upregulation of the MCT4 isoform in the three 3-BrPA-R cell lines as a direct and necessary consequence of the epigenetic silencing of MCT1 (**Figure 33**). MCT4 thereby became the exclusive transporter to extrude lactate and maintain a sustained glycolytic activity within the resistant cancer cells. This « isoform switching » phenomenon is a well-known mechanism of acquired resistance in cancer. For instance, four clinical cases have identified mutant IDH switching, either from mutant IDH1 to mutant IDH2 or vice versa, as a mechanism of acquired clinical resistance to IDH inhibition in solid and liquid tumors [350]. Similarly, a GLS isoform switch was recently documented to drive therapeutic resistance and disease progression of prostate cancer [351]. In our study, the precise molecular mechanisms supporting MCT4 upregulation are still unknown, even though we showed that HIF-1α is not involved in the process. Still, we can hypothesize the occurrence of a metabolic feedback mechanism triggered by intracellular accumulation of protons and lactate in glycolytic cancer cells [352]. This new acquired phenotype offers 3-BrPA-R cells with several advantages, notably a better resistance to hypoxia and loss of sensitivity to various OXPHOS inhibitors (**Figure 33**). Of note, low proliferative 3-BrPA-R cancer cells localized in the hypoxic core of 3D spheroid models also showed cross-resistance to the chemotherapy compound 5-FU, while this result was not recapitulated with 2D cell monolayers. This last observation also highlighted the importance of considering the influence of TME peculiarities when analyzing drug exposure outcomes since 5-FU did not reveal this mode of resistance when cells were cultured in normal incubator under ambient pO_2. Besides the above

advantages in terms of survival and proliferation, the strict reliance of 3-BrPA-R cancer cells for MCT4 expression to support glycolysis represented the vulnerability we were aiming to. To pharmacologically target MCT4, we used a repurposed drug, namely diclofenac, a NSAID exhibiting MCT4 inhibitory activity in the µM range (with a 10-fold selectivity over MCT1) [142]. Diclofenac was able to induce 3-BrPA-R cell death in 3D spheroids, and interestingly to prevent 3-BrPA resistance establishment in parental cells *in vitro* and *in vivo* (**Figure 33**). While we were using diclofenac in our 3D tumor spheroid and mouse models, other MCT4 inhibitors were reported including AZD0095, a nanomolar range MCT4 inhibitor (with a >1000-fold selectivity over MCT1) [311]. Further investigation is warranted to determine whether this more potent compound could lead to tumor eradication when used in combination with 3-BrPA (instead of tumor growth delay as reported in our study).

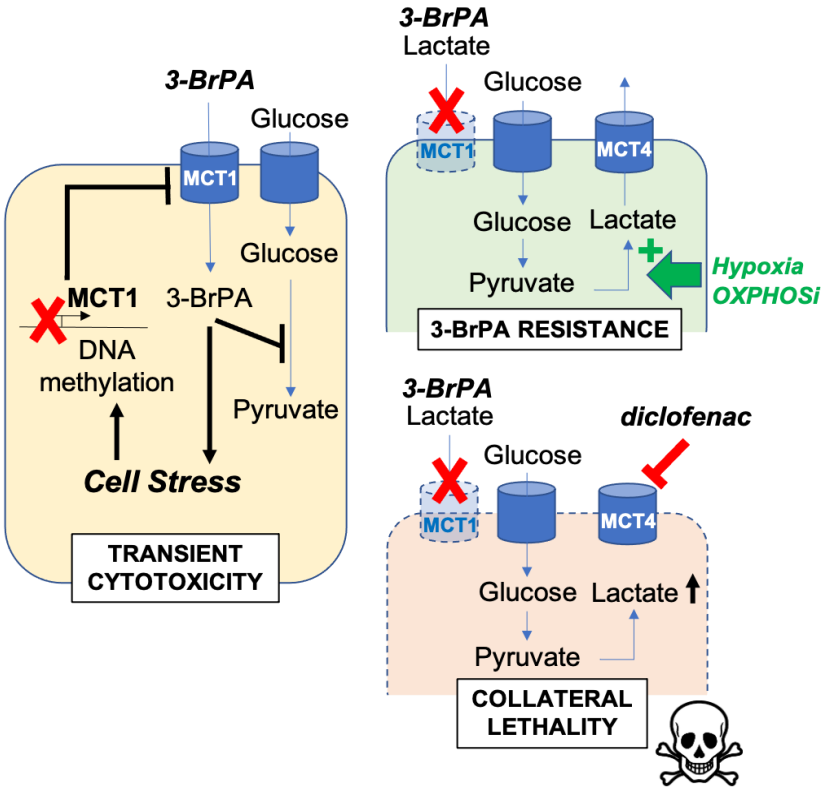

Figure 33: Graphical summary of main achievements related to Results chapter 1. *Cancer cell exposure to the glycolytic inhibitor 3-bromopyruvate (3-BrPA) leads to DNA methylation-dependent silencing of monocarboxylate transporter (MCT)-1, the main entry path for this drug. Resistant cancer cells in turn rely on MCT4 activity, a metabolic vulnerability that can be targeted by repurposed anti-inflammatory drug diclofenac. Abbreviations: OXPHOSi, inhibitor of oxidative phosphorylation.*

In the second part of the thesis, we have investigated the effects of three different metabolism-targeting agents on CD8+ T cells. This study was inspired by the increasing evidence that manipulating the ability of T cells to withstand metabolic stress can enhance the therapeutic potential of T cell-based therapies [220]. Among the drugs that we tested, the FAOi etomoxir

appeared to be particularly suited to enhance CD8+ T cell proliferation and cytotoxic potential *in vitro*, including in an OVA-based model of cancer cell killing using murine melanoma cells and T cells derived from OT-1 mouse model (**Table 3**). With the inhibitor of the ETC complex I CIM203070, an interesting finding was a higher proportion of CD8+ memory T cells after long-time treatment with CIM203070, in adequation with our hypothesis that forcing the use of ETC complex II (to bypass CIM203070-induced complex I inhibition) would favor FAO to furnish the reduced cofactor $FADH_2$. We have however documented that long-term treatment of CD8+ T cells with CIM203070 led to a higher expression of the co-inhibitory molecule PD-1 (**Table 3**). This result further confirms the observation of Scharping et al. that impaired mitochondrial biogenesis in T cells enhances the expression of co-inhibitory molecules and favors the exhaustion phenotype [332]. Finally, treatment with the MCT1/4 inhibitor diclofenac strongly delayed T cell division and eventually led to cell death. The capacity of diclofenac to inhibit cyclo-oxygenase (COX) (described in paragraph « 3. Limitations ») is likely to contribute to the detrimental effects of this drugs on T cells.

Table 3: Summary of main achievements related to Results chapter 2.
This table summarizes the effects of CIM203070, diclofenac and etomoxir treatments on CD8+ T cell phenotype. Abbreviations: FAOi, inhibitor of fatty acid oxidation; MCTi, inhibitor of monocarboxylate transporters; n.d., non determined; OXPHOSi, inhibitor of oxidative phosphorylation; PD-1, programmed cell-death protein 1.

	OXPHOSi (CIM203070)	MCTi (diclofenac)	FAOi (etomoxir)
Cytolytic activity	-	-	+
Memory phenotype	++	n.d. (too toxic)	=
PD-1 expression	++	n.d. (too toxic)	=
Cytolytic activity after exhaustion	=	n.d. (too toxic)	++

2. Therapeutic implications

About the concept of collateral lethality elicited by the 3-BrPA and repurposed diclofenac.

One main innovative idea of this thesis is that instead of a long-term treatment administration leading almost unavoidably to tumor resistance establishment and therapy failure, we could come with a short-term exposure to a first metabolism-targeting drug to shape new metabolic addictions of cancer cells (*i.e*. induction of a « metabolic bottleneck ») that can be specifically targeted with a second treatment, to avoid a potential escape of plastic cancer cells. To the best of our knowledge, this approach was not exploited yet in clinic, neither reported in the scientific literature. Of note, inhibition of glucose metabolism by glycolytic inhibitors including 3-

BrPA, although not used to force the addiction to specific metabolic routes (our study), was previously reported to re-sensitize prednisolone-resistant acute lymphoblastic leukemia cell lines to glucocorticoids [353] or to sensitize myeloid leukemic cells K-562 to anti-leukemic drug daunorubicin [354]. Importantly, limiting the exposure to the first drug may also be beneficial to decrease the extent of potential adverse effects of highly toxic compounds. This may actually apply to 3-BrPA since this drug can cause anasarca (*i.e.* a severe and generalized form of edema, with subcutaneous tissue swelling throughout the body) and a burning sensation at the infusion site [355].

More generally, evolution-based therapeutic strategies consisting in combinatorial or sequential treatments with metabolic inhibitors are currently increasingly investigated. For instance, by tracking leukemia cells *in vivo* and conducting metabolomics on persisting cells following chemotherapy, van Gastel et al. have recently documented that persisting cells use glutamine to preferentially fuel pyrimidine and glutathione generation, (*i.e.*, in a distinctive manner from the pre-chemo growth phase where glutamine fuels the mitochondrial TCA cycle) [356]. In consequence, blunting glutamine metabolism or pyrimidine synthesis selected against residual leukemia-initiating cells and improved survival in leukemia mouse models. Further studies are warranted to determine whether best therapeutic outcomes will be obtained by sequential or simultaneous administration of the drug that induces addiction and the drug that takes advantage of it. Also the strategy may be particularly relevant when drugs directed against two major isoforms of a transporter or an enzyme do exist.

In our hand, we were actually able to recapitulate the upregulation of MCT4 expression with the MCT1 inhibitor AZD3965. The use of a clinically approved compound such as AZD3965 may concretely provide a more favorable regulatory affairs context to launch a clinical study. For the latter, the level of expression of MCT1 could represent a predictive biomarker and would certainly support the selection of cancers with high levels of MCT1 that are associated with poor prognosis and metastasis (*e.g.* cervical cancer, bladder cancer, lung cancer, melanoma and esophageal adenocarcinoma [103, 104, 357-359]).

The use of the NSAID diclofenac to inhibit MCT4 activity in our study supports the growing interest for drug repurposing. Indeed, given the high costs and slow pace of new drug discovery and development, repurposing « old » drugs to treat both common and rare diseases is increasingly becoming an attractive proposition. Repurposing involves the use of de-risked compounds, with potentially lower overall development costs and timelines [360]. The first step of a drug repurposing strategy consists in the identification of a candidate molecule for a given indication. As some NSAIDs, including diclofenac, are monocarboxylates, Renner et al. have hypothesized that diclofenac might directly target MCTs and investigated the effect of different NSAIDs on MCT transport activity in *Xenopus laevis* oocytes expressing either MCT1 or MCT4 [142]. Doing this, they found that diclofenac inhibits transport activity of both MCT1 and MCT4, with a half maximal inhibitory concentration (IC_{50}) of 1.45 ±0.04 µM for MCT1 and 0.14 ±0.01 µM for MCT4. Among the other NSAIDs, lumiracoxib also blocked

MCT1 and MCT4 activity at higher IC_{50} values (of 4.15 µM and 1.12 µM, respectively) and ketoprofen inhibited MCT activity with an almost 100-fold higher IC_{50} than diclofenac; aspirin had no impact on transport activity even at a concentration of 1 mM, thereby adding evidence that diclofenac-mediated inhibitory effects on MCT activity were COX-independent [142]. Recently, the anti-hypertensive drug syrosingopine has also been identified as a dual MCT1 and MCT4 inhibitor, with 60-fold higher potency on MCT4 [297].

About the in vitro prechallenge of T cells before adoptive transfer.

Despite the breakthrough in medical oncology provoked by immune checkpoint inhibitors, many cancer patients do not respond and some initial responders can even become resistant. The search for new immunotherapeutic modalities and/or adjuvant treatments that may benefit immunotherapy is thus always vivid. Among them, ACT using either autologous TILs or engineered CAR T cell have a great potential in mediating long lasting responses against tumors [361]. Of interest, ACT makes possible the *in vitro* treatment of lymphocytes with a given drug or the engineering of CAR T cells with DNA transduction while tumors may be pre-challenged by a drug targeting another metabolic routes. Such option is actually supported by our findings promoting the *in vitro* T cell treatment with etomoxir whilst OXPHOSi could preferentially be administered *in vivo* to impact cancer cells before the adoptive transfer.

Several studies have documented that metabolic conditioning of T cells *in vitro* before autologous transfer to the patient could be useful to promote a strong immune response [269, 335, 362]. Surprisingly, previous reports have shown that T cells expanded in the presence of metabolic stress such as nutrient starvation are better at delaying tumor growth [362, 363]. While we have shown in our study that redirecting CD8+ T cell metabolism towards glycolysis by inhibiting FAO with etomoxir leads to higher proliferation rates and better cytotoxic capacities, Sukumar et al. have found that depriving T cells of glucose *in vitro* supports their stem-like and central memory profiles [362]. These authors also showed that these glucose-starved T cells regained potent effector functions in the tumor when infused to mice. More recently, these results were further supported by Klein Geltink et al., who reported that transient glucose restriction in activated CD8+ T cells metabolically primes effector functions and enhances tumor clearance in mice [335]. Since glucose availability is a requirement for T cell-mediated immunity *in vivo*, one hypothesis explaining why depriving T cells of glucose *in vitro* enhances tumor immunity resides in a metabolic adaptation driven by mitochondrial compensation [220]. Supporting this idea, Chamoto et al. have shown that direct activators of mTOR, AMPK, or PGC-1α promote mitochondrial function in T cells and thereby synergize with PD-1 blockade therapy leading to better immune response against tumors [364]. These observation may actually be related to our demonstration that disturbing mitochondrial function with ETC I inhibitor CIM203070 leads to decreased proliferation rates and lower cytotoxic potential. Altogether, these findings

tend to suggest that as cancer cells, T cells may also exhibit metabolic plasticity to adapt to the local environment.

3. Limitations

The main obstacle encountered during this project is the lack of specificity for metabolism-targeting drugs. Indeed, besides the CIM203070 compound which has been documented to have strong selectivity for ETC complex I (unpublished data from our laboratory), off-target effects have to be considered with 3-bromopyruvate, diclofenac and etomoxir.

3-BrPA is a strong inhibitor of a wide variety of molecules due to its alkylating properties. Hence, 3-BrPA has been shown to inhibit/interfere with the activity of succinate dehydrogenase [365], red cell carbonic anhydrase isoenzyme [366], vacuolar ATPase [367], pyruvate kinase [368], macrophage migration inhibitory factor [369], and ribonuclease A [370]. From a chemistry perspective, it has been shown to alkylate multiple amino acids including cysteine [371], glutamic acid [372], and histidine [373], having the strongest affinity for cysteine residues. While proteomic studies have actually identified numerous potential targets of 3-BrPA alkylation [374], 3-BrPA is today mainly recognized as an anti-glycolytic drug due to the inhibition of HKII and GAPDH enzymes. In a very elegant study, Birsoy et al. have metabolically profiled KBM7 human leukemia cells treated 1 hour with 50 µM of 3-BrPA and showed an accumulation of the glycolytic intermediates preceding the synthesis of GA3P, a substrate for GAPDH, but

a depletion of those that are synthesized later (**Figure 34**). Furthermore, 3-BrPA-treated KBM7 cells accumulated intermediates of the PPP, which branches off from glycolysis above the GAPDH-mediated step [115]. Moreover, since Wang et al. postulated that the coordination of the carboxylate group of the MCT1 inhibitor BAY-8002 may represent the general binding mode for the carboxylate in all monocarboxylate substrates, one may also hypothesize that 3-BrPA binds to the central substrate binding site of MCT1 [108]. Importantly, although several 3-BrPA off-targets unrelated to glycolysis have been identified (see above), it should be emphasized that all the experiments on native and 3-BrPA-R cancer cells reported in our study have been performed in the absence of 3-BrPA since MCT1 epigenetic silencing and subsequent metabolic rewiring of the resistant cells are stable in time. Our main goal here was to induce, characterize and exploit new metabolic addictions in cancer cells after a first metabolism-targeting drug, and 3-BrPA has been used to deliver a proof of concept that is all the more relevant that it was obtained from three independent cancer cell lines.

NSAID drugs such as diclofenac have been shown to exhibit potent anticancer effects, through their classical role of COX inhibitors. Indeed, COX-2, a key isoenzyme responsible for conversion of arachidonic acid to prostaglandins, is induced by various agents such as growth factors and oncogenic signals and is thereby frequently overexpressed in various tumors [375]. Interestingly, in addition to MCT targeting, diclofenac has also been reported to significantly diminish MYC expression and to modulate glucose metabolism through inhibition of GLUT1 and LDHA gene expression in

melanoma, leukemia and carcinoma cell lines whereas aspirin had no similar effect [376]. Even though we have documented that diclofenac kills 3-BrPA-R cancer cells through a likely inhibitory activity on lactate efflux, possible effects on the above other targets should be further evaluated. Also, aspirin should be routinely used as a negative control to exclude any influence of COX inhibitory effects. In our hands, diclofenac has shown to be extremely toxic on mouse CD8+ lymphocytes. The working dose of 0.1 mM was chosen based on a previous study of Renner et al. (*i.e.* the authors who documented the repurposed activity toward MCT4) who reported that affecting glycolysis in T cells with 0.1-0.2 mM of diclofenac does not compromise T cell effector functions and only slightly delays CD8+ T cell proliferation after 7 days of treatment [142]. Of note, while 3-BrPA-R cancer cells do not express MCT1 and the effects of diclofenac were related to MCT4 inhibition in these cells, diclofenac at the dose used in our study has the potential to exert significant inhibitory effects on both MCT1 and MCT4 activity in T cells (see **Table 2**). If T cell activation has been reported to rapidly induce MCT1 protein expression (*vs.* quiescent T cells), MCT4 induction requires more time [142]. Considering the acute toxic effect of diclofenac on activated T cells observed in our hands, if inhibition of lactate transport is involved, it is thus more likely to result from MCT1 inhibition. A direct deleterious effect of COX inhibition on T cells cells can however not be excluded based on the previous reports. For instance, in B cell lymphoma patients treated with CAR T cells targeting CD19 and receiving concomitant NSAIDs, COX inhibition-dependent impairment of the quantity and quality of CAR T cells was documented [377]. NSAIDs have also been reported to block transcription factors

required for the expression of inducible response genes triggered by TCR engagement [378]. The authors have further identified COX-1 and COX-2 as integral and sequential components of TCR signaling to p38 MAP kinase activation. These data may in part explain the deleterious effects of diclofenac in CD8+ T cells that we have reported.

Finally, etomoxir is a widely used small-molecule inhibitor of FAO, through its irreversible inhibitory effects on the CPT1A protein. Using a shRNA approach to reduce CPT1A in T cells, O'Connor et al. have demonstrated that the inhibition of oxidative metabolism in T cells by etomoxir is independent of its effects on FAO at concentrations exceeding 5 µM [379]. These off-target effects are associated with inhibition of oxidative metabolism and induction of severe oxidative stress in T cells through ROS production. This study illustrates the challenges of using (metabolic) inhibitors, and indicates that results derived from etomoxir treatment used for the purpose of CPT1A inhibition must be interpreted cautiously, especially at high concentrations. In our study, we used etomoxir at a working concentration of 3 µM to treat CD8+ T cells thereby *a priori* excluding any major non-CPT1a related effects.

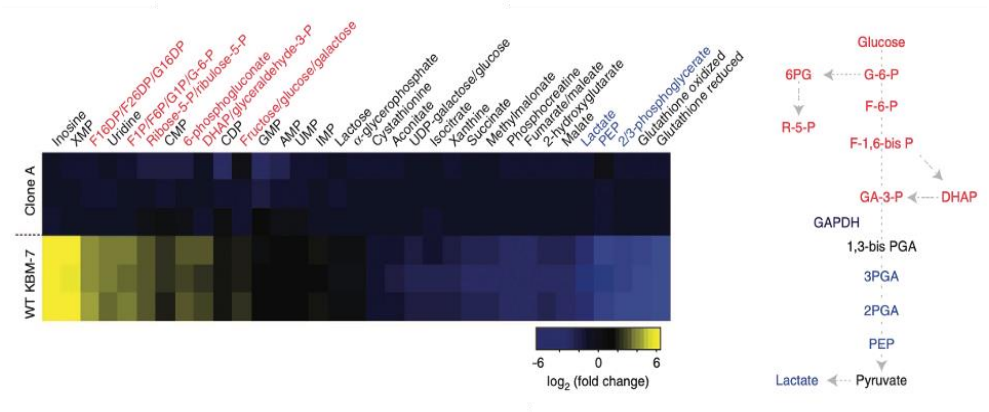

Figure 34: Degree of change in glycolysis-related metabolite abundance upon 3-bromopyruvate treatment.

This figure depicts a heatmap of relative changes in metabolite concentrations between wild-type (WT) and monocarboxylate transporter (MCT)-1-null (clone A) KBM7 cells after 1h of treatment with 50 µM of 3-bromopyruvate (3-BrPA). Intracellular metabolites were obtained and analyzed by liquid chromatography-mass spectrometry. On the right, a schematic of the metabolites that are increased (red) or decreased (blue) in WT and MCT1-null KBM7 cells upon 3-BrPA treatment. Reproduced from [115].

Another obstacle faced during this project was the fragility of T cells when cultured *in vitro*. Indeed, all the steps from spleen isolation to lymphocyte acquisition have to be carried out very cautiously, and many parameters (*e.g.* cell density, degree of activation with anti-CD3 and/or anti-CD28 antibodies, pH of the medium, ratio for co-culture with cancer cells) have to be accurately set up to avoid cell death. The use of primary cultures also induces intrinsic difficulties in the reproducibility of experiments and the generation of reliable data due to inter-animal variability. For instance, the size of isolated spleen and thereby the starting number of splenocytes

can vary according to mouse age or weight. Since genetically engineered OT-1 mice are immunodeficient, they are more subject to infections when hosted in non-SPF animal facilities and any mouse not completely healthy can severely affect lymphocyte quality and experiment outcomes. Nevertheless, the use of model antigens such as OVA has been extremely beneficial to the field of immunology, and the availability of transgenic OT-1 mice that have a T cell repertoire with a defined specificity has provided an important tool to study the selection, activation, and memory response of T cells [380].

4. Conclusions and future directions

In conclusion, our work has brought new insights regarding the use of metabolism-targeting treatments as anticancer therapies. More specifically, our study has contributed to shed some lights on the following issues:

- how to optimize treatment schedule to prevent the escape of metabolically plastic cancer cells;
- how to take advantage of repurposed drugs when the target is difficult to reach due to lack of existing specific drugs;
- how to use metabolism-targeting drugs to metabolically condition CD8+ T cells *in vitro* and thereby increase immunotherapy efficiency.

Our work has also opened several perspectives. The applicability of the sequential (or concomitant) administration of two metabolism-targeting drugs that mutually reinforce their efficacy should be further explored (with drugs more specific than 3-BrPA and diclofenac). Since anticancer treatment resistance often occurs through remodeling of DNA methylation [381], a deeper dissection of the triggering events could unravel generic resistance mechanisms and identify new sets of metabolic addictions. *In vivo* experiments are also needed to confirm that priming CD8+ T cells with etomoxir can lead to higher tumor clearance in mice. Another option that would allow the evaluation of a larger set of drugs interfering with fatty acid metabolism could be to use 3D tumor spheroids or more recently developed patient-derived tumor organoids. Hence, a recently described model of T cells co-cultured with tumor organoids proved to be exploitable to evaluate *ex vivo* T-cell based immunotherapy [382].

Bibliography

1. Mattiuzzi, C. and G. Lippi, *Current Cancer Epidemiology.* J Epidemiol Glob Health, 2019. 9(4): p. 217-222.
2. Chene, G., et al., *[Lucy's cancer(s): A prehistorical origin?].* Gynecol Obstet Fertil, 2016. 44(12): p. 690-700.
3. Ngeow, J. and C. Eng, *Precision medicine in heritable cancer: when somatic tumour testing and germline mutations meet.* NPJ Genom Med, 2016. 1: p. 15006.
4. Stratton, M.R., P.J. Campbell, and P.A. Futreal, *The cancer genome.* Nature, 2009. 458(7239): p. 719-24.
5. Cahill, D.P., et al., *Genetic instability and darwinian selection in tumours.* Trends Cell Biol, 1999. 9(12): p. M57-60.
6. Cusnir, M. and L. Cavalcante, *Inter-tumor heterogeneity.* Hum Vaccin Immunother, 2012. 8(8): p. 1143-5.
7. Hanahan, D. and R.A. Weinberg, *The hallmarks of cancer.* Cell, 2000. 100(1): p. 57-70.
8. Hanahan, D. and R.A. Weinberg, *Hallmarks of cancer: the next generation.* Cell, 2011. 144(5): p. 646-74.
9. McGuirk, S., Y. Audet-Delage, and J. St-Pierre, *Metabolic Fitness and Plasticity in Cancer Progression.* Trends Cancer, 2020. 6(1): p. 49-61.
10. Dai, C., et al., *Metabolomics of oncogene-specific metabolic reprogramming during breast cancer.* Cancer Metab, 2018. 6: p. 5.
11. Min, H.Y. and H.Y. Lee, *Oncogene-Driven Metabolic Alterations in Cancer.* Biomol Ther (Seoul), 2018. 26(1): p. 45-56.
12. Fendt, S.M., C. Frezza, and A. Erez, *Targeting Metabolic Plasticity and Flexibility Dynamics for Cancer Therapy.* Cancer Discov, 2020. 10(12): p. 1797-1807.
13. Marusyk, A. and K. Polyak, *Tumor heterogeneity: causes and consequences.* Biochim Biophys Acta, 2010. 1805(1): p. 105-17.
14. Elia, I., G. Doglioni, and S.M. Fendt, *Metabolic Hallmarks of Metastasis Formation.* Trends Cell Biol, 2018. 28(8): p. 673-684.
15. Scheepers, A., H.G. Joost, and A. Schürmann, *The glucose transporter families SGLT and GLUT: molecular basis of normal and aberrant function.* JPEN J Parenter Enteral Nutr, 2004. 28(5): p. 364-71.

16. Nokin, M.J., et al., *Methylglyoxal, a glycolysis metabolite, triggers metastasis through MEK/ERK/SMAD1 pathway activation in breast cancer.* Breast Cancer Res, 2019. 21(1): p. 11.
17. de Bari, L., et al., *Synthesis and metabolism of methylglyoxal, S-D-lactoylglutathione and D-lactate in cancer and Alzheimer's disease. Exploring the crossroad of eternal youth and premature aging.* Ageing Res Rev, 2019. 53: p. 100915.
18. Martínez-Reyes, I. and N.S. Chandel, *Mitochondrial TCA cycle metabolites control physiology and disease.* Nat Commun, 2020. 11(1): p. 102.
19. Gatenby, R.A. and R.J. Gillies, *Why do cancers have high aerobic glycolysis?* Nat Rev Cancer, 2004. 4(11): p. 891-9.
20. Cardaci, S. and M.R. Ciriolo, *TCA Cycle Defects and Cancer: When Metabolism Tunes Redox State.* Int J Cell Biol, 2012. 2012: p. 161837.
21. Sajnani, K., et al., *Genetic alterations in Krebs cycle and its impact on cancer pathogenesis.* Biochimie, 2017. 135: p. 164-172.
22. Eniafe, J. and S. Jiang, *The functional roles of TCA cycle metabolites in cancer.* Oncogene, 2021. 40(19): p. 3351-3363.
23. López-Lázaro, M., *The warburg effect: why and how do cancer cells activate glycolysis in the presence of oxygen?* Anticancer Agents Med Chem, 2008. 8(3): p. 305-12.
24. Liberti, M.V. and J.W. Locasale, *The Warburg Effect: How Does it Benefit Cancer Cells?* Trends Biochem Sci, 2016. 41(3): p. 211-218.
25. Newsholme, E.A., B. Crabtree, and M.S. Ardawi, *The role of high rates of glycolysis and glutamine utilization in rapidly dividing cells.* Biosci Rep, 1985. 5(5): p. 393-400.
26. DeBerardinis, R.J. and N.S. Chandel, *We need to talk about the Warburg effect.* Nat Metab, 2020. 2(2): p. 127-129.
27. Eales, K.L., K.E. Hollinshead, and D.A. Tennant, *Hypoxia and metabolic adaptation of cancer cells.* Oncogenesis, 2016. 5(1): p. e190.
28. Lee, J.W., et al., *Hypoxia signaling in human diseases and therapeutic targets.* Exp Mol Med, 2019. 51(6): p. 1-13.
29. Nagao, A., et al., *HIF-1-Dependent Reprogramming of Glucose Metabolic Pathway of Cancer Cells and Its Therapeutic Significance.* Int J Mol Sci, 2019. 20(2).

30. Ratcliffe, P.J., *HIF-1 and HIF-2: working alone or together in hypoxia?* J Clin Invest, 2007. 117(4): p. 862-5.
31. Vander Linden, C. and C. Corbet, *Therapeutic Targeting of Cancer Stem Cells: Integrating and Exploiting the Acidic Niche.* Front Oncol, 2019. 9: p. 159.
32. Corbet, C., et al., *The SIRT1/HIF2α axis drives reductive glutamine metabolism under chronic acidosis and alters tumor response to therapy.* Cancer Res, 2014. 74(19): p. 5507-19.
33. Covello, K.L., et al., *HIF-2alpha regulates Oct-4: effects of hypoxia on stem cell function, embryonic development, and tumor growth.* Genes Dev, 2006. 20(5): p. 557-70.
34. Hjelmeland, A.B., et al., *Acidic stress promotes a glioma stem cell phenotype.* Cell Death Differ, 2011. 18(5): p. 829-40.
35. Iommarini, L., et al., *Non-Canonical Mechanisms Regulating Hypoxia-Inducible Factor 1 Alpha in Cancer.* Front Oncol, 2017. 7: p. 286.
36. Hosios, A.M., et al., *Amino Acids Rather than Glucose Account for the Majority of Cell Mass in Proliferating Mammalian Cells.* Dev Cell, 2016. 36(5): p. 540-9.
37. Cormerais, Y., et al., *The glutamine transporter ASCT2 (SLC1A5) promotes tumor growth independently of the amino acid transporter LAT1 (SLC7A5).* J Biol Chem, 2018. 293(8): p. 2877-2887.
38. Bothwell, P.J., et al., *Targeted Suppression and Knockout of ASCT2 or LAT1 in Epithelial and Mesenchymal Human Liver Cancer Cells Fail to Inhibit Growth.* Int J Mol Sci, 2018. 19(7).
39. Oizel, K., et al., *Glutamine uptake and utilization of human mesenchymal glioblastoma in orthotopic mouse model.* Cancer Metab, 2020. 8: p. 9.
40. Bott, A.J., et al., *Oncogenic Myc Induces Expression of Glutamine Synthetase through Promoter Demethylation.* Cell Metab, 2015. 22(6): p. 1068-77.
41. Hernandez-Davies, J.E., et al., *Vemurafenib resistance reprograms melanoma cells towards glutamine dependence.* J Transl Med, 2015. 13: p. 210.
42. Schito, L. and G.L. Semenza, *Hypoxia-Inducible Factors: Master Regulators of Cancer Progression.* Trends Cancer, 2016. 2(12): p. 758-770.

43. Xiang, L., et al., *Glutaminase 1 expression in colorectal cancer cells is induced by hypoxia and required for tumor growth, invasion, and metastatic colonization.* Cell Death Dis, 2019. 10(2): p. 40.
44. Fendt, S.M., et al., *Reductive glutamine metabolism is a function of the α-ketoglutarate to citrate ratio in cells.* Nat Commun, 2013. 4: p. 2236.
45. Corbet, C. and O. Feron, *Tumour acidosis: from the passenger to the driver's seat.* Nat Rev Cancer, 2017. 17(10): p. 577-593.
46. Dierge, E. and O. Feron, *Dealing with saturated and unsaturated fatty acid metabolism for anticancer therapy.* Curr Opin Clin Nutr Metab Care, 2019. 22(6): p. 427-433.
47. Koundouros, N. and G. Poulogiannis, *Reprogramming of fatty acid metabolism in cancer.* Br J Cancer, 2020. 122(1): p. 4-22.
48. Bonnefont, J.P., et al., *Carnitine palmitoyltransferases 1 and 2: biochemical, molecular and medical aspects.* Mol Aspects Med, 2004. 25(5-6): p. 495-520.
49. Corbet, C. and O. Feron, *Emerging roles of lipid metabolism in cancer progression.* Curr Opin Clin Nutr Metab Care, 2017. 20(4): p. 254-260.
50. van Beek, J., *The dynamic side of the Warburg effect: glycolytic intermediate storage as buffer for fluctuating glucose and O (2) supply in tumor cells.* F1000Res, 2018. 7: p. 1177.
51. Modre-Osprian, R., et al., *Dynamic simulations on the mitochondrial fatty acid beta-oxidation network.* BMC Syst Biol, 2009. 3: p. 2.
52. Melone, M.A.B., et al., *The carnitine system and cancer metabolic plasticity.* Cell Death Dis, 2018. 9(2): p. 228.
53. Camarda, R., et al., *Inhibition of fatty acid oxidation as a therapy for MYC-overexpressing triple-negative breast cancer.* Nat Med, 2016. 22(4): p. 427-32.
54. Kloska, A., et al., *Lipophagy and Lipolysis Status in Lipid Storage and Lipid Metabolism Diseases.* Int J Mol Sci, 2020. 21(17).
55. Petan, T., E. Jarc, and M. Jusović, *Lipid Droplets in Cancer: Guardians of Fat in a Stressful World.* Molecules, 2018. 23(8).
56. Garcia-Bermudez, J., et al., *Aspartate is a limiting metabolite for cancer cell proliferation under hypoxia and in tumours.* Nat Cell Biol, 2018. 20(7): p. 775-781.
57. Sullivan, L.B., et al., *Aspartate is an endogenous metabolic limitation for tumour growth.* Nat Cell Biol, 2018. 20(7): p. 782-788.

58. Jain, M., et al., *Metabolite profiling identifies a key role for glycine in rapid cancer cell proliferation.* Science, 2012. 336(6084): p. 1040-4.
59. Possemato, R., et al., *Functional genomics reveal that the serine synthesis pathway is essential in breast cancer.* Nature, 2011. 476(7360): p. 346-50.
60. Maddocks, O.D., et al., *Serine starvation induces stress and p53-dependent metabolic remodelling in cancer cells.* Nature, 2013. 493(7433): p. 542-6.
61. Comerford, S.A., et al., *Acetate dependence of tumors.* Cell, 2014. 159(7): p. 1591-602.
62. Mashimo, T., et al., *Acetate is a bioenergetic substrate for human glioblastoma and brain metastases.* Cell, 2014. 159(7): p. 1603-14.
63. Schug, Z.T., et al., *Acetyl-CoA synthetase 2 promotes acetate utilization and maintains cancer cell growth under metabolic stress.* Cancer Cell, 2015. 27(1): p. 57-71.
64. Peng, H., Y. Wang, and W. Luo, *Multifaceted role of branched-chain amino acid metabolism in cancer.* Oncogene, 2020. 39(44): p. 6747-6756.
65. Sivanand, S. and M.G. Vander Heiden, *Emerging Roles for Branched-Chain Amino Acid Metabolism in Cancer.* Cancer Cell, 2020. 37(2): p. 147-156.
66. Boroughs, L.K. and R.J. DeBerardinis, *Metabolic pathways promoting cancer cell survival and growth.* Nat Cell Biol, 2015. 17(4): p. 351-9.
67. Stow, J.L., Y. Hung, and A.A. Wall, *Macropinocytosis: Insights from immunology and cancer.* Curr Opin Cell Biol, 2020. 65: p. 131-140.
68. Commisso, C., et al., *Macropinocytosis of protein is an amino acid supply route in Ras-transformed cells.* Nature, 2013. 497(7451): p. 633-7.
69. Kamerkar, S., et al., *Exosomes facilitate therapeutic targeting of oncogenic KRAS in pancreatic cancer.* Nature, 2017. 546(7659): p. 498-503.
70. Strohecker, A.M., et al., *Autophagy sustains mitochondrial glutamine metabolism and growth of BrafV600E-driven lung tumors.* Cancer Discov, 2013. 3(11): p. 1272-85.
71. Yang, S., et al., *Pancreatic cancers require autophagy for tumor growth.* Genes Dev, 2011. 25(7): p. 717-29.

72. Guo, J.Y., et al., *Autophagy suppresses progression of K-ras-induced lung tumors to oncocytomas and maintains lipid homeostasis.* Genes Dev, 2013. 27(13): p. 1447-61.
73. Marin-Valencia, I., et al., *Analysis of tumor metabolism reveals mitochondrial glucose oxidation in genetically diverse human glioblastomas in the mouse brain in vivo.* Cell Metab, 2012. 15(6): p. 827-37.
74. Yuneva, M.O., et al., *The metabolic profile of tumors depends on both the responsible genetic lesion and tissue type.* Cell Metab, 2012. 15(2): p. 157-70.
75. Hui, S., et al., *Glucose feeds the TCA cycle via circulating lactate.* Nature, 2017. 551(7678): p. 115-118.
76. Fan, T.W., et al., *Altered regulation of metabolic pathways in human lung cancer discerned by (13)C stable isotope-resolved metabolomics (SIRM).* Mol Cancer, 2009. 8: p. 41.
77. Maher, E.A., et al., *Metabolism of [U-13 C]glucose in human brain tumors in vivo.* NMR Biomed, 2012. 25(11): p. 1234-44.
78. Sellers, K., et al., *Pyruvate carboxylase is critical for non-small-cell lung cancer proliferation.* J Clin Invest, 2015. 125(2): p. 687-98.
79. Hensley, C.T., et al., *Metabolic Heterogeneity in Human Lung Tumors.* Cell, 2016. 164(4): p. 681-94.
80. Faubert, B., et al., *Lactate Metabolism in Human Lung Tumors.* Cell, 2017. 171(2): p. 358-371.e9.
81. Courtney, K.D., et al., *Isotope Tracing of Human Clear Cell Renal Cell Carcinomas Demonstrates Suppressed Glucose Oxidation In Vivo.* Cell Metab, 2018. 28(5): p. 793-800.e2.
82. Buescher, J.M., et al., *A roadmap for interpreting (13)C metabolite labeling patterns from cells.* Curr Opin Biotechnol, 2015. 34: p. 189-201.
83. Davidson, S.M., et al., *Environment Impacts the Metabolic Dependencies of Ras-Driven Non-Small Cell Lung Cancer.* Cell Metab, 2016. 23(3): p. 517-28.
84. Dang, C.V., *MYC on the path to cancer.* Cell, 2012. 149(1): p. 22-35.
85. Horiuchi, D., et al., *MYC pathway activation in triple-negative breast cancer is synthetic lethal with CDK inhibition.* J Exp Med, 2012. 209(4): p. 679-96.

86. Bartman, C.R., et al., *Slow TCA flux implies low ATP production in tumors.* 2021.
87. Corbet, C. and O. Feron, *Metabolic and mind shifts: from glucose to glutamine and acetate addictions in cancer.* Curr Opin Clin Nutr Metab Care, 2015. 18(4): p. 346-53.
88. Corbet, C. and O. Feron, *Cancer cell metabolism and mitochondria: Nutrient plasticity for TCA cycle fueling.* Biochim Biophys Acta Rev Cancer, 2017. 1868(1): p. 7-15.
89. Nakazawa, M.S., B. Keith, and M.C. Simon, *Oxygen availability and metabolic adaptations.* Nat Rev Cancer, 2016. 16(10): p. 663-73.
90. Lyssiotis, C.A. and A.C. Kimmelman, *Metabolic Interactions in the Tumor Microenvironment.* Trends Cell Biol, 2017. 27(11): p. 863-875.
91. Kallinowski, F. and P. Vaupel, *pH distributions in spontaneous and isotransplanted rat tumours.* Br J Cancer, 1988. 58(3): p. 314-21.
92. Schornack, P.A. and R.J. Gillies, *Contributions of cell metabolism and H+ diffusion to the acidic pH of tumors.* Neoplasia, 2003. 5(2): p. 135-45.
93. Mookerjee, S.A., et al., *The contributions of respiration and glycolysis to extracellular acid production.* Biochim Biophys Acta, 2015. 1847(2): p. 171-181.
94. Vaupel, P.W., S. Frinak, and H.I. Bicher, *Heterogeneous oxygen partial pressure and pH distribution in C3H mouse mammary adenocarcinoma.* Cancer Res, 1981. 41(5): p. 2008-13.
95. Helmlinger, G., et al., *Interstitial pH and pO2 gradients in solid tumors in vivo: high-resolution measurements reveal a lack of correlation.* Nat Med, 1997. 3(2): p. 177-82.
96. Corbet, C., et al., *Acidosis Drives the Reprogramming of Fatty Acid Metabolism in Cancer Cells through Changes in Mitochondrial and Histone Acetylation.* Cell Metab, 2016. 24(2): p. 311-23.
97. Corbet, C., et al., *TGFβ2-induced formation of lipid droplets supports acidosis-driven EMT and the metastatic spreading of cancer cells.* Nat Commun, 2020. 11(1): p. 454.
98. Lamonte, G., et al., *Acidosis induces reprogramming of cellular metabolism to mitigate oxidative stress.* Cancer Metab, 2013. 1(1): p. 23.

99. Sonveaux, P., et al., *Targeting lactate-fueled respiration selectively kills hypoxic tumor cells in mice.* J Clin Invest, 2008. 118(12): p. 3930-42.
100. Boidot, R., et al., *Regulation of monocarboxylate transporter MCT1 expression by p53 mediates inward and outward lactate fluxes in tumors.* Cancer Res, 2012. 72(4): p. 939-48.
101. Feron, O., *Pyruvate into lactate and back: from the Warburg effect to symbiotic energy fuel exchange in cancer cells.* Radiother Oncol, 2009. 92(3): p. 329-33.
102. Johnson, J.M., et al., *MCT1 in Invasive Ductal Carcinoma: Monocarboxylate Metabolism and Aggressive Breast Cancer.* Front Cell Dev Biol, 2017. 5: p. 27.
103. Zhang, G., et al., *MCT1 regulates aggressive and metabolic phenotypes in bladder cancer.* J Cancer, 2018. 9(14): p. 2492-2501.
104. Tasdogan, A., et al., *Metabolic heterogeneity confers differences in melanoma metastatic potential.* Nature, 2020. 577(7788): p. 115-120.
105. Payen, V.L., et al., *Monocarboxylate transporters in cancer.* Mol Metab, 2020. 33: p. 48-66.
106. Pierre, K. and L. Pellerin, *Monocarboxylate transporters in the central nervous system: distribution, regulation and function.* J Neurochem, 2005. 94(1): p. 1-14.
107. Draoui, N. and O. Feron, *Lactate shuttles at a glance: from physiological paradigms to anti-cancer treatments.* Dis Model Mech, 2011. 4(6): p. 727-32.
108. Wang, N., et al., *Structural basis of human monocarboxylate transporter 1 inhibition by anti-cancer drug candidates.* Cell, 2021. 184(2): p. 370-383.e13.
109. Wilson, M.C., et al., *Studies on the DIDS-binding site of monocarboxylate transporter 1 suggest a homology model of the open conformation and a plausible translocation cycle.* J Biol Chem, 2009. 284(30): p. 20011-21.
110. Garcia, C.K., et al., *Molecular characterization of a membrane transporter for lactate, pyruvate, and other monocarboxylates: implications for the Cori cycle.* Cell, 1994. 76(5): p. 865-73.
111. Juel, C., *Lactate-proton cotransport in skeletal muscle.* Physiol Rev, 1997. 77(2): p. 321-58.

112. Doherty, J.R., et al., *Blocking lactate export by inhibiting the Myc target MCT1 Disables glycolysis and glutathione synthesis.* Cancer Res, 2014. 74(3): p. 908-20.
113. Halestrap, A.P. and D. Meredith, *The SLC16 gene family-from monocarboxylate transporters (MCTs) to aromatic amino acid transporters and beyond.* Pflugers Arch, 2004. 447(5): p. 619-28.
114. Wilson, M.C., et al., *Basigin (CD147) is the target for organomercurial inhibition of monocarboxylate transporter isoforms 1 and 4: the ancillary protein for the insensitive MCT2 is EMBIGIN (gp70).* J Biol Chem, 2005. 280(29): p. 27213-21.
115. Birsoy, K., et al., *MCT1-mediated transport of a toxic molecule is an effective strategy for targeting glycolytic tumors.* Nat Genet, 2013. 45(1): p. 104-8.
116. Vijay, N. and M.E. Morris, *Role of monocarboxylate transporters in drug delivery to the brain.* Curr Pharm Des, 2014. 20(10): p. 1487-98.
117. Halestrap, A.P., *The monocarboxylate transporter family--Structure and functional characterization.* IUBMB Life, 2012. 64(1): p. 1-9.
118. Dhup, S., et al., *Multiple biological activities of lactic acid in cancer: influences on tumor growth, angiogenesis and metastasis.* Curr Pharm Des, 2012. 18(10): p. 1319-30.
119. Bröer, S., et al., *Characterization of the monocarboxylate transporter 1 expressed in Xenopus laevis oocytes by changes in cytosolic pH.* Biochem J, 1998. 333 (Pt 1)(Pt 1): p. 167-74.
120. Garcia, C.K., et al., *cDNA cloning of MCT2, a second monocarboxylate transporter expressed in different cells than MCT1.* J Biol Chem, 1995. 270(4): p. 1843-9.
121. Philp, N.J., H. Yoon, and L. Lombardi, *Mouse MCT3 gene is expressed preferentially in retinal pigment and choroid plexus epithelia.* Am J Physiol Cell Physiol, 2001. 280(5): p. C1319-26.
122. Pérez de Heredia, F., I.S. Wood, and P. Trayhurn, *Hypoxia stimulates lactate release and modulates monocarboxylate transporter (MCT1, MCT2, and MCT4) expression in human adipocytes.* Pflugers Arch, 2010. 459(3): p. 509-18.
123. Bröer, S., et al., *Characterization of the high-affinity monocarboxylate transporter MCT2 in Xenopus laevis oocytes.* Biochem J, 1999. 341 (Pt 3)(Pt 3): p. 529-35.

124. Dimmer, K.S., et al., *The low-affinity monocarboxylate transporter MCT4 is adapted to the export of lactate in highly glycolytic cells.* Biochem J, 2000. 350 Pt 1(Pt 1): p. 219-27.
125. Li, F. and M.C. Simon, *Cancer Cells Don't Live Alone: Metabolic Communication within Tumor Microenvironments.* Dev Cell, 2020. 54(2): p. 183-195.
126. Sahai, E., et al., *A framework for advancing our understanding of cancer-associated fibroblasts.* Nat Rev Cancer, 2020. 20(3): p. 174-186.
127. Pavlides, S., et al., *The reverse Warburg effect: aerobic glycolysis in cancer associated fibroblasts and the tumor stroma.* Cell Cycle, 2009. 8(23): p. 3984-4001.
128. Whitaker-Menezes, D., et al., *Evidence for a stromal-epithelial "lactate shuttle" in human tumors: MCT4 is a marker of oxidative stress in cancer-associated fibroblasts.* Cell Cycle, 2011. 10(11): p. 1772-83.
129. Sousa, C.M., et al., *Pancreatic stellate cells support tumour metabolism through autophagic alanine secretion.* Nature, 2016. 536(7617): p. 479-83.
130. Yang, L., et al., *Targeting Stromal Glutamine Synthetase in Tumors Disrupts Tumor Microenvironment-Regulated Cancer Cell Growth.* Cell Metab, 2016. 24(5): p. 685-700.
131. Donohoe, C.L., et al., *Emerging Concepts Linking Obesity with the Hallmarks of Cancer.* Trends Endocrinol Metab, 2017. 28(1): p. 46-62.
132. Hoy, A.J., S. Balaban, and D.N. Saunders, *Adipocyte-Tumor Cell Metabolic Crosstalk in Breast Cancer.* Trends Mol Med, 2017. 23(5): p. 381-392.
133. Cao, Y., *Adipocyte and lipid metabolism in cancer drug resistance.* J Clin Invest, 2019. 129(8): p. 3006-3017.
134. Ladanyi, A., et al., *Adipocyte-induced CD36 expression drives ovarian cancer progression and metastasis.* Oncogene, 2018. 37(17): p. 2285-2301.
135. Salimian Rizi, B., et al., *Nitric oxide mediates metabolic coupling of omentum-derived adipose stroma to ovarian and endometrial cancer cells.* Cancer Res, 2015. 75(2): p. 456-71.
136. Vera, J.C., et al., *Direct inhibition of the hexose transporter GLUT1 by tyrosine kinase inhibitors.* Biochemistry, 2001. 40(3): p. 777-90.

137. Zambrano, A., et al., *Glut 1 in Cancer Cells and the Inhibitory Action of Resveratrol as A Potential Therapeutic Strategy.* Int J Mol Sci, 2019. 20(13).
138. Ganapathy-Kanniappan, S. and J.F. Geschwind, *Tumor glycolysis as a target for cancer therapy: progress and prospects.* Mol Cancer, 2013. 12: p. 152.
139. Végran, F., et al., *Lactate influx through the endothelial cell monocarboxylate transporter MCT1 supports an NF-κB/IL-8 pathway that drives tumor angiogenesis.* Cancer Res, 2011. 71(7): p. 2550-60.
140. Doherty, J.R. and J.L. Cleveland, *Targeting lactate metabolism for cancer therapeutics.* J Clin Invest, 2013. 123(9): p. 3685-92.
141. Quanz, M., et al., *Preclinical Efficacy of the Novel Monocarboxylate Transporter 1 Inhibitor BAY-8002 and Associated Markers of Resistance.* Mol Cancer Ther, 2018. 17(11): p. 2285-2296.
142. Renner, K., et al., *Restricting Glycolysis Preserves T Cell Effector Functions and Augments Checkpoint Therapy.* Cell Rep, 2019. 29(1): p. 135-150.e9.
143. Butler, L.M., et al., *Lipids and cancer: Emerging roles in pathogenesis, diagnosis and therapeutic intervention.* Adv Drug Deliv Rev, 2020. 159: p. 245-293.
144. Broadfield, L.A., et al., *Lipid metabolism in cancer: New perspectives and emerging mechanisms.* Dev Cell, 2021. 56(10): p. 1363-1393.
145. Feng, W.W., et al., *CD36-Mediated Metabolic Rewiring of Breast Cancer Cells Promotes Resistance to HER2-Targeted Therapies.* Cell Rep, 2019. 29(11): p. 3405-3420.e5.
146. Pike, L.S., et al., *Inhibition of fatty acid oxidation by etomoxir impairs NADPH production and increases reactive oxygen species resulting in ATP depletion and cell death in human glioblastoma cells.* Biochim Biophys Acta, 2011. 1807(6): p. 726-34.
147. Ricciardi, M.R., et al., *Targeting the leukemia cell metabolism by the CPT1a inhibition: functional preclinical effects in leukemias.* Blood, 2015. 126(16): p. 1925-9.
148. Wei, J., et al., *An allosteric mechanism for potent inhibition of human ATP-citrate lyase.* Nature, 2019. 568(7753): p. 566-570.
149. Svensson, R.U., et al., *Inhibition of acetyl-CoA carboxylase suppresses fatty acid synthesis and tumor growth of non-small-cell lung cancer in preclinical models.* Nat Med, 2016. 22(10): p. 1108-1119.

150. Lally, J.S.V., et al., *Inhibition of Acetyl-CoA Carboxylase by Phosphorylation or the Inhibitor ND-654 Suppresses Lipogenesis and Hepatocellular Carcinoma.* Cell Metab, 2019. 29(1): p. 174-182.e5.
151. Zadra, G., et al., *Inhibition of de novo lipogenesis targets androgen receptor signaling in castration-resistant prostate cancer.* Proc Natl Acad Sci U S A, 2019. 116(2): p. 631-640.
152. Dierge, E., et al., *Peroxidation of n-3 and n-6 polyunsaturated fatty acids in the acidic tumor environment leads to ferroptosis-mediated anticancer effects.* Cell Metab, 2021. 33(8): p. 1701-1715.e5.
153. Altman, B.J., Z.E. Stine, and C.V. Dang, *From Krebs to clinic: glutamine metabolism to cancer therapy.* Nat Rev Cancer, 2016. 16(10): p. 619-34.
154. Willems, L., et al., *Inhibiting glutamine uptake represents an attractive new strategy for treating acute myeloid leukemia.* Blood, 2013. 122(20): p. 3521-32.
155. Ashton, T.M., et al., *Oxidative Phosphorylation as an Emerging Target in Cancer Therapy.* Clin Cancer Res, 2018. 24(11): p. 2482-2490.
156. Molina, J.R., et al., *An inhibitor of oxidative phosphorylation exploits cancer vulnerability.* Nat Med, 2018. 24(7): p. 1036-1046.
157. Shi, Y., et al., *Gboxin is an oxidative phosphorylation inhibitor that targets glioblastoma.* Nature, 2019. 567(7748): p. 341-346.
158. Lissanu Deribe, Y., et al., *Mutations in the SWI/SNF complex induce a targetable dependence on oxidative phosphorylation in lung cancer.* Nat Med, 2018. 24(7): p. 1047-1057.
159. Fischer, G.M., et al., *Molecular Profiling Reveals Unique Immune and Metabolic Features of Melanoma Brain Metastases.* Cancer Discov, 2019. 9(5): p. 628-645.
160. Chang, E., et al., *18F-FAZA PET imaging response tracks the reoxygenation of tumors in mice upon treatment with the mitochondrial complex I inhibitor BAY 87-2243.* Clin Cancer Res, 2015. 21(2): p. 335-46.
161. Corbet, C., et al., *Interruption of lactate uptake by inhibiting mitochondrial pyruvate transport unravels direct antitumor and radiosensitizing effects.* Nat Commun, 2018. 9(1): p. 1208.
162. Xu, R.H., et al., *Inhibition of glycolysis in cancer cells: a novel strategy to overcome drug resistance associated with mitochondrial respiratory defect and hypoxia.* Cancer Res, 2005. 65(2): p. 613-21.

163. Wagner, W., W.M. Ciszewski, and K.D. Kania, *L- and D-lactate enhance DNA repair and modulate the resistance of cervical carcinoma cells to anticancer drugs via histone deacetylase inhibition and hydroxycarboxylic acid receptor 1 activation.* Cell Commun Signal, 2015. 13: p. 36.
164. Chakraborty, P.K., et al., *MICU1 drives glycolysis and chemoresistance in ovarian cancer.* Nat Commun, 2017. 8: p. 14634.
165. McGuirk, S., et al., *Resistance to different anthracycline chemotherapeutics elicits distinct and actionable primary metabolic dependencies in breast cancer.* Elife, 2021. 10.
166. Shen, W., et al., *Targeting SREBP1 chemosensitizes colorectal cancer cells to gemcitabine by caspase-7 upregulation.* Bioengineered, 2019. 10(1): p. 459-468.
167. Schlaepfer, I.R., et al., *Progestin modulates the lipid profile and sensitivity of breast cancer cells to docetaxel.* Mol Cell Endocrinol, 2012. 363(1-2): p. 111-21.
168. Morandi, A. and S. Indraccolo, *Linking metabolic reprogramming to therapy resistance in cancer.* Biochim Biophys Acta Rev Cancer, 2017. 1868(1): p. 1-6.
169. Sirois, I., et al., *A Unique Morphological Phenotype in Chemoresistant Triple-Negative Breast Cancer Reveals Metabolic Reprogramming and PLIN4 Expression as a Molecular Vulnerability.* Mol Cancer Res, 2019. 17(12): p. 2492-2507.
170. Lièvre, A., et al., *Clinical value of mitochondrial mutations in colorectal cancer.* J Clin Oncol, 2005. 23(15): p. 3517-25.
171. Guerra, F., et al., *Mitochondrial DNA mutation in serous ovarian cancer: implications for mitochondria-coded genes in chemoresistance.* J Clin Oncol, 2012. 30(36): p. e373-8.
172. Weerts, M.J.A., et al., *Low Tumor Mitochondrial DNA Content Is Associated with Better Outcome in Breast Cancer Patients Receiving Anthracycline-Based Chemotherapy.* Clin Cancer Res, 2017. 23(16): p. 4735-4743.
173. Woo, Y.M., et al., *Inhibition of Aerobic Glycolysis Represses Akt/mTOR/HIF-1α Axis and Restores Tamoxifen Sensitivity in Antiestrogen-Resistant Breast Cancer Cells.* PLoS One, 2015. 10(7): p. e0132285.

174. Ruprecht, B., et al., *Lapatinib Resistance in Breast Cancer Cells Is Accompanied by Phosphorylation-Mediated Reprogramming of Glycolysis.* Cancer Res, 2017. 77(8): p. 1842-1853.
175. Bader, D.A., et al., *Mitochondrial pyruvate import is a metabolic vulnerability in androgen receptor-driven prostate cancer.* Nat Metab, 2019. 1(1): p. 70-85.
176. Viale, A., et al., *Oncogene ablation-resistant pancreatic cancer cells depend on mitochondrial function.* Nature, 2014. 514(7524): p. 628-32.
177. Apicella, M., et al., *Increased Lactate Secretion by Cancer Cells Sustains Non-cell-autonomous Adaptive Resistance to MET and EGFR Targeted Therapies.* Cell Metab, 2018. 28(6): p. 848-865.e6.
178. Hudson, C.D., et al., *Resistance to the tyrosine kinase inhibitor axitinib is associated with increased glucose metabolism in pancreatic adenocarcinoma.* Cell Death Dis, 2014. 5(4): p. e1160.
179. Gao, R., et al., *USP29-mediated HIF1α stabilization is associated with Sorafenib resistance of hepatocellular carcinoma cells by upregulating glycolysis.* Oncogenesis, 2021. 10(7): p. 52.
180. Allen, E., et al., *Metabolic Symbiosis Enables Adaptive Resistance to Anti-angiogenic Therapy that Is Dependent on mTOR Signaling.* Cell Rep, 2016. 15(6): p. 1144-60.
181. Pisarsky, L., et al., *Targeting Metabolic Symbiosis to Overcome Resistance to Anti-angiogenic Therapy.* Cell Rep, 2016. 15(6): p. 1161-74.
182. Jiménez-Valerio, G., et al., *Resistance to Antiangiogenic Therapies by Metabolic Symbiosis in Renal Cell Carcinoma PDX Models and Patients.* Cell Rep, 2016. 15(6): p. 1134-43.
183. Park, S., et al., *ERRα-Regulated Lactate Metabolism Contributes to Resistance to Targeted Therapies in Breast Cancer.* Cell Rep, 2016. 15(2): p. 323-35.
184. Correnti, M., et al., *Stemness features in liver cancer.* Hepatoma Res, 2018: p. 4:69.
185. Muller, F.L., E.A. Aquilanti, and R.A. DePinho, *Collateral Lethality: A new therapeutic strategy in oncology.* Trends Cancer, 2015. 1(3): p. 161-173.
186. Singer, K., et al., *Immunometabolism in cancer at a glance.* Dis Model Mech, 2018. 11(8).

187. Fridman, W.H., et al., *The immune contexture in human tumours: impact on clinical outcome.* Nat Rev Cancer, 2012. 12(4): p. 298-306.
188. Balkwill, F. and A. Mantovani, *Inflammation and cancer: back to Virchow?* Lancet, 2001. 357(9255): p. 539-45.
189. Dieu-Nosjean, M.C., et al., *Long-term survival for patients with non-small-cell lung cancer with intratumoral lymphoid structures.* J Clin Oncol, 2008. 26(27): p. 4410-7.
190. Mantovani, A., et al., *Cancer-related inflammation.* Nature, 2008. 454(7203): p. 436-44.
191. Halama, N., et al., *Localization and density of immune cells in the invasive margin of human colorectal cancer liver metastases are prognostic for response to chemotherapy.* Cancer Res, 2011. 71(17): p. 5670-7.
192. Farhood, B., M. Najafi, and K. Mortezaee, *CD8(+) cytotoxic T lymphocytes in cancer immunotherapy: A review.* J Cell Physiol, 2019. 234(6): p. 8509-8521.
193. Weissman, I., *Lymphocytes, Jim Gowans and in vivo veritas.* Nat Immunol, 2010. 11(12): p. 1073-5.
194. Raskov, H., et al., *Cytotoxic CD8(+) T cells in cancer and cancer immunotherapy.* Br J Cancer, 2021. 124(2): p. 359-367.
195. Brazin, K.N., et al., *Structural Features of the αβTCR Mechanotransduction Apparatus That Promote pMHC Discrimination.* Front Immunol, 2015. 6: p. 441.
196. Bettini, M.L., et al., *Membrane association of the CD3ε signaling domain is required for optimal T cell development and function.* J Immunol, 2014. 193(1): p. 258-67.
197. Gascoigne, N.R., *Do T cells need endogenous peptides for activation?* Nat Rev Immunol, 2008. 8(11): p. 895-900.
198. Schwartz, R.H., *T cell anergy.* Annu Rev Immunol, 2003. 21: p. 305-34.
199. Choi, S. and R.H. Schwartz, *Molecular mechanisms for adaptive tolerance and other T cell anergy models.* Semin Immunol, 2007. 19(3): p. 140-52.
200. Verma, N.K. and D. Kelleher, *An Introduction to LFA-1/ICAM-1 Interactions in T-Cell Motility.* Methods Mol Biol, 2019. 1930: p. 1-9.
201. Kupfer, A., G. Dennert, and S.J. Singer, *The reorientation of the Golgi apparatus and the microtubule-organizing center in the cytotoxic*

effector cell is a prerequisite in the lysis of bound target cells. J Mol Cell Immunol, 1985. 2(1): p. 37-49.
202. Yagi, H., et al., *Structural Basis for Ca2+-mediated Interaction of the Perforin C2 Domain with Lipid Membranes.* J Biol Chem, 2015. 290(42): p. 25213-26.
203. Alimonti, J.B., et al., *Granzyme B induces BID-mediated cytochrome c release and mitochondrial permeability transition.* J Biol Chem, 2001. 276(10): p. 6974-82.
204. Wiedemann, A., et al., *Cytotoxic T lymphocytes kill multiple targets simultaneously via spatiotemporal uncoupling of lytic and stimulatory synapses.* Proc Natl Acad Sci U S A, 2006. 103(29): p. 10985-90.
205. Fu, Q., et al., *Structural Basis and Functional Role of Intramembrane Trimerization of the Fas/CD95 Death Receptor.* Mol Cell, 2016. 61(4): p. 602-613.
206. Dornell, J., *CD8+ T Cells.* Technology Networks, 2021.
207. Oppenheim, J.J., *Cytokines: past, present, and future.* Int J Hematol, 2001. 74(1): p. 3-8.
208. St Paul, M. and P.S. Ohashi, *The Roles of CD8(+) T Cell Subsets in Antitumor Immunity.* Trends Cell Biol, 2020. 30(9): p. 695-704.
209. Croft, M., et al., *Generation of polarized antigen-specific CD8 effector populations: reciprocal action of interleukin (IL)-4 and IL-12 in promoting type 2 versus type 1 cytokine profiles.* J Exp Med, 1994. 180(5): p. 1715-28.
210. Boyman, O. and J. Sprent, *The role of interleukin-2 during homeostasis and activation of the immune system.* Nat Rev Immunol, 2012. 12(3): p. 180-90.
211. Cho, J.H., et al., *Unique features of naive CD8+ T cell activation by IL-2.* J Immunol, 2013. 191(11): p. 5559-73.
212. Yang, Y., et al., *Identification of a distant T-bet enhancer responsive to IL-12/Stat4 and IFNgamma/Stat1 signals.* Blood, 2007. 110(7): p. 2494-500.
213. Joller, N. and V.K. Kuchroo, *Tim-3, Lag-3, and TIGIT.* Curr Top Microbiol Immunol, 2017. 410: p. 127-156.
214. Arasanz, H., et al., *PD1 signal transduction pathways in T cells.* Oncotarget, 2017. 8(31): p. 51936-51945.

215. Patsoukis, N., et al., *PD-1 alters T-cell metabolic reprogramming by inhibiting glycolysis and promoting lipolysis and fatty acid oxidation.* Nat Commun, 2015. 6: p. 6692.
216. Schneider, H., et al., *Reversal of the TCR stop signal by CTLA-4.* Science, 2006. 313(5795): p. 1972-5.
217. Wherry, E.J. and M. Kurachi, *Molecular and cellular insights into T cell exhaustion.* Nat Rev Immunol, 2015. 15(8): p. 486-99.
218. Sakuishi, K., et al., *TIM3(+)FOXP3(+) regulatory T cells are tissue-specific promoters of T-cell dysfunction in cancer.* Oncoimmunology, 2013. 2(4): p. e23849.
219. Buck, M.D., D. O'Sullivan, and E.L. Pearce, *T cell metabolism drives immunity.* J Exp Med, 2015. 212(9): p. 1345-60.
220. Rangel Rivera, G.O., et al., *Fundamentals of T Cell Metabolism and Strategies to Enhance Cancer Immunotherapy.* Front Immunol, 2021. 12: p. 645242.
221. Surh, C.D. and J. Sprent, *Homeostasis of naive and memory T cells.* Immunity, 2008. 29(6): p. 848-62.
222. Wofford, J.A., et al., *IL-7 promotes Glut1 trafficking and glucose uptake via STAT5-mediated activation of Akt to support T-cell survival.* Blood, 2008. 111(4): p. 2101-11.
223. Chang, C.H., et al., *Posttranscriptional control of T cell effector function by aerobic glycolysis.* Cell, 2013. 153(6): p. 1239-51.
224. Gubser, P.M., et al., *Rapid effector function of memory CD8+ T cells requires an immediate-early glycolytic switch.* Nat Immunol, 2013. 14(10): p. 1064-72.
225. Buck, M.D., et al., *Mitochondrial Dynamics Controls T Cell Fate through Metabolic Programming.* Cell, 2016. 166(1): p. 63-76.
226. Peng, M., et al., *Aerobic glycolysis promotes T helper 1 cell differentiation through an epigenetic mechanism.* Science, 2016. 354(6311): p. 481-484.
227. Wellen, K.E., et al., *ATP-citrate lyase links cellular metabolism to histone acetylation.* Science, 2009. 324(5930): p. 1076-80.
228. Somarribas Patterson, L.F. and S.A. Vardhana, *Metabolic regulation of the cancer-immunity cycle.* Trends Immunol, 2021.
229. Scalise, M., et al., *The Human SLC1A5 (ASCT2) Amino Acid Transporter: From Function to Structure and Role in Cell Biology.* Front Cell Dev Biol, 2018. 6: p. 96.

230. Zhang, L. and P. Romero, *Metabolic Control of CD8(+) T Cell Fate Decisions and Antitumor Immunity.* Trends Mol Med, 2018. 24(1): p. 30-48.
231. Hörig, H., et al., *Exogenous glutamine requirement is confined to late events of T cell activation.* J Cell Biochem, 1993. 53(4): p. 343-51.
232. Cobbold, S.P., et al., *Infectious tolerance via the consumption of essential amino acids and mTOR signaling.* Proc Natl Acad Sci U S A, 2009. 106(29): p. 12055-60.
233. Chi, H., *Regulation and function of mTOR signalling in T cell fate decisions.* Nat Rev Immunol, 2012. 12(5): p. 325-38.
234. Youngblood, B., C.W. Davis, and R. Ahmed, *Making memories that last a lifetime: heritable functions of self-renewing memory CD8 T cells.* Int Immunol, 2010. 22(10): p. 797-803.
235. Bantug, G.R., et al., *Mitochondria-Endoplasmic Reticulum Contact Sites Function as Immunometabolic Hubs that Orchestrate the Rapid Recall Response of Memory CD8(+) T Cells.* Immunity, 2018. 48(3): p. 542-555.e6.
236. van der Windt, G.J., et al., *Mitochondrial respiratory capacity is a critical regulator of CD8+ T cell memory development.* Immunity, 2012. 36(1): p. 68-78.
237. Rambold, A.S. and E.L. Pearce, *Mitochondrial Dynamics at the Interface of Immune Cell Metabolism and Function.* Trends Immunol, 2018. 39(1): p. 6-18.
238. Mayer, A., et al., *AMP-activated protein kinase regulates lymphocyte responses to metabolic stress but is largely dispensable for immune cell development and function.* Eur J Immunol, 2008. 38(4): p. 948-56.
239. Pearce, E.L., et al., *Enhancing CD8 T-cell memory by modulating fatty acid metabolism.* Nature, 2009. 460(7251): p. 103-7.
240. Cui, G., et al., *IL-7-Induced Glycerol Transport and TAG Synthesis Promotes Memory CD8+ T Cell Longevity.* Cell, 2015. 161(4): p. 750-61.
241. Chen, D.S. and I. Mellman, *Oncology meets immunology: the cancer-immunity cycle.* Immunity, 2013. 39(1): p. 1-10.
242. Wagner, S., C.S. Mullins, and M. Linnebacher, *Colorectal cancer vaccines: Tumor-associated antigens vs neoantigens.* World J Gastroenterol, 2018. 24(48): p. 5418-5432.

243. Motz, G.T. and G. Coukos, *Deciphering and reversing tumor immune suppression.* Immunity, 2013. 39(1): p. 61-73.
244. Palucka, K. and J. Banchereau, *Dendritic-cell-based therapeutic cancer vaccines.* Immunity, 2013. 39(1): p. 38-48.
245. Doix, B., et al., *Low Photosensitizer Dose and Early Radiotherapy Enhance Antitumor Immune Response of Photodynamic Therapy-Based Dendritic Cell Vaccination.* Front Oncol, 2019. 9: p. 811.
246. Pardoll, D.M., *The blockade of immune checkpoints in cancer immunotherapy.* Nat Rev Cancer, 2012. 12(4): p. 252-64.
247. Hamanishi, J., et al., *PD-1/PD-L1 blockade in cancer treatment: perspectives and issues.* Int J Clin Oncol, 2016. 21(3): p. 462-73.
248. Velu, V., et al., *Enhancing SIV-specific immunity in vivo by PD-1 blockade.* Nature, 2009. 458(7235): p. 206-10.
249. Holstein, S.A. and M.A. Lunning, *CAR T-Cell Therapy in Hematologic Malignancies: A Voyage in Progress.* Clin Pharmacol Ther, 2020. 107(1): p. 112-122.
250. Mohanty, R., et al., *CAR T cell therapy: A new era for cancer treatment (Review).* Oncol Rep, 2019. 42(6): p. 2183-2195.
251. Ramos, C.A., et al., *Anti-CD30 CAR-T Cell Therapy in Relapsed and Refractory Hodgkin Lymphoma.* J Clin Oncol, 2020. 38(32): p. 3794-3804.
252. Schneider, D., et al., *Trispecific CD19-CD20-CD22-targeting duoCAR-T cells eliminate antigen-heterogeneous B cell tumors in preclinical models.* Sci Transl Med, 2021. 13(586).
253. Yang, J.C. and S.A. Rosenberg, *Adoptive T-Cell Therapy for Cancer.* Adv Immunol, 2016. 130: p. 279-94.
254. Manfredi, F., et al., *TCR Redirected T Cells for Cancer Treatment: Achievements, Hurdles, and Goals.* Front Immunol, 2020. 11: p. 1689.
255. Cham, C.M. and T.F. Gajewski, *Glucose availability regulates IFN-gamma production and p70S6 kinase activation in CD8+ effector T cells.* J Immunol, 2005. 174(8): p. 4670-7.
256. Chang, C.H., et al., *Metabolic Competition in the Tumor Microenvironment Is a Driver of Cancer Progression.* Cell, 2015. 162(6): p. 1229-41.
257. Singer, K., et al., *Warburg phenotype in renal cell carcinoma: high expression of glucose-transporter 1 (GLUT-1) correlates with low*

CD8(+) T-cell infiltration in the tumor. Int J Cancer, 2011. 128(9): p. 2085-95.
258. Fischer, K., et al., *Inhibitory effect of tumor cell-derived lactic acid on human T cells.* Blood, 2007. 109(9): p. 3812-9.
259. Gottfried, E., et al., *Tumor-derived lactic acid modulates dendritic cell activation and antigen expression.* Blood, 2006. 107(5): p. 2013-21.
260. Dietl, K., et al., *Lactic acid and acidification inhibit TNF secretion and glycolysis of human monocytes.* J Immunol, 2010. 184(3): p. 1200-9.
261. Liao, Y.P., D. Schaue, and W.H. McBride, *Modification of the tumor microenvironment to enhance immunity.* Front Biosci, 2007. 12: p. 3576-600.
262. Brand, A., et al., *LDHA-Associated Lactic Acid Production Blunts Tumor Immunosurveillance by T and NK Cells.* Cell Metab, 2016. 24(5): p. 657-671.
263. Angelin, A., et al., *Foxp3 Reprograms T Cell Metabolism to Function in Low-Glucose, High-Lactate Environments.* Cell Metab, 2017. 25(6): p. 1282-1293.e7.
264. Pilon-Thomas, S., et al., *Neutralization of Tumor Acidity Improves Antitumor Responses to Immunotherapy.* Cancer Res, 2016. 76(6): p. 1381-90.
265. Calcinotto, A., et al., *Modulation of microenvironment acidity reverses anergy in human and murine tumor-infiltrating T lymphocytes.* Cancer Res, 2012. 72(11): p. 2746-56.
266. Ohta, A., et al., *Hypoxia-induced and A2A adenosine receptor-independent T-cell suppression is short lived and easily reversible.* Int Immunol, 2014. 26(2): p. 83-91.
267. Ohta, A. and M. Sitkovsky, *Extracellular adenosine-mediated modulation of regulatory T cells.* Front Immunol, 2014. 5: p. 304.
268. Ma, X., et al., *Cholesterol Induces CD8(+) T Cell Exhaustion in the Tumor Microenvironment.* Cell Metab, 2019. 30(1): p. 143-156.e5.
269. Geiger, R., et al., *L-Arginine Modulates T Cell Metabolism and Enhances Survival and Anti-tumor Activity.* Cell, 2016. 167(3): p. 829-842.e13.
270. Mazzone, M., A. Menga, and A. Castegna, *Metabolism and TAM functions-it takes two to tango.* Febs j, 2018. 285(4): p. 700-716.
271. Fallarino, F., et al., *The combined effects of tryptophan starvation and tryptophan catabolites down-regulate T cell receptor zeta-chain and*

induce a regulatory phenotype in naive T cells. J Immunol, 2006. 176(11): p. 6752-61.
272. Boulland, M.L., et al., *Human IL4I1 is a secreted L-phenylalanine oxidase expressed by mature dendritic cells that inhibits T-lymphocyte proliferation.* Blood, 2007. 110(1): p. 220-7.
273. Chon, S.Y., H.H. Hassanain, and S.L. Gupta, *Cooperative role of interferon regulatory factor 1 and p91 (STAT1) response elements in interferon-gamma-inducible expression of human indoleamine 2,3-dioxygenase gene.* J Biol Chem, 1996. 271(29): p. 17247-52.
274. Harris, I.S. and G.M. DeNicola, *The Complex Interplay between Antioxidants and ROS in Cancer.* Trends Cell Biol, 2020. 30(6): p. 440-451.
275. Noman, M.Z., et al., *PD-L1 is a novel direct target of HIF-1α, and its blockade under hypoxia enhanced MDSC-mediated T cell activation.* J Exp Med, 2014. 211(5): p. 781-90.
276. Zhu, B., et al., *Targeting the upstream transcriptional activator of PD-L1 as an alternative strategy in melanoma therapy.* Oncogene, 2018. 37(36): p. 4941-4954.
277. Sadik, A., et al., *IL4I1 Is a Metabolic Immune Checkpoint that Activates the AHR and Promotes Tumor Progression.* Cell, 2020. 182(5): p. 1252-1270.e34.
278. Dell'Antone, P., *Targets of 3-bromopyruvate, a new, energy depleting, anticancer agent.* Med Chem, 2009. 5(6): p. 491-6.
279. Ko, Y.H., P.L. Pedersen, and J.F. Geschwind, *Glucose catabolism in the rabbit VX2 tumor model for liver cancer: characterization and targeting hexokinase.* Cancer Lett, 2001. 173(1): p. 83-91.
280. Inoue, T., et al., *Inhibition of COX-2 expression by topical diclofenac enhanced radiation sensitivity via enhancement of TRAIL in human prostate adenocarcinoma xenograft model.* BMC Urol, 2013. 13: p. 1.
281. Abdel-aleem, S., et al., *Regulation of glucose utilization during the inhibition of fatty acid oxidation in rat myocytes.* Horm Metab Res, 1994. 26(2): p. 88-91.
282. Luengo, A., D.Y. Gui, and M.G. Vander Heiden, *Targeting Metabolism for Cancer Therapy.* Cell Chem Biol, 2017. 24(9): p. 1161-1180.
283. Wise, D.R., et al., *Myc regulates a transcriptional program that stimulates mitochondrial glutaminolysis and leads to glutamine addiction.* Proc Natl Acad Sci U S A, 2008. 105(48): p. 18782-7.

284. Ying, H., et al., *Oncogenic Kras maintains pancreatic tumors through regulation of anabolic glucose metabolism.* Cell, 2012. 149(3): p. 656-70.
285. Haq, R., et al., *Oncogenic BRAF regulates oxidative metabolism via PGC1α and MITF.* Cancer Cell, 2013. 23(3): p. 302-15.
286. Zecchini, V. and C. Frezza, *Metabolic synthetic lethality in cancer therapy.* Biochim Biophys Acta Bioenerg, 2017. 1858(8): p. 723-731.
287. Lehuédé, C., et al., *Metabolic Plasticity as a Determinant of Tumor Growth and Metastasis.* Cancer Res, 2016. 76(18): p. 5201-8.
288. Enriquez-Navas, P.M., J.W. Wojtkowiak, and R.A. Gatenby, *Application of Evolutionary Principles to Cancer Therapy.* Cancer Res, 2015. 75(22): p. 4675-80.
289. Gatenby, R.A., J. Brown, and T. Vincent, *Lessons from applied ecology: cancer control using an evolutionary double bind.* Cancer Res, 2009. 69(19): p. 7499-502.
290. Maley, C.C., B.J. Reid, and S. Forrest, *Cancer prevention strategies that address the evolutionary dynamics of neoplastic cells: simulating benign cell boosters and selection for chemosensitivity.* Cancer Epidemiol Biomarkers Prev, 2004. 13(8): p. 1375-84.
291. Antonia, S.J., et al., *Combination of p53 cancer vaccine with chemotherapy in patients with extensive stage small cell lung cancer.* Clin Cancer Res, 2006. 12(3 Pt 1): p. 878-87.
292. Ramakrishnan, R., et al., *Chemotherapy enhances tumor cell susceptibility to CTL-mediated killing during cancer immunotherapy in mice.* J Clin Invest, 2010. 120(4): p. 1111-24.
293. Salgia, R. and P. Kulkarni, *The Genetic/Non-genetic Duality of Drug 'Resistance' in Cancer.* Trends Cancer, 2018. 4(2): p. 110-118.
294. Ganapathy-Kanniappan, S., et al., *Glyceraldehyde-3-phosphate dehydrogenase (GAPDH) is pyruvylated during 3-bromopyruvate mediated cancer cell death.* Anticancer Res, 2009. 29(12): p. 4909-18.
295. Rodrigues-Ferreira, C., A.P. da Silva, and A. Galina, *Effect of the antitumoral alkylating agent 3-bromopyruvate on mitochondrial respiration: role of mitochondrially bound hexokinase.* J Bioenerg Biomembr, 2012. 44(1): p. 39-49.
296. Ullah, M.S., A.J. Davies, and A.P. Halestrap, *The plasma membrane lactate transporter MCT4, but not MCT1, is up-regulated by hypoxia*

through a HIF-1alpha-dependent mechanism. J Biol Chem, 2006. 281(14): p. 9030-7.
297. Benjamin, D., et al., *Dual Inhibition of the Lactate Transporters MCT1 and MCT4 Is Synthetic Lethal with Metformin due to NAD+ Depletion in Cancer Cells.* Cell Rep, 2018. 25(11): p. 3047-3058.e4.
298. Fan, T., et al., *Tumor Energy Metabolism and Potential of 3-Bromopyruvate as an Inhibitor of Aerobic Glycolysis: Implications in Tumor Treatment.* Cancers (Basel), 2019. 11(3).
299. Robertson, K.D., et al., *DNMT1 forms a complex with Rb, E2F1 and HDAC1 and represses transcription from E2F-responsive promoters.* Nat Genet, 2000. 25(3): p. 338-42.
300. Di Croce, L., et al., *Methyltransferase recruitment and DNA hypermethylation of target promoters by an oncogenic transcription factor.* Science, 2002. 295(5557): p. 1079-82.
301. Keshet, I., et al., *Evidence for an instructive mechanism of de novo methylation in cancer cells.* Nat Genet, 2006. 38(2): p. 149-53.
302. Estécio, M.R. and J.P. Issa, *Dissecting DNA hypermethylation in cancer.* FEBS Lett, 2011. 585(13): p. 2078-86.
303. Ferreri, A.J., et al., *Aberrant methylation in the promoter region of the reduced folate carrier gene is a potential mechanism of resistance to methotrexate in primary central nervous system lymphomas.* Br J Haematol, 2004. 126(5): p. 657-64.
304. Polański, R., et al., *Activity of the monocarboxylate transporter 1 inhibitor AZD3965 in small cell lung cancer.* Clin Cancer Res, 2014. 20(4): p. 926-937.
305. Oshima, N., et al., *Dynamic Imaging of LDH Inhibition in Tumors Reveals Rapid In Vivo Metabolic Rewiring and Vulnerability to Combination Therapy.* Cell Rep, 2020. 30(6): p. 1798-1810.e4.
306. Beloueche-Babari, M., et al., *MCT1 Inhibitor AZD3965 Increases Mitochondrial Metabolism, Facilitating Combination Therapy and Noninvasive Magnetic Resonance Spectroscopy.* Cancer Res, 2017. 77(21): p. 5913-5924.
307. Muller, F.L., et al., *Passenger deletions generate therapeutic vulnerabilities in cancer.* Nature, 2012. 488(7411): p. 337-42.
308. Mavrakis, K.J., et al., *Disordered methionine metabolism in MTAP/CDKN2A-deleted cancers leads to dependence on PRMT5.* Science, 2016. 351(6278): p. 1208-13.

309. Dey, P., et al., *Genomic deletion of malic enzyme 2 confers collateral lethality in pancreatic cancer.* Nature, 2017. 542(7639): p. 119-123.
310. Nowak-Sliwinska, P., L. Scapozza, and A. Ruiz i Altaba, *Drug repurposing in oncology: Compounds, pathways, phenotypes and computational approaches for colorectal cancer.* Biochim Biophys Acta Rev Cancer, 2019. 1871(2): p. 434-454.
311. Critchlow, S.E., et al., *Abstract 1207: Reversing lactate-driven immunosuppression using the novel, potent and selective MCT4 inhibitor AZD0095.* Cancer Res, 2019.
312. Hambrush, N., et al., *Abstract 3588: Identification of a potent, orally bioavailable and selective MCT4 Inhibitor for the treatment of solid Warburg tumors.* Cancer Res, 2019.
313. DeBerardinis, R.J. and N.S. Chandel, *Fundamentals of cancer metabolism.* Sci Adv, 2016. 2(5): p. e1600200.
314. Phan, L.M., S.C. Yeung, and M.H. Lee, *Cancer metabolic reprogramming: importance, main features, and potentials for precise targeted anti-cancer therapies.* Cancer Biol Med, 2014. 11(1): p. 1-19.
315. Qin, C., et al., *Metabolism of pancreatic cancer: paving the way to better anticancer strategies.* Mol Cancer, 2020. 19(1): p. 50.
316. Waldman, A.D., J.M. Fritz, and M.J. Lenardo, *A guide to cancer immunotherapy: from T cell basic science to clinical practice.* Nat Rev Immunol, 2020. 20(11): p. 651-668.
317. Maleki Vareki, S., *High and low mutational burden tumors versus immunologically hot and cold tumors and response to immune checkpoint inhibitors.* J Immunother Cancer, 2018. 6(1): p. 157.
318. Marceaux, C., et al., *Holding our breath: the promise of tissue-resident memory T cells in lung cancer.* Transl Lung Cancer Res, 2021. 10(6): p. 2819-2829.
319. Cheng, W.C. and P.C. Ho, *Metabolic tug-of-war in tumors results in diminished T cell antitumor immunity.* Oncoimmunology, 2016. 5(4): p. e1119355.
320. Xu, K., A. Shyu, and M.O. Li, *A Tug-of-War Over Methionine.* Cell Metab, 2020. 32(5): p. 699-701.
321. Pallett, L.J., et al., *A glutamine 'tug-of-war': targets to manipulate glutamine metabolism for cancer immunotherapy.* Immunother Adv, 2021. 1(1): p. ltab010.

322. Huang, S.C., et al., *Cell-intrinsic lysosomal lipolysis is essential for alternative activation of macrophages.* Nat Immunol, 2014. 15(9): p. 846-55.
323. Nomura, M., et al., *Fatty acid oxidation in macrophage polarization.* Nat Immunol, 2016. 17(3): p. 216-7.
324. Shao, H., et al., *Carnitine palmitoyltransferase 1A functions to repress FoxO transcription factors to allow cell cycle progression in ovarian cancer.* Oncotarget, 2016. 7(4): p. 3832-46.
325. Yao, C.H., et al., *Identifying off-target effects of etomoxir reveals that carnitine palmitoyltransferase I is essential for cancer cell proliferation independent of β-oxidation.* PLoS Biol, 2018. 16(3): p. e2003782.
326. Erra Díaz, F., E. Dantas, and J. Geffner, *Unravelling the Interplay between Extracellular Acidosis and Immune Cells.* Mediators Inflamm, 2018. 2018: p. 1218297.
327. Najjar, Y.G., et al., *Tumor cell oxidative metabolism as a barrier to PD-1 blockade immunotherapy in melanoma.* JCI Insight, 2019. 4(5).
328. Chen, D., et al., *Combination treatment with radiotherapy and a novel oxidative phosphorylation inhibitor overcomes PD-1 resistance and enhances antitumor immunity.* J Immunother Cancer, 2020. 8(1).
329. Wherry, E.J., *T cell exhaustion.* Nat Immunol, 2011. 12(6): p. 492-9.
330. Raud, B., et al., *Fatty acid metabolism in CD8(+) T cell memory: Challenging current concepts.* Immunol Rev, 2018. 283(1): p. 213-231.
331. Lipson, E.J., et al., *Relatlimab (RELA) plus nivolumab (NIVO) versus NIVO in first-line advanced melanoma: Primary phase III results from RELATIVITY-047 (CA224-047).* Meeting Abstract | 2021 ASCO Annual Meeting, 2021.
332. Scharping, N.E., et al., *The Tumor Microenvironment Represses T Cell Mitochondrial Biogenesis to Drive Intratumoral T Cell Metabolic Insufficiency and Dysfunction.* Immunity, 2016. 45(2): p. 374-88.
333. Rosenberg, S.A., et al., *Adoptive cell transfer: a clinical path to effective cancer immunotherapy.* Nat Rev Cancer, 2008. 8(4): p. 299-308.
334. Anagnostou, T., et al., *Anti-CD19 chimeric antigen receptor T-cell therapy in acute lymphocytic leukaemia: a systematic review and meta-analysis.* Lancet Haematol, 2020. 7(11): p. e816-e826.

335. Klein Geltink, R.I., et al., *Metabolic conditioning of CD8(+) effector T cells for adoptive cell therapy.* Nat Metab, 2020. 2(8): p. 703-716.
336. Abou-Alfa, G.K., et al., *Ivosidenib in IDH1-mutant, chemotherapy-refractory cholangiocarcinoma (ClarIDHy): a multicentre, randomised, double-blind, placebo-controlled, phase 3 study.* Lancet Oncol, 2020. 21(6): p. 796-807.
337. Choe, S., et al., *Molecular mechanisms mediating relapse following ivosidenib monotherapy in IDH1-mutant relapsed or refractory AML.* Blood Adv, 2020. 4(9): p. 1894-1905.
338. Quek, L., et al., *Clonal heterogeneity of acute myeloid leukemia treated with the IDH2 inhibitor enasidenib.* Nat Med, 2018. 24(8): p. 1167-1177.
339. Intlekofer, A.M., et al., *Acquired resistance to IDH inhibition through trans or cis dimer-interface mutations.* Nature, 2018. 559(7712): p. 125-129.
340. Singleton, D.C., et al., *Pyruvate anaplerosis is a mechanism of resistance to pharmacological glutaminase inhibition in triple-receptor negative breast cancer.* BMC Cancer, 2020. 20(1): p. 470.
341. Azevedo-Silva, J., et al., *The anticancer agent 3-bromopyruvate: a simple but powerful molecule taken from the lab to the bedside.* J Bioenerg Biomembr, 2016. 48(4): p. 349-62.
342. Geschwind, J.F., et al., *Novel therapy for liver cancer: direct intraarterial injection of a potent inhibitor of ATP production.* Cancer Res, 2002. 62(14): p. 3909-13.
343. Cao, X., et al., *Synergistic antipancreatic tumor effect by simultaneously targeting hypoxic cancer cells with HSP90 inhibitor and glycolysis inhibitor.* Clin Cancer Res, 2008. 14(6): p. 1831-9.
344. Famuyiwa, T.O., et al., *Interaction between 3-Bromopyruvate and SC-514 in prostate cancer treatment.* J Cancer Prev Curr Res., 2018.
345. Hanafy, N.A., et al., *Inihibition of Glycolysis by Using a Micro/Nano-Lipid Bromopyruvic Chitosan Carrier as a Promising Tool to Improve Treatment of Hepatocellular Carcinoma.* Nanomaterials (Basel), 2018. 8(1).
346. Chang, X., et al., *Identification of hypermethylated genes associated with cisplatin resistance in human cancers.* Cancer Res, 2010. 70(7): p. 2870-9.

347. Chen, M. and S. Xie, *Therapeutic targeting of cellular stress responses in cancer.* Thorac Cancer, 2018. 9(12): p. 1575-1582.
348. Akhter, Z., et al., *In Response to Abiotic Stress, DNA Methylation Confers EpiGenetic Changes in Plants.* Plants (Basel), 2021. 10(6).
349. Bird, A., *DNA methylation patterns and epigenetic memory.* Genes Dev, 2002. 16(1): p. 6-21.
350. Harding, J.J., et al., *Isoform Switching as a Mechanism of Acquired Resistance to Mutant Isocitrate Dehydrogenase Inhibition.* Cancer Discov, 2018. 8(12): p. 1540-1547.
351. Xu, L., et al., *A glutaminase isoform switch drives therapeutic resistance and disease progression of prostate cancer.* Proc Natl Acad Sci U S A, 2021. 118(13).
352. Parks, S.K., J. Chiche, and J. Pouysségur, *Disrupting proton dynamics and energy metabolism for cancer therapy.* Nat Rev Cancer, 2013. 13(9): p. 611-23.
353. Hulleman, E., et al., *Inhibition of glycolysis modulates prednisolone resistance in acute lymphoblastic leukemia cells.* Blood, 2009. 113(9): p. 2014-21.
354. Rai, Y., et al., *Hexokinase II inhibition by 3-bromopyruvate sensitizes myeloid leukemic cells K-562 to anti-leukemic drug, daunorubicin.* Biosci Rep, 2019. 39(9).
355. El Sayed, S.M., et al., *Safety and outcome of treatment of metastatic melanoma using 3-bromopyruvate: a concise literature review and case study.* Chin J Cancer, 2014. 33(7): p. 356-64.
356. van Gastel, N., et al., *Induction of a Timed Metabolic Collapse to Overcome Cancer Chemoresistance.* Cell Metab, 2020. 32(3): p. 391-403.e6.
357. Pinheiro, C., et al., *Monocarboxylate transporters 1 and 4 are associated with CD147 in cervical carcinoma.* Dis Markers, 2009. 26(3): p. 97-103.
358. Izumi, H., et al., *Monocarboxylate transporters 1 and 4 are involved in the invasion activity of human lung cancer cells.* Cancer Sci, 2011. 102(5): p. 1007-13.
359. Huhta, H., et al., *Intratumoral lactate metabolism in Barrett's esophagus and adenocarcinoma.* Oncotarget, 2017. 8(14): p. 22894-22902.

360. Pushpakom, S., et al., *Drug repurposing: progress, challenges and recommendations.* Nat Rev Drug Discov, 2019. 18(1): p. 41-58.
361. Rosenberg, S.A., et al., *Durable complete responses in heavily pretreated patients with metastatic melanoma using T-cell transfer immunotherapy.* Clin Cancer Res, 2011. 17(13): p. 4550-7.
362. Sukumar, M., et al., *Inhibiting glycolytic metabolism enhances CD8+ T cell memory and antitumor function.* J Clin Invest, 2013. 123(10): p. 4479-88.
363. Eil, R., et al., *Ionic immune suppression within the tumour microenvironment limits T cell effector function.* Nature, 2016. 537(7621): p. 539-543.
364. Chamoto, K., et al., *Mitochondrial activation chemicals synergize with surface receptor PD-1 blockade for T cell-dependent antitumor activity.* Proc Natl Acad Sci U S A, 2017. 114(5): p. E761-e770.
365. Sanborn, B.M., N.T. Felberg, and T.C. Hollocher, *The inactivation of succinate dehydrogenase by bromopyruvate.* Biochim Biophys Acta, 1971. 227(2): p. 219-31.
366. Conroy, C.W. and T.H. Maren, *The determination of osteopetrotic phenotypes by selective inactivation of red cell carbonic anhydrase isoenzymes.* Clin Chim Acta, 1985. 152(3): p. 347-54.
367. Dell'Antone, P., *Inactivation of H+-vacuolar ATPase by the energy blocker 3-bromopyruvate, a new antitumour agent.* Life Sci, 2006. 79(21): p. 2049-55.
368. Acan, N.L. and N. Ozer, *Modification of human erythrocyte pyruvate kinase by an active site-directed reagent: bromopyruvate.* J Enzyme Inhib, 2001. 16(5): p. 457-64.
369. Bendrat, K., et al., *Biochemical and mutational investigations of the enzymatic activity of macrophage migration inhibitory factor.* Biochemistry, 1997. 36(49): p. 15356-62.
370. Wang, M.H., Z.X. Wang, and K.Y. Zhao, *Kinetics of inactivation of bovine pancreatic ribonuclease A by bromopyruvic acid.* Biochem J, 1996. 320 (Pt 1)(Pt 1): p. 187-92.
371. Hanau, S., et al., *Bromopyruvate for the affinity labelling of a single cysteine residue near the carboxylate binding site of lamb liver 6-phosphogluconate dehydrogenase.* Biochem Mol Biol Int, 1995. 37(4): p. 785-93.

372. Vlahos, C.J. and E.E. Dekker, *Active-site residues of 2-keto-4-hydroxyglutarate aldolase from Escherichia coli. Bromopyruvate inactivation and labeling of glutamate 45.* J Biol Chem, 1990. 265(33): p. 20384-9.
373. Urban, P. and F. Lederer, *Inactivation of flavocytochrome b2 with fluoropyruvate. Reaction at the active-site histidine.* Eur J Biochem, 1988. 173(1): p. 155-62.
374. Darabedian, N., et al., *Bioorthogonal Profiling of a Cancer Cell Proteome Identifies a Large Set of 3-Bromopyruvate Targets beyond Glycolysis.* ACS Chem Biol, 2018. 13(11): p. 3054-3058.
375. Xu, X.C., *COX-2 inhibitors in cancer treatment and prevention, a recent development.* Anticancer Drugs, 2002. 13(2): p. 127-37.
376. Gottfried, E., et al., *New aspects of an old drug--diclofenac targets MYC and glucose metabolism in tumor cells.* PLoS One, 2013. 8(7): p. e66987.
377. Yang, M., et al., *Dual Effects of Cyclooxygenase Inhibitors in Combination With CD19.CAR-T Cell Immunotherapy.* Front Immunol, 2021. 12: p. 670088.
378. Paccani, S.R., et al., *Nonsteroidal anti-inflammatory drugs suppress T-cell activation by inhibiting p38 MAPK induction.* J Biol Chem, 2002. 277(2): p. 1509-13.
379. O'Connor, R.S., et al., *The CPT1a inhibitor, etomoxir induces severe oxidative stress at commonly used concentrations.* Sci Rep, 2018. 8(1): p. 6289.
380. Pritchard, G.H., et al., *Spontaneous partial loss of the OT-I transgene.* Nat Immunol, 2016. 17(5): p. 471.
381. Quagliano, A., A. Gopalakrishnapillai, and S.P. Barwe, *Understanding the Mechanisms by Which Epigenetic Modifiers Avert Therapy Resistance in Cancer.* Front Oncol, 2020. 10: p. 992.
382. Cattaneo, C.M., et al., *Tumor organoid-T-cell coculture systems.* Nat Protoc, 2020. 15(1): p. 15-39.